PolyPublie
Polytechnique Montréal

POLYTECHNIQUE MONTRÉAL
UNIVERSITÉ D'INGÉNIERIE

Titre: Title: Calculation and Verification of Assembly Discontinuity Factors for the DRAGON/PARCS Code Sequence

Auteur: Author: Luca Liponi

Date: 2017

Type: Mémoire ou thèse / Dissertation or Thesis

Référence: Citation: Liponi, L. (2017). Calculation and Verification of Assembly Discontinuity Factors for the DRAGON/PARCS Code Sequence [Mémoire de maîtrise, École Polytechnique de Montréal]. PolyPublie. https://publications.polymtl.ca/2726/

Document en libre accès dans PolyPublie
Open Access document in PolyPublie

URL de PolyPublie: PolyPublie URL: https://publications.polymtl.ca/2726/

Directeurs de recherche: Advisors: Alain Hébert, & Julien Taforeau

Programme: Program: Génie énergétique

Ce fichier a été téléchargé à partir de PolyPublie, le dépôt institutionnel de Polytechnique Montréal
This file has been downloaded from PolyPublie, the institutional repository of Polytechnique Montréal

https://publications.polymtl.ca

UNIVERSITÉ DE MONTRÉAL

CALCULATION AND VERIFICATION OF ASSEMBLY DISCONTINUITY FACTORS FOR THE DRAGON/PARCS CODE SEQUENCE

LUCA LIPONI
DÉPARTEMENT DE GÉNIE PHYSIQUE
ÉCOLE POLYTECHNIQUE DE MONTRÉAL

MÉMOIRE PRÉSENTÉ EN VUE DE L'OBTENTION
DU DIPLÔME DE MAÎTRISE ÈS SCIENCES APPLIQUÉES
(GÉNIE ÉNERGÉTIQUE)
JUILLET 2017

© Luca Liponi, 2017.

UNIVERSITÉ DE MONTRÉAL

ÉCOLE POLYTECHNIQUE DE MONTRÉAL

Ce mémoire intitulé:

CALCULATION AND VERIFICATION OF ASSEMBLY DISCONTINUITY FACTORS FOR THE DRAGON/PARCS CODE SEQUENCE

présenté par: LIPONI Luca
en vue de l'obtention du diplôme de: Maîtrise ès sciences appliquées
a été dûment accepté par le jury d'examen constitué de:

M. MARLEAU Guy, Ph. D., président
M. HÉBERT Alain, Doctorat, membre et directeur de recherche
M. TAFOREAU Julien, Ph. D., membre et codirecteur de recherche
M. CHAMBON Richard, Ph. D., membre externe

DÉDICACE

À mes parents,
à mon frère

REMERCIEMENTS

Je tiens tout d'abord à remercier mon directeur de recherche, prof. Alain Hébert, de m'avoir accepté comme étudiant et de m'avoir donné la possibilité de participer à ce projet et d'effectuer un stage au sein de l'IRSN. Sa patience et sa disponibilité ainsi que ses précieux conseils ont joué un rôle essentiel dans la réussite de cette maitrise de recherche. De la même manière, j'aimerais également remercier Julien Taforeau, mon maître de stage à l'IRSN et co-directeur de recherche, de m'avoir encouragé et guidé pendant ce projet de recherche. Je lui suis très reconnaissant d'avoir réussi à me motiver alors que j'en avais besoin et de m'avoir orienté vers la réalisation de cet objectif.

Concernant mon stage à l'IRSN, je tiens à remercier Mme Sophie Pignet pour son accueil au sein du LNR et tous les collègues qui ont contribué à rendre ce stage très profitable sur le plan humain et professionnel. Surtout, je tiens à remercier Antoine et Vivian pour les précieux conseils et les discussions fructueuses qui ont activement influencé mon travail.

Au sein du l'Institut de Génie Nucléaire (IGN) à Polytechnique de Montréal, je tiens à remercier tous les étudiants, les professeurs et le personnel que j'ai rencontrés au cours de cette expérience. Je remercie prof. Guy Marleau, directeur de l'IGN, pour sa disponibilité et ses conseils pertinents, et Richard Chambon, qui m'a donné des informations importantes afin de poursuivre le travail qu'il a commencé. Merci aussi à Lyne Dénommé pour sa grande patience. De plus, j'aimerais remercier ceux qui ont contribué de manière significative, même indirectement, à ce mémoire : Bastien, Aaron, Atyab, Clément, Alvaro, Najoua, Ahmed.

Enfin, un grand merci à ma famille et à Maria, qui m'ont soutenu tout au long de cette période, surtout dans les moments difficiles, et qui ont été essentiels afin d'atteindre cet objectif.

RÉSUMÉ

Cette étude est dédiée à la génération et à la validation des Facteurs de Discontinuité d'Assemblage (FDA) pour la chaine de calcul DRAGON5-PARCS.

Dans le cadre du projet ORON, l'IRSN a travaillé sur le couplage entre le code de réseau DRAGON5 et le code de simulation cœur-entier PARCS. Dans un premier temps, les efforts ont été mis sur la validation de la technique SPH conformément à l'approche traditionnelle utilisée en France pour les REP. Ce travail propose d'améliorer la flexibilité de la chaine de calcul DRAGON/PARCS en étudiant une méthode alternative basée sur l'homogénéisation des assemblages par la méthode des facteurs de discontinuité.

La première partie du document est axée sur le calcul d'un assemblage en milieu infini et sur l'impact des différentes stratégies envisagées pour la génération des FDA. Dans cette optique, différents schémas de calcul ont été évalués conformément aux approches actuellement adoptées par l'IRSN et par l'EPM. La première méthode, historiquement utilisé à l'IRSN, s'appuie sur un schéma simple niveau basé sur la méthode des probabilités de collisions. Le second schéma, récemment mis au point par l'EPM et correspondant à l'état de l'art actuel, a également été considéré; il correspond à une approche double niveaux (Pij/MOC).

L'impact des sections efficaces et des facteurs de discontinuités ainsi générés est évalué via des motifs d'assemblages et comparé à un calcul de référence Monte Carlo utilisant le code SERPENT2. La validation a été réalisée sur des motifs 2x2 et 3x3 composés de trois types d'assemblages: UOX, UOX avec barres de contrôles AIC et MOX. L'étude a porté sur trois paramètres présentant un intérêt particulier : la réactivité du massif, la puissance des assemblages, et la reconstruction fine de puissance. Cette dernière peut être considérée comme particulièrement sensible aux facteurs de discontinuités. De plus, un motif plus réaliste, entouré d'un réflecteur neutronique, a également été envisagé. Cette partie à donné lieu à un développement spécifique du réflecteur, basé sur la méthode proposée par Koebke.

Cette étude démontre l'impact significatif des facteurs de discontinuité sur les configurations évaluées. Les améliorations observées en utilisant des FDA sont importantes : jusqu'à 600 pcm en ce qui concerne la réactivité et 8% pour la puissance assemblage. En outre, une meilleure reconstruction a également été observée en ce qui concerne la distribution de puissance crayon par crayon. Au terme de cette étude, il apparait que le schéma de calcul double niveau fournit les résultats les plus proches de la référence Monte Carlo. Pour chaque configuration testée, les meilleures options de schéma de calculs sont identifiées. Les calculs DRAGON/PARCS avec réflecteur neutronique démontrent par ailleurs un bon accord comparé aux calculs Monte

Carlo. Pour conclure, les écarts importants observés sur le motif UOX-MOX suggèrent une étude plus approfondie concernant le traitement des assemblages MOX par le code réseau et en particulier l'approximation du milieu infini qui ne tient pas compte des phénomènes environnementaux particulièrement prononcés à l'interface UOX/MOX.

ABSTRACT

This study is dedicated to the generation and validation of Assembly Discontinuity Factor (ADF) for the DRAGON5-PARCS code sequence. Over the past few years, within the framework of the ORION project, IRSN has worked on the coupling between the lattice code DRAGON5 and the full-core simulation code PARCS. Initially, efforts have been placed on the validation of the SPH technique in accordance with the traditional strategy used in France for PWR. This work aims to improve the flexibility of the code sequence by adding an alternative method for the assembly homogenization technique, based on discontinuity factors.

The first part of the document is focused on the lattice calculation, and the impact of different strategies envisaged for the generation of ADF. With this in mind, various lattice schemes have been evaluated following the approaches currently adopted by IRSN and by the EPM. The first method, historically used at IRSN, consists in a single level scheme based on the collision probabilities method. Then a state of the art design, recently developed by the EPM is also considered; it corresponds to a two-level approach (Pij/MOC).

The impact of the cross sections and discontinuity factors generated were assessed on simplified PWR motifs and compared to a reference Monte Carlo calculation using SERPENT2. The validation exercise was first performed on 2x2 and 3x3 clusters composed of three types of assemblies: UOX, UOX with AIC control rods and MOX. The study focuses on three parameters of particular interest: reactivity, assembly power, and reconstructed pin power, which are expected to be highly sensitive to the discontinuity factors. Afterward, a more realistic problem is considered by including a reflector region. This task is achieved by the specific development of a reflector model, based on the methodology proposed by Koebke.

In conclusion, this research demonstrates the significant impact of the discontinuity factors on the evaluated configurations. The extent of the amelioration varies according to the case: up to 600 pcm in reactivity and 8% in assembly power. Furthermore, the positive influence has also been assessed in the reconstruction process. At the end of the study, it appears that the two-level calculation scheme is the most reliable design compared with the Monte Carlo reference. For each configuration tested, the best combination of options was identified. Moreover, a good accuracy of the DRAGON/PARCS code sequence is observed for PWR motifs containing a neutron reflector. Finally, significant differences observed for the configuration UOX-MOX suggest further study on the treatment of MOX fuel assemblies by the lattice code; the limit of the infinite-lattice approximation, which does not take into

account the environmental effects, are pronounced at the UOX-MOX interface.

TABLE OF CONTENTS

LIST OF TABLES

LIST OF FIGURES

LIST OF APPENDICES

CHAPTER 1 INTRODUCTION

1.1 Context

The Institut de Radioprotection et de Sûreté Nucléaire (IRSN) is the technical support of French Nuclear Safety Authority (ASN) regarding nuclear plant safety and radiological risk. As an embedded sub-structure, the Service de Neutronique et des Risques de Criticité (SNC) represents the part of IRSN devoted to expertise and Research and Development (R&D) in the criticality safety and reactor physics domain. The Laboratoire d'expertise et de Recherche en Neutronique des Reacteurs (LNR), a component of SNC, is in charge of expertise and R&D in neutronic of nuclear reactors. Since 2012, IRSN has been working on a R&D project called ORION dedicated to the optimization and improvement of computational tools and skills relative to neutronic deterministic simulations[1].

The aim is to refine the tools currently in use for Pressurized Water Reactors (PWR) simulations to perform independent assessment regarding criticality safety and general reactor physics activities. The reason that drives this renew of the deterministic computational tools derives mainly from three aspects:

- the needs of a flexible tool able to adjust to different models and approximations;
- the improvement of independent cross-checking capabilities;
- a wider opening to the international reactor physics community to guarantee the state-of-the-art knowledge and know how.

Given that a direct reactor simulation is not feasible due to the high complexity and time computation, a neutronic deterministic calculation is generally performed through three distinct and separate stages: evaluation and gathering of nuclear data, assembly calculation, and full-core calculation. The focus of the ORION project is dedicated to the latter two steps of the reactor "calculation scheme". In this context, the project is related to knowledge acquisition on criticality and reactor physics that can be adopted as new standards for IRSN safety assessment. Another project carried on by LNR, called INSIDER, is dedicated to the first stage of the neutronic calculation, and their work focuses on the evaluation of nuclear data uncertainties. In order to find suitable software to work alongside the traditional tools used at IRSN to perform complete reactor simulations, several options from different sources are currently in use and under analysis.

Concerning the assembly calculation, historically IRSN has been using the lattice code APOLLO2[2] developed by the Commissariat à l'Energie Atomique (CEA) for criticality safety and reactor physics applications. As an alternative software alongside APOLLO2, two lattice codes are currently in use and under investigations at LNR: DRAGON (Version 4 and 5) from École Polytechnique de Montréal (EPM)[3] and CASMO5 from Studvisk, Inc[4]. DRAGON5 is employed under an LGPL license, and it presents the significant interest of being developed for an academic purpose and being built in a way to facilitate the implementation of new calculation techniques. However, the high flexibility meets with a low validation process and optimization of computation time. CASMO5 on the other side is an industrial code, widely validated and widespread for lattice calculation worldwide. However, the high cost and primarily the proprietary aspect, make it unattractive for a R&D purpose and is principally employed as an independent reference tool.

CRONOS2[5], another software supplied by CEA, is historically used to execute the full-core simulation. The available alternatives considered are DONJON5/TRIVAC[3], the corresponding code of DRAGON5 for full-core calculation, and PARCS[6] developed by the University of Michigan (previously Purdue University) with the financing of US NRC (the United States Nuclear Regulatory Commission). DONJON5 and TRIVAC present the same technical advantages and disadvantages of DRAGON5, LGPL license, high flexibility but a limited validation process. PARCS is a free license code firstly developed for academic purposes now operate under the aegis of US NRC. It is widely adopted, especially by safety organizations like the German GRS (Gesellschaft fur Anlagen- und Reaktorscerheit). Thanks to a bilateral collaboration between IRSN and NRC, IRSN holds the license for use, and has access to the source code. The primary challenge is then to accomplish the coupling between different codes through the development of original tools that can guarantee this capability. In the aftermath of this, the prospects that have been investigated are presented in the following framework (Figure 1.1):

In conclusion, the practical objectives that ORION project is trying to pursue concerning PWR reactor physics applications are:

- performing assembly and full-core calculation with the neutronic deterministic tools previously introduced, to estimate the parameters applied directly for safety assessments;
- carrying out the validation of these newly developed schemes through reference results and experiments, giving priority to international benchmarks and benefit from a broad experience and knowledge.

Both these goals will lead to the creation and development of new means capable of maintaining

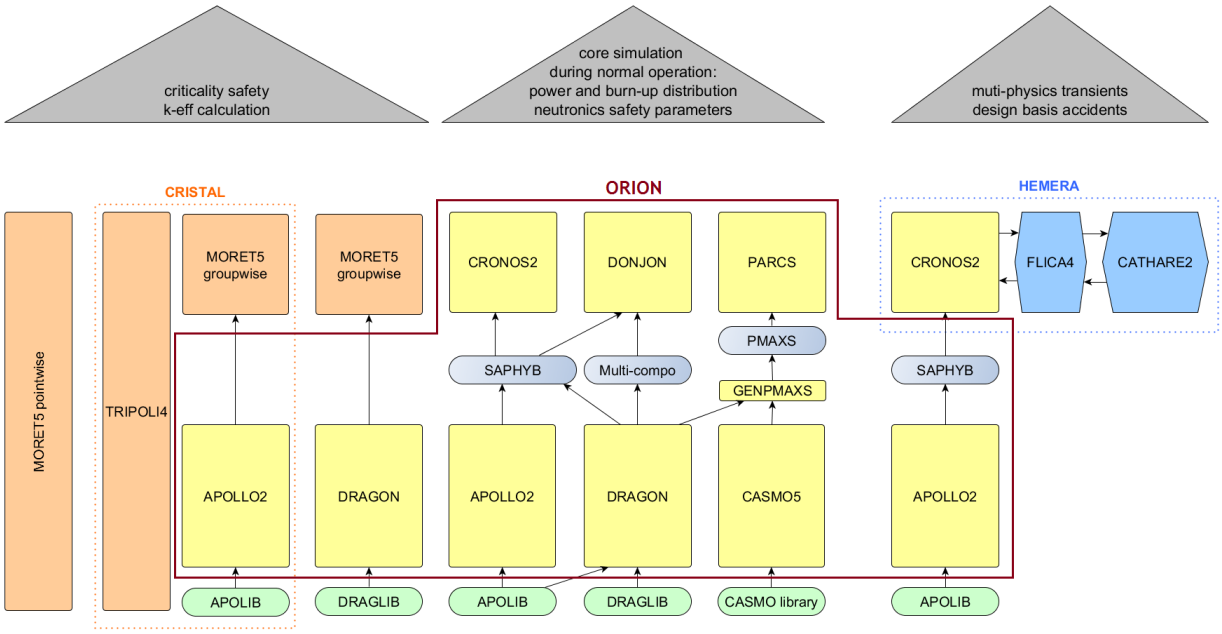

Figure 1.1 Neutronic codes considered for the ORION project and their possible coupling. The relationship with other IRSN projects is also shown.

the IRSN up-to-date with respect to the future modernization of industrial codes.

1.2 Objective of the Thesis

A central issue that must be taken into account in the implementation of a calculation scheme is the flux of information between the lattice and the core code (Figure 1.2).

In fact, to be able to perform a full reactor calculation, a spatial homogenization of cross sections needs to be considered at the end of the assembly calculation to generate the database of information required in the latter step. This database consists of macroscopic cross sections and other homogenized parameters that describe the piecewise homogenized model of the entire reactor. The primary aspects that have to be analyzed during this process:

- the homogenization technique employed to create the reactor database;
- the information required by the full-core code compared to the output generated by the lattice code, and the format in which this information is stored.

For PWR, two approaches are generally considered to perform the complete reactor calculation:

- pin-cell homogenization;

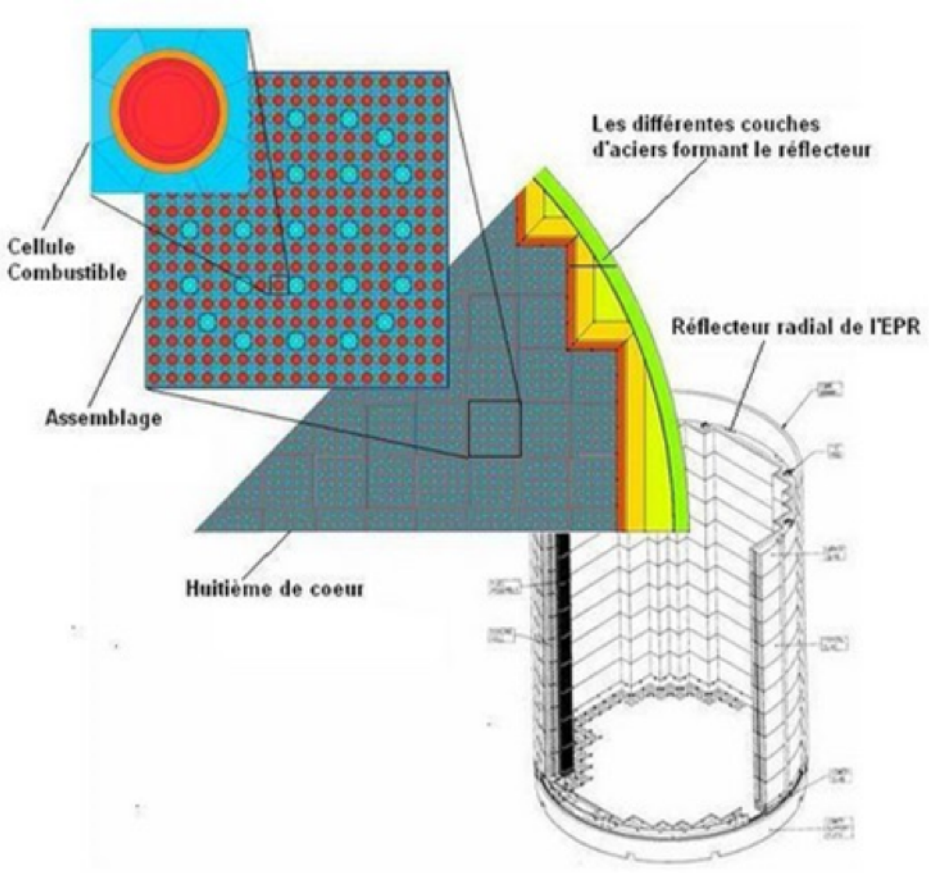

Figure 1.2 Review of the calculation steps usually considered in an LWR reactor nuclear simulation.

- assembly homogenization.

The first one relies on a reactor database built on the nuclear properties gained from the homogenization of each distinct pin-cell (fuel surrounded by coolant). The latter uses homogeneous nuclear properties that are defined for the whole assembly.

The present work is devoted to the implementation of the flux of information between the lattice code DRAGON5 and the full-core simulation tool PARCS, and to perform diffusion calculation using the homogenized assembly parameters produced during the lattice calculation according to the General Equivalence Theory (GET)[7]. The coupling of DRAGON5-PARCS is a unique capability under development at IRSN to address reactor criticality and safety issues. DRAGON5 indeed is suited to perform the *superhomogénéisation* (SPH) equivalence technique[8], which includes the correction of the homogenized cross sections directly inside the code after the transport calculation. However, currently, DRAGON5 is not able to generate

the homogenized parameters required to implement the direct use of the GET equivalence technique using Assembly Discontinuity Factor (ADF). The purpose of the study has been to validate a calculation scheme between DRAGON5 and PARCS, through the modeling of a single assembly calculation to generate homogenized parameters; for this reason, the environmental effects have not been taken into account, and all the lattice calculation are performed in infinite lattice approximation.

1.3 Content of the Thesis

The first part of the research is dedicated to the validation of several lattice schemes for single assembly calculation with the purpose of maintaining consistency with the work currently performed both at IRSN and at EPM, and furthermore to highlight the sources of discrepancies that can be expected in the full-core calculation. The EPM has been working for several years to the implementation of up to date lattice schemes to be used with DRAGON5, focusing in particular on the development of an efficient two-level calculation scheme[9, 10]. IRSN on the other side is currently working on the transposition of qualified APOLLO2 calculation into DRAGON5 and is looking towards recent developments for lattice simulations. Hence, following the recent improvements in the geometry module of DRAGON5, different lattice schemes have been considered to generate the nuclear reactor database for full-core calculations. Following the single assembly calculation, the central aspect of the project has been to validate the generation of the cross-sections database required to perform nodal core calculation according to GET theory. The simulations were carried out on multiple simplified reactor configurations. Besides, following the recent work of Chambon[11], the pin power reconstruction implemented by the nodal solver PARCS has been investigated. The final part deals with a configuration derived from a widely used benchmark[12], already used for a similar purpose[13]. Since at the time of this project, a model for the reflector region was under development, several possibilities have been investigated and are synthetically described. The result both of lattice calculation and the core calculations are validated using the Monte Carlo code SERPENT2[14].

CHAPTER 2 OVERVIEW OF THE HOMOGENIZATION PROBLEMATIC

This chapter is dedicated to the presentation of the main topic of this research project. Since this work is not devoted to an original theoretical approach toward the reactor analysis, we decided to avoid the specification of the legacy models that are usually implemented in a reactor simulation, principally to reduce the extent of the thesis. A comprehensive and detailed description of the majority of the methods used in the study can be found in the references[15, 16, 17].

2.1 Introduction of a Calculation Scheme

As a result of the dimension and heterogeneities that constitute a nuclear reactor, it is not feasible to perform a complete and exact simulation in a reasonable computation time. A calculation scheme represents the ensemble of approximations and models that are employed to simplify the issue of the simulation of a complete reactor, which ensure the required accuracy in an acceptable computing time. For a PWR it is possible to identify three main levels that characterized the calculation scheme[17]:

- nuclear data evaluation;
- lattice calculation;
- full-core calculation.

First, the data that emerge from nuclear measurement are properly evaluated and then collected in a database described in a peculiar format (ENDF, JEFF, JENDL, etc.). Then a cross-section processing code (NJOY, AMPX, etc.) is used to process this data and to produce an isotopic cross-section library that is going to feed the lattice code. Two main operations are performed during the treatment of raw data: the grouping of data in energy groups (around a few hundred) and the tabulation of the parameters required for resonant absorptions. The second level corresponds to the simulation of a limited part of the core (usually of the dimension of an assembly) with approximate boundary conditions. Since the actual environment about this element is not known, typically a reflective boundary condition is chosen in order to re-create a simplified representation of the reactor where the calculation geometry repeats itself to infinity. This system is called infinite regular lattice. The lattice is a 2-D structure where the mesh elements are fictitious cell structure assumed to be axially infinite; in turn, each cell is subdivided into volumes that might be discretized with a finer

mesh (a fuel cell, for example, is divided into at least three volume elements: fuel, cladding, and associated moderator). To partially correct this strong approximation and to ensure that the neutron flux is stationary, a leakage model based on the heterogeneous or homogeneous B_n theory is usually applied. The lattice calculation is performed for several combinations of parameters (for example burnup, temperature/density of fuel, temperature/density of the moderator, boron concentration) solving the steady state transport equation over the infinite domain. Finally, the full-core calculation is accomplished by solving a simplified transport equation (generally diffusion or simplified P_n equation) over the whole reactor using few energy groups (generally two). The data that feeds this last simulation are recovered from so-called reactor database (MULTICOMPO, SAPHYB, etc.) where are stored the condensed and homogenized information evaluated in the lattice calculation. The homogenization can be done over each cell (cell-by-cell homogenization) or the full assembly (complete assembly homogenization). The latter has the advantage to allow the use of numerical methods with large mesh elements (finite elements or nodal methods) that are more economical regarding the computational time. The full-core calculation can be performed in transient or steady-state condition and produce neutron flux and reaction rates over the whole assembly.

2.2 Homogenization Theory

The idea of homogenization is to replace heterogeneous components with homogeneous ones to reduce the computation time of large and complicated systems[8]. The homogenized problem is also solved using a lower order operator (derived as an asymptotic limit of the exact one) to eliminate some of the variables of the original problem. Since it is not feasible to preserve all the details of the heterogeneous calculation, the purpose of the computation of a homogenized system is to obtain accurate global averaged values representative of the exact original system. Bear in mind the loss of information, a choice has to be made to define the reference averaged values to be preserved by the homogenization.

A first problem regards the definition of the reference problem which as to be close as possible to the solution that would be obtained in the case the heterogeneous system would be exactly evaluated. As mentioned before, the common idea is to divide the heterogeneous system into representative components and to perform the homogenization in these restricted reference problems; however this procedure leads to an inaccurate reproduction of the boundary values that would be obtained in the complete heterogeneous system. To amend this practical approximation, a basic principle proposed by Selengut is usually employed: the homogeneous components are constructed in the way that if substituted in place of the heterogeneous component in the exact system, they would not modify the global solution.

Two common homogenization technique are currently in use for PWR reactors: super homogenization equivalence (SPH) and General Equivalence Theory (GET). The first one was firstly developed for the Pin-By-Pin homogenization problem and includes the correction directly inside the homogenized cross sections after the transport calculation. The GET instead was firstly established to be applied for an assembly homogenization approach and is characterized by introducing discontinuity coefficients on the surface of the homogenized component to preserve flux boundary values of the heterogeneous problem.

2.2.1 Transport-Diffusion Equivalence

In order to highlight the problematic that arises from spatial homogenization, let's assume we know the exact steady-state solution of the multigroup transport equation over the complete reactor domain[7]. Let's refer to it as the heterogenous or reference solution for the whole domain.

A contracted group dependent form of the neutron balance transport equation for the heterogeneous problem is given by:

$$\vec{\nabla} \cdot \vec{J}_g^* (\vec{r}) + \Sigma_g^* (\vec{r}) \phi_g^* (\vec{r}) = Q_g^* (\vec{r}) \tag{2.1}$$

where

$\phi_g^* \left(\vec{r}, \vec{\Omega}\right)$ is the *group-averaged angular flux*

$\phi_g^* (\vec{r}) = \int \phi_g^* \left(\vec{r}, \vec{\Omega}\right) d^2\Omega$ is the *group-averaged integrated flux*;

$\vec{J}_g^* (\vec{r}) = \int \vec{\Omega} \cdot \phi_g^* \left(\vec{r}, \vec{\Omega}\right) d^2\Omega$ is the *group-averaged neutron current*;

$\Sigma_g^* (\vec{r})$ is the macroscopic total cross section;

$Q_g^* (\vec{r})$ is the neutronic source density.

A first step in the definition of a homogenization process is to choose reactors properties that should be reproduced by the homogeneous problem; only the preservation of the spatial integrals of quantities of interest is considered. Usually, the most relevant quantities are:

- averaged group reaction rates;
- surface-averaged group current;
- reactor eigenvalue.

To highlight the definition of those quantities of interest, let's consider the balance equation for the homogenized model of the reactor. It can be written as:

$$\vec{\nabla} \cdot \tilde{\vec{J}}_g(\vec{r}) + \tilde{\Sigma}_g \tilde{\phi}_g(\vec{r}) = \tilde{Q}_g(\vec{r}) \tag{2.2}$$

Let's remark that we denote with "*" the solution of the exact heterogeneous problem and with "˜" the correspondant homogeneous problem.

For every energy group g and each cross section, according to the preservation of the spatial integrals of quantities of interest, the following relations need to be satisfied:

$$\int_{V_i} \tilde{\Sigma}_g \tilde{\phi}_g(\vec{r}) d^3r = \int_{V_i} \Sigma_g^*(\vec{r}) \phi_g^*(\vec{r}) d^3r \tag{2.3}$$

$$\int_{S_i^k} \vec{\nabla} \cdot \tilde{\vec{J}}_g(\vec{r}) d^2S = \int_{S_i^k} \vec{\nabla} \cdot \vec{J}_g^*(\vec{r}) d^2S \tag{2.4}$$

where

V_i is the volume of the i-th homogenized region.

S_i^k is the limiting surface of the volume V_i.

The previous equations correspond respectively to the preservation of the average-group reaction rate (Eq. 2.3) and surface-averaged group current (Eq.2.4). The preservation of the reactor eigenvalue is instead ensured by the relation:

$$k_{eff}^* = \tilde{k}_{eff} \tag{2.5}$$

It should be emphasized that if the first two equations are satisfied (Eqs. 2.3 and 2.4), the latter is automatically fulfilled (Eq. 2.5).

So if the homogenized parameters are assumed to be spatially constant, an *ideal* homogenized cross section can be defined by the first of the previous relations (Eq. 2.3):

$$\tilde{\Sigma}_g^i = \frac{\int_{V_i} \Sigma_g^*(\vec{r}) \phi_g^*(\vec{r}) d^3r}{\int_{V_i} \tilde{\phi}_g(\vec{r}) d^3r}. \tag{2.6}$$

The preservation of the integrated surface current instead depends on the low-order operator chosen to simplify the homogenized system. Since only the diffusion approximation is considered for the full-core calculation with PARCS, this case will be presented.

If the Fick law is assumed to define a heuristic relation between the neutron current and the

gradient of the flux[16]

$$\tilde{\vec{J}}_g(\vec{r}) = -\tilde{D}_g \vec{\nabla} \tilde{\phi}_g(\vec{r}) \tag{2.7}$$

it follows that:

$$\tilde{D}_g^i = \frac{-\int_{S_i^k} \vec{J}_g^*(\vec{r})\, d^2S}{\int_{S_i^k} \vec{\nabla} \tilde{\phi}_g(\vec{r})\, d^2S} \tag{2.8}$$

where $\tilde{D}_g^i$ is the group-averaged diffusion coefficient for region i.

From the previous relation, it can be observed that nonlinearity is introduced since both the solution of the exact problem and the homogenized system must be known to satisfy Eqs. (2.6) and (2.8). Then an issue needs to be addressed in the definition of the homogenized diffusion coefficient of Eq. (2.8). Since each node is characterized by many surfaces of indices k, the diffusion coefficients need to be defined, and it is impossible to determine a unique spatially constant parameter that preserves both the average reaction rate and the surface-averaged group current.

2.2.2 Direct Homogenization

To overcome the first problem, the most common employed practice has been to obtain the exact solution by solving a 2-D heterogeneous transport equation on a limited part of the exact system (the assembly to be homogenized), assuming an infinite lattice calculation by imposing reflective boundary conditions (net current equal to 0).

Since all the details are represented in the lattice calculation, the only approximation regards the boundary conditions. Furthermore, if the average value of the homogeneous flux is replaced by the heterogeneous one, the homogenized total cross sections are simply defined as a flux-volume averaged of the heterogeneous ones:

$$\tilde{\Sigma}_g^{\,i,\infty} = \frac{\int_{V_i} \Sigma_g^*(\vec{r})\, \phi_g^*(\vec{r})\, d^3r}{\int_{V_i} \phi_g^*(\vec{r})\, d^3r}. \tag{2.9}$$

and the diffusion coefficient as:

$$\tilde{D}_g^{i,\infty} = \frac{-\int_{S_i^k} \vec{J}_g^*(\vec{r})\, d^2S}{\int_{S_i^k} \vec{\nabla} \phi_g^*(\vec{r})\, d^2S} \tag{2.10}$$

where "∞" stand for infinite lattice approximation.

The reaction rates of an infinite lattice are strictly preserved by the previous relations Eqs. (2.9) and (2.10). However, this method appears to be particularly inaccurate when the real environment surrounding the studied assembly cannot be represented assuming close boundary

conditions. In fact, this method is particularly inaccurate when large spatial flux gradients are generated at the interface of different nodes, due to the use of spatially-constant diffusion coefficients that are unable to solve the problem of preservation of surface-integrated currents.

2.2.3 Beyond Direct Homogenization

One of the major limits of the direct homogenization is the inaccurate approximation of the leakage term that arises from the use of spatially constant diffusion constants that are unable to solve the problem of preservation of surface integrated currents.

In order to exploit the difficulties in the determination of proper diffusion coefficients, let's consider a 1-D monoenergetic reactor and let's suppose the heterogeneous flux distribution of the exact problem; only nodes i and $i+1$ will be presented (Figure 2.1[7]).

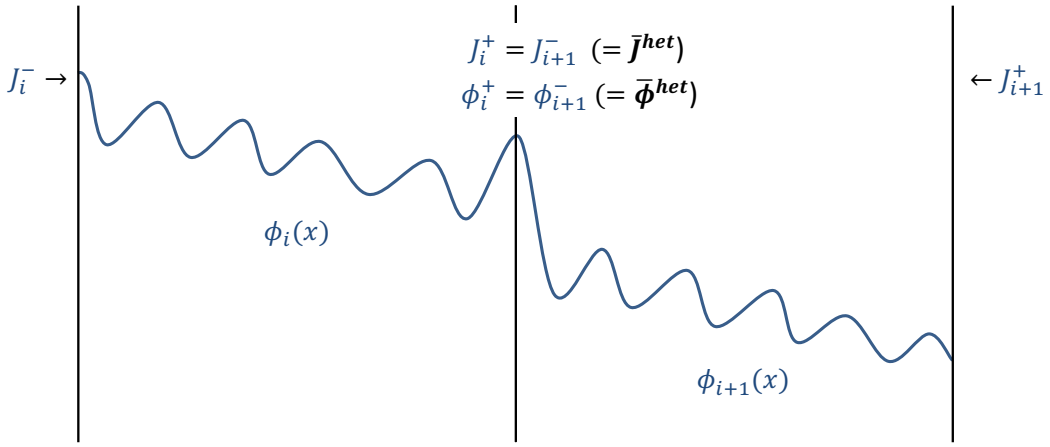

Figure 2.1 Heterogeneous flux distribution of a 1-D reactor (two nodes considered).

The heterogeneous solution allows the calculation of the *exact* homogenized cross sections and conventional diffusion coefficients; the homogenized parameters are evaluated through a flux-volume weighting, and it can be underlined that it does not correspond to a standard homogenization evaluated with an infinite-medium approximation (the exact heterogeneous solution is known). Using the *exact* homogenized parameters and imposing the averaged heterogeneous surface currents at the boundaries of the node, it is possible to solve the diffusion equation on a homogenized system for each single separated node. A unique solution can be calculated for the homogenized flux for a problem of this kind that preserved the averaged surface current (Figure 2.2[7]).

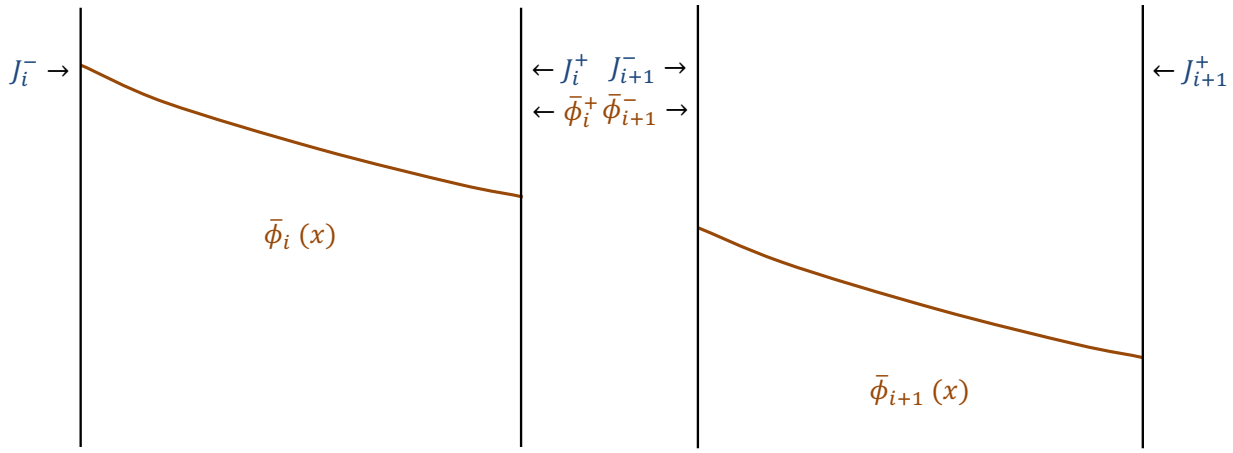

Figure 2.2 Homogeneous flux distribution in each node evaluated using exact homogenized parameters and the imposition of exact average current at the boundaries.

When the homogenized flux distributions assessed for each separate node are compared, almost for sure, it will be observed that the two fluxes will be different (Figure 2.3[7]) even if the exact surface current have been imposed. This discrepancy is due to the fact that the definition of the diffusion coefficient with a flux weighting approximation is arbitrary, and it affects directly the homogenized flux distribution.

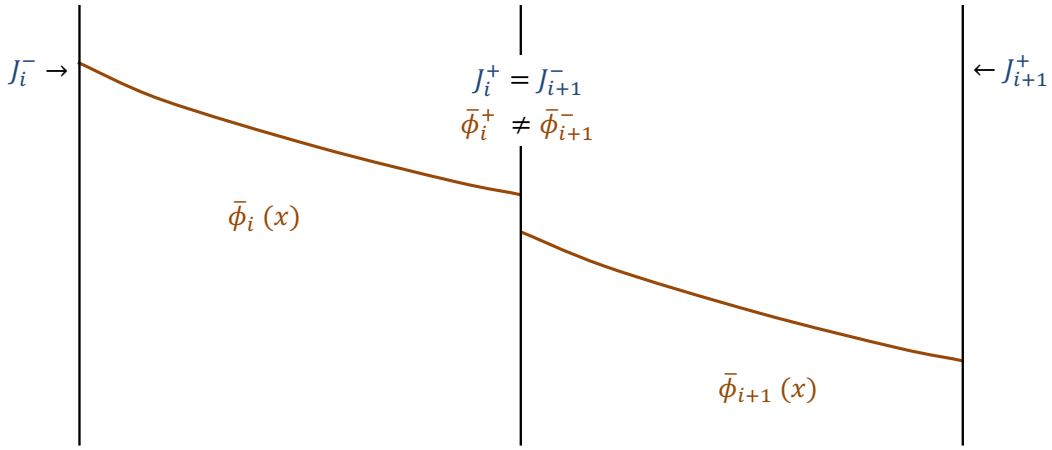

Figure 2.3 Comparison of the homogenized flux distibutions obtained from single node problems with exact boundary conditions. The surface flux is discontinuous.

A further case can be considered where the constraint of the imposed surface currents at the interface of the two nodes are relaxed, and the homogenized problem is solved with exact

surface current at the external boundaries but only the continuity of fluxes and currents at the interface of the nodes (Figure 2.4[7]).

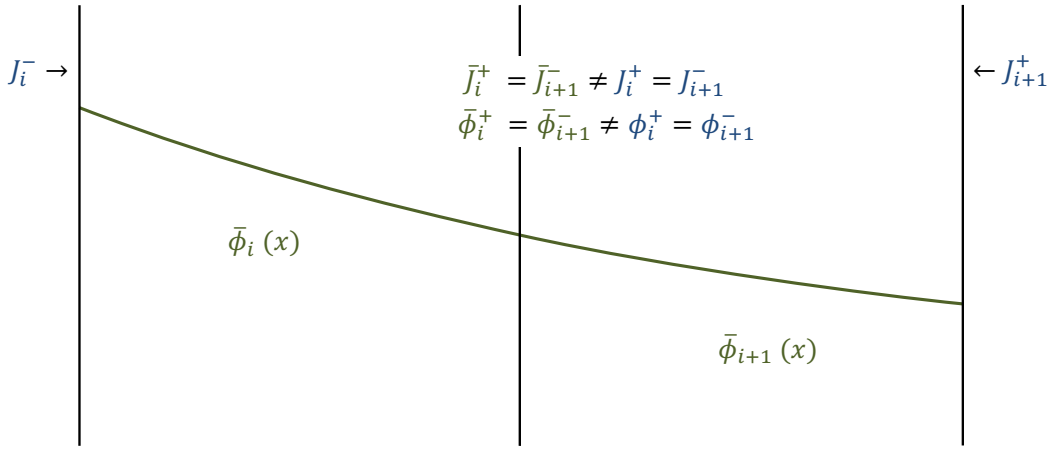

Figure 2.4 The homogeneous flux distribution is obtained assuming the continuity of flux and current at the interface between nodes. Neither the exact flux or the exact current will be preserved.

The result will be a homogenized flux distribution different compared to the heterogeneous one and furthermore, the averaged current will not be preserved at the interfaces. This assessment is valid for whatever diffusion coefficient employed. From the previous examples it can be concluded that the limit for the preservation of the surface currents is the continuity of flux at the interface of the nodes and does not originate from the diffusion coefficient. The conclusion from this simplified case problem is that the continuity of flux at the interfaces is a limit for the diffusion calculation both to preserve reaction rates and surface current from heterogenous calculation.

2.2.4 General Equivalence Theory

The General Equivalence Theory (GET) proposed by Smith [7], suggests the introduction of an additional degree of freedom to account for the preservation of the surface current. It provides discontinuity factors at each surface of the node in order to relax the continuity of fluxes and preserve both average reaction rates and net currents from the heterogeneous system. A new interface condition for each energy group is then defined to ensure the continuity of the homogeneous flux between adjacent nodes:

$$f_{g,j}^{+} \int_{S_j} \tilde{\phi}_g^{+}(\vec{r}) d^2S = f_{g,j}^{-} \int_{S_j} \tilde{\phi}_g^{-}(\vec{r}) d^2S \tag{2.11}$$

Where $f^+_{g,j}$ and $f^-_{g,j}$ are the energy-dependent discontinuity factors at the surface S_j, $\tilde{\phi}^+_g$ and $\tilde{\phi}^-_g$ the surface average homogeneous fluxes, respectively. This relation assures the preservation of both reaction rates and net currents from heterogeneous reactor problems, by stating that the heterogeneous flux is continuous at the interface.

Assembly Discontinuity Factor

To evaluate the discontinuity factors, the knowledge of the heterogeneous solution is required; in GET, this problem is circumvented by solving the heterogeneous problem on a representative colorset in order to take into account the environmental effect for a particular configuration of assemblies. This approach allows the computation of very accurate homogenized parameters but not practical to use: each combination of assemblies in the colorset must be treated separately and each time it requires an expensive calculation.

In the case where the heterogeneous solution is evaluated on a single assembly with reflective boundary conditions, the homogenized cross sections and diffusion coefficients prove to be equivalent to the flux-volume weighted one. Since the homogeneous flux can be assumed to be spatially flat in the homogenized node, and since the average heterogeneous flux and the averaged homogeneous flux are equal by definition, a new expression can be obtained:

$$\mathrm{adf}_{g,j} = \frac{\phi^*_{g,j}}{\bar{\phi}_{g,j}} \tag{2.12}$$

where $\mathrm{adf}_{g,j}$ is the assembly discontinuity factor (ADF) for each group and each surface of the node. This approach reduces the computational time and limits the calculation of equivalence parameters to each different type of assembly. However, it introduces large homogenization errors when the composition of the core is highly heterogeneous; in fact, the environmental effect is strongly approximated and appears to be inaccurate when there is significant leakage across nodal interfaces.

In this project, only the approximation of ADF has been considered to treat the homogenization problematic.

2.2.5 Dehomogenization

Once the nodal calculation is performed, a reconstruction process is needed to regenerate the actual heterogenous structure inside each node. This procedure is usually called dehomogenization. The detailed description of the method implemented in PARCS is presented in the theory manual[18]. The output from the nodal flux solution is employed together with

so called form functions to assure a proper reconstruction of the heterogenous power inside each node. Group Form Fuction (GFF) are computed from lattice calculation, considering the same approximation of ADF concerning the infinite lattice approximation. The GFF are groupwise factors defined as a function of the pincell fission rates as:

$$f_g(x,y) = \frac{\kappa\bar{\Sigma}_{fg}\varphi_g(x,y)}{\kappa\bar{\Sigma}_{fg}\bar{\varphi}_g} \tag{2.13}$$

where $\kappa\bar{\Sigma}_{fg}$ is the macroscopic fission cross section of the fuel in group g multiplied by the energy produced by fission. Due to the pin power reconstruction methodology, so called *Corner Discontinuity Factors* (CDF) also needs to be obtain to account for the local heterogeneities at the interface between assemblies. They are defined similarly to the ADFs, with the flux recovered at the corner of the assembly:

$$\mathrm{cdf}_{g,j} = \frac{\phi^*_{g,j,corner}}{\bar{\phi}_{g,j}} \tag{2.14}$$

2.2.6 SPH Equivalence Procedure

At the end of this presentation, it is also interesting to describe the method employed for the SPH equivalence procedure when full assembly homogenization is performed. This is the technique currently adopted by IRSN.

As mentioned before, the Super homogenization methodology was first developed to correct the direct homogenization procedure by introducing a renormalization of the cross sections in order to guaranty the reaction rate conservation. It was first proposed by Kavenoky[19] and subsequently implemented in DRAGON5 by Hebert et al. [20, 21] through several algorithms for the transport-transport and transport-diffusion equivalence. The heterogeneous solution is obtained from a single assembly calculation with reflective boundary conditions and a critical leakage model as in the direct homogenization method. Similar to what presented for the equivalence between transport and diffusion calculation, to account for the non-linearity observed for the conservation of average heterogenous quantity, an iterative process is usually defined to compute homogenized cross sections. Starting from the flux-volume averaged cross section (as defined in the direct homogenization approximation) the iterative procedure is applied through the implementation of the following relation; for each macroregion M and macro energy-group g for which the homogeneous domain is discretized:

$$\tilde{\Sigma}^M_{\rho,g} = \mu^M_g \tilde{\Sigma}^{M,\infty}_{\rho,g} \tag{2.15}$$

where

μ_g^M is the group SPH factor;

$\tilde{\Sigma}_{\rho,g}^M$ is the corrected group homogenized cross section for reaction ρ;

$\tilde{\Sigma}_{\rho,g}^{M,\infty}$ is the group homogenized cross section for reaction ρ.

However, for conservative boundary conditions (net current equal to zero), a degenerate non-linear problem is defined, and an infinite number of solutions are admitted. A supplementary constraint needs to be considered to obtain a unique solution, as the conservation of the assembly average heterogeneous flux. In this particular case of interest, when of a full assembly homogenization ($M = 1$) is considered, the total reaction rate is preserved regardless the value of the SPH factor.

However, a condition that provides the conservation of assembly average flux generates a set of SPH factor equal to unity, corresponding to a solution equivalent to the direct homogenization approximation. A more meaningful choice is to drop the average flux normalization, and to consider a different condition called Selengut's normalization: it involves the correction of the cross sections in order to preserve the global heterogeneous partial current. This approach can be implemented by assuming that the homogenized assembly average flux can be expressed by the relation[8]:

$$\bar{\tilde{\phi}}_g = 4J_g^{\pm} \tag{2.16}$$

where

$\bar{\tilde{\phi}}_g$ is the homogenized assembly averaged flux;

$J_g^{\pm}$ is the heterogeneous partial current averaged over the surface of the assembly.

From the preservation of the reaction rates, the homogenized cross section can then be defined as:

$$\tilde{\Sigma}_g = \frac{\tau_g}{4J_g^{\pm}} \tag{2.17}$$

with τ_g the assembly heterogeneous group reaction rate. Subsequently, if we assume the linear anisotropic flux approximation at the surface of the assembly, for perfectly reflective boundary conditions we can express the SPH factor using the following non-iterative relation:

$$\mu_{g,Selengut}^{M=1} = \frac{\bar{\phi^*}_g}{\phi_{g,surface}^*} \tag{2.18}$$

where $\phi^*_{g,surface} = 4J^{\pm}_g$ is the average heterogeneous surface flux. $\mu^{M=1}_{g,Selengut}$ is the SPH factor computed through the Selengut's normalization.

It should be remarked that the previous expression corresponds just to the inverse of an ADF:

$$\mu^{M=1}_{g,Selengut} = \frac{1}{adf_g} \tag{2.19}$$

Furthermore, it has been demonstrated that for full assembly homogenization, performed with infinite-lattice approximation, the SPH formulation is equivalent to the ADF formulation, under the two following conditions[13]:

- a mesh-centered finite difference formulation is employed to discretize the diffusion equation, and
- the ADFs are equal on each side of each assembly.

CHAPTER 3 IMPACT OF THE LATTICE CALCULATION ON THE GENERATION OF HOMOGENIZED PARAMETERS

In this chapter, we give a brief description of the models that we implemented in the lattice calculation and the methodology applied for the generation of the nuclear reactor database.

3.1 PWR Configurations

A realistic assembly of a French PWR 900 MW has been examined for the research.
The layout has been designed in the attempt to build a PWR in which a portion of the UOX fuel is substituted by a MOX fuel, characterized by an equivalent fission content. The assembly is disposed as a square of 17x17 pins, composed of 264 fuel pins, 1 instrument tube and 24 guide tubes, which can be interchanged with absorber rods (Figure 3.1).
Two kinds of cladding compositions are contemplated for the different elements inside the assembly: *zircalloy4* is employed for the fuel pins while stainless steel has been adopted for the cladding around the control rods. It should be remarked that the gas gap is not explicitly discretized but diluted inside the metal mixture; however, for the instrument tube, pure *zircalloy4* is used. Furthermore, the grid has been diluted in the moderator generating five different compositions related to the position within the fuel assembly (center, lateral, and corner, inside/outside the tube). The internal guide tube is filled with pure water, without dilution. Concerning the dimensions, "hot values" has been used; actually, DRAGON5 does not take into account the thermal expansion of the materials during the computation. The same criterion has been applied for the reference calculation with SERPENT2.

The study has been carried on by considering two types of fuel: UOX and MOX; moreover, a configuration of UOX with "black" control rods has been investigated (24 control rods inserted). For the whole study, the boron concentration has been assumed equal to zero.

3.1.1 UOX

For the UOX assembly (UX), an enrichment of 3.7 % (wt) of ^{235}U is assumed, and the concentration of other fissile isotopes is considered almost negligible. The density of the UOX pellet has been chosen according to the enrichment. As previously mentioned, in the absence of absorber rods, the guide tubes are designed analogously as the instrument tube: the internal region is filled with pure water while the external moderator includes the diluted grid.

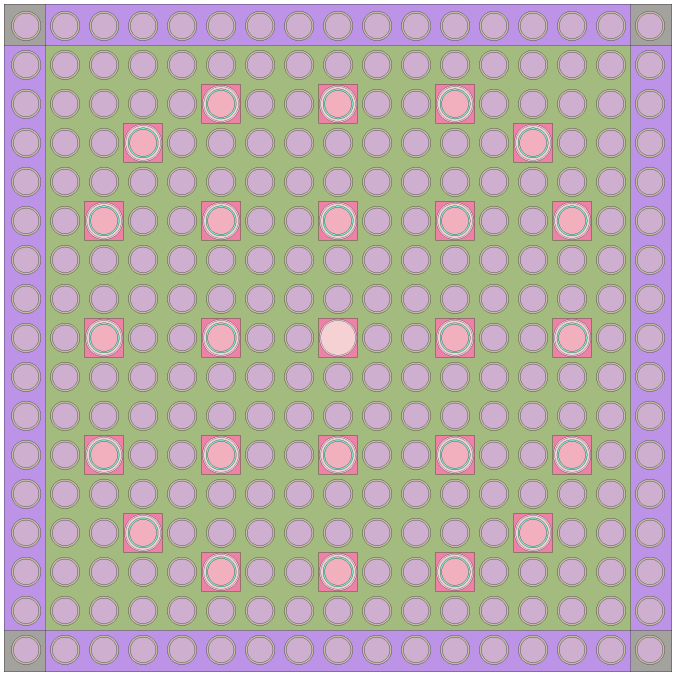

Figure 3.1 PWR configuration for an UOX fuel assembly with absorber rods (geometry output from SERPENT2 computation). In the picture are highlight the mixtures implemeted in the design of the geometry.

3.1.2 UOX with AIC

For the UOX assembly with absorber rods (UA), so-called "black" AIC control rods has been considered for the project. AIC is a metal mixture composed of Silver, Indium, and Cadmium. It is a conventional absorber adopted in nuclear reactors design due to its capacity to withstand long irradiation times; one of the main advantages is that it does not undergo (n,α) reactions that may induce the swelling of the pin. As discussed in a previous study [22], mainly four isotopes have a practical impact on the absorption property of the metal mixture, as shown in Table 3.1[22].

Table 3.1 Percentages of total absorption for the main isotopes of AIC metal mixture.

	Total Absorption Portion (%)
^{107}Ag	16.4
^{109}Ag	36.2
^{115}In	25.5
^{113}Cd	20.7
$Others$	1.2

Furthermore, these isotopes exhibit important nuclear properties that justify their interest for

nuclear safety applications; the absorption macroscopic cross section of these four isotopes covers the entire neutron spectrum [22]. The disadvantage lies in the resonant structure of Silver (^{107}Ag and ^{109}Ag) and Indium (^{115}In) that requires a careful treatment. Consequently, a proper self-shielding procedure needs to be adopted.

3.1.3 MOX

The MOX assembly has been designed to be equivalent to a UOX assembly enriched with 3.7 % (wt) of ^{235}U. As shown in (Figure 3.2), the geometry is arranged with a three-zone Pu-content structure, where the content of Pu increases from the center towards the corner:

- High content of Pu in the central zone (**green**);
- Medium content of Pu in the intermediate zone (**amaranth**);
- Low content of Pu in the corner zone (**blue**).

3.2 Lattice Schemes

The validation of several lattice schemes utilized for the production of the nuclear reactor database allows us to introduce the investigation of the sources of inaccuracy that can be expected in the diffusion calculation. Concerning the lattice computation with DRAGON5, different calculation options are considered based on the work currently performed at IRSN and EPM.

Currently, IRSN is employing an assembly scheme based on the CEA-97 single level approach proposed by CEA[23], whereas at EPM, a two-level computation design based on the REL2005 by CEA[24] has been promoted over the last years. Since the concepts behind the different schemes have been already discussed in other works[9, 10, 23, 24, 25], in the following chapter, we propose just a summary of the principal characteristics that we implemented for the design of our lattice calculations with DRAGON5. Considering the flexibility of DRAGON5, certain modifications of the original schemes have been adopted to examine the impact of various approaches in the creation of the multi-parameter cross-section database.

The multigroup neutron library used for the calculations is a DRAGLIB format library, based on the *Jeff 3.1.1* nuclear data evaluation. The energy mesh employed is the SHEM295 energy mesh: it is based on the 281-groupoup Santamarina Hfaiedh Energy Mesh (SHEM)[26] and the refined 361-groupoup energy mesh (SHEM361) proposed by Hébert and Santamarina[27]. This energy mesh represents an optimization of the original SHEM structure to allow the

use of the subgroup projection method (SPM)[28] between 11.14 keV and 4.63 eV, the lower limit for the self-shielding calculation; above this energy range, a statistical approach with physical probability tables (ST) is used. In the CEA-97 scheme recommendation, the use of the original CEA93V7 library in APOLIB format is suggested; however it is not available for the CEA-97 based scheme of IRSN and cannot be implemented in the calculation. This library is designed for the 172-group European XMAS library based on the *Jeff 2.2* evaluation. Due to the compatibility in the validation process, we decided to primarily perform our calculation employing the same SHEM295 library adopted for the Canbakan scheme based on the *Jeff 3.1.1* evaluation. This is also because a corresponding version of the CEA93V7 library is not available for the stochastic computation, and the only alternative, a continuous-energy ACE format data library based on the *Jeff 2.2* nuclear data evaluation, does not present the isotopic re-evaluation made by CEA.

Three options are evaluated concerning the flux calculation and the leakage model: without any leakage model, with a B_1 homogeneous leakage, and with a P_1 homogeneous leakage[15, 16]. The reason is embedded in the impact of the spatial and spectral form of the transport solution in the computation of homogenized parameters, both macroscopic cross sections and the discontinuity factors. As mention in the first chapter, without any leakage model, the eigenvalue to be computed is the effective multiplication factor with a fixed buckling equal to zero. For the other two cases, the eigenvalue is selected from the Monte Carlo calculations performed on the PWR motifs, which will be presented in the next chapters. To accomplish this, the keyword `KEFF` has been used in the leakage model specification structure of the `FLU:` module. Even if the effective multiplication constant is usually fixed to 1.0 for deterministic simulations on critical reactors, we decided to perform a critical buckling search with the k_{eff} recovered from Monte Carlo motif calculations, to be more consistent with the leakage model approximation.
It should be remarked that a critical occurence happens with the B_1 model in some low-reactivity cases[16]. For this reason, in the newest version of DRAGON5, a dynamic correction is performed such that the B_1 model is replaced by the P_1 model if particular subcritical conditions occur. However, this is not the case for our study.

At the end of the calculation, the flux is used to collapse cross sections to two groups (threshold at 0.625 eV), and the homogenization is performed over the whole assembly. The generated nuclear data are then stored in a DRAGON5 data structure of type `MULTICOMPO`; it also contains the information required to compute ADF, CDF, and GFF. It should be noted that the geometry considered is an eight of assembly, specified for the North-East quadrant (Figure 3.2).

At the first stage of the project, the DRAGON5 lattice scheme developed by Vallerent[9] has been employed for the generation of the multi-parameter database; the aim was to retrace the work already performed by Chambon[11] to compute adequate homogenized parameters. However, following the recent improvements in the geometry module of DRAGON5 was envisaged the possibility of defining a windmill-type geometry discretization directly in the code (through the `G2S:` module) without the need of external geometry CAD-software[29]. Moreover, the appeal of using the SHEM295 energy mesh, encouraged us to replace the former calculations with the most up to date lattice scheme validated at EPM by Canbakan[10]. We also wish to emphasize that the task of this study was not the validation of the lattice scheme and the investigation of the inaccuracies observed at the assembly level. Therefore, we relied mostly on previous researches, and we addressed our sensitivities studies only to the calculation choices that we considered of primary relevance in the computation of discontinuity factors. As an example, to reduce the burden of results, we decided not to include some possibilities that we investigated, such as a lattice scheme based on the SHEM281 energy mesh, which was presented at a recent conference[30].

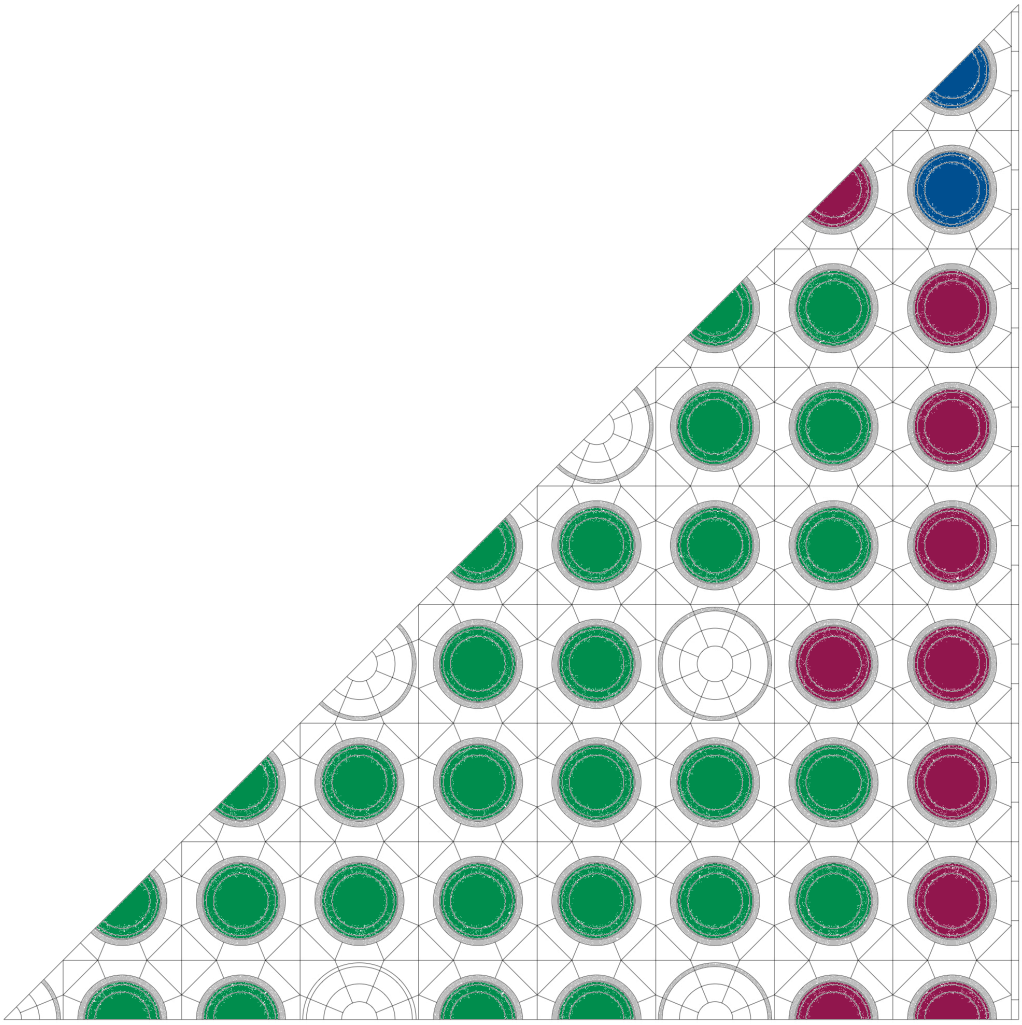

Figure 3.2 Eight of PWR represented with windmill type spatial discretization. The picture highlights the three Pu enrichment of MOX assembly

3.2.1 Canbakan's Schemes

As previously mentioned, recently developments in DRAGON5 led Canbakan to validate a single level and two-level schemes based on the Method of Characteristic (MOC) and optimized for the SHEM295 refined energy mesh[10]. Prior to a further description, we would like to emphasise the motivation that brought to the definition of a multi-level computation method. Since a single level calculation with a detailed energy mesh demands considerable computational time when a fine spatial discretization is required on complicated assembly geometries, this concept has been introduced with the target of reducing the computational cost by dimishing the number of groups employed in the flux calculation. Hence, the flux calculation performed in the initial levels is necessary to compute the weighting-flux for the collapsing of group cross sections to a coarser energy mesh, whereas the main flux calculation represents a compromise between a certain degree of accuracy and an acceptable computational time. Accordigly, a step-by-step description is presented as follow for the two-level and single level scheme.

Two-level Scheme

The resonance self-shielding is performed above 4.63 eV using the SPM subgroup approach implemented in the `USS:` module of DRAGON5[28]; the CALENDF-type mathematical probability tables (without slowing-down correlated weight matrices) are activated with the keyword `PT` in the `LIB:` module. The subgroup equations are solved adopting a double P_1 interface current (IC) calculation, where the linear anisotropic components of the inter-cells current are used. It should be noted that the calculation is implemented with a transport-corrected P_0 scattering source. A coarse spatial mesh geometry is defined through the `GEO:` module, at this stage there is no need for the discretization of the moderator. To take in account the spatial self-shielding, the fuel rods are split in four rings (50 %, 30 %, 15 %, 5 % of the total volume of the pellet); this procedure allows an accurate representation of the resonant absorption of ^{238}U and other isotope inside the pin. Therefore, following the consideration of UOX with AIC, the same discretization is applied for the control rods to account for the resonances in the AIC mixture. A cell grouping assumption is also made to reduce the computational cost: this means that cells with similar fluxes are merged into a so-called physical cells and evaluated together. The cell grouping is performed considering eleven types of physical cells and applied for the three configurations considered in this study. In particular, eight kinds of physical cells are envisaged for the fuel, one for each assembly ring of control rods (or guide tubes) and one for the instrument tube. A flux-current iterative technique (keyword `ARM`) is also adopted to speed up the calculation due to the high number

of physical cells considered in the grouping.

The self-shielded cross sections are then used for the first-level double-P_1 IC flux calculation that is performed over a 295-energy group energy mesh library. A coarse spatial mesh similar to the one employed for the self-shielding is considered; only an additional ring in the moderator is designed for the fuel pins. At this stage no grouping is considered, and each pin is treated separately. Subsequently, the fine-group flux is used to collapse the cross section from 295-energy groups to 26-energy groups without any spatial homogenization; the number of mixture is expanded to account for the finer spatial discretization of the following calculation. An SPH equivalence procedure can then be performed in order to collapse the cross sections. In fact this equivalence procedure can account for the loss of accuracy caused by the condensation process.

The collapsed cross sections are then used to carry out the 26-groupoup flux calculation using the Method Of Characteristic (MOC) on the refined spatial 2-D geometry. The weighting flux computed in the previous steps is used as a starting point and it is expected to allow a faster convergence of the MOC calculation. As mentioned before, following the developments in the `G2S:` module of DRAGON5[29], it is now possible to generate a windmill-type spatial discretization (Figure 3.2) for the detailed MOC calculation without the use of an external software. This optimized mesh is used to properly take account of the spatial distribution of the thermal flux shape in each fuel cell. We chose to mantain the same tracking parameter in the `SALT:` module as the one employed by Canbakan for the validation of the scheme. In particular, the trajectories are characterized by a tracking option `TSPC 8 20.0` that defines respectively the angular parameter and the density of the integration lines.

The geometries employed in the different steps of the calculation scheme are presented in Figure 3.3. A resume of the two-level scheme is displayed in Figure 3.4.

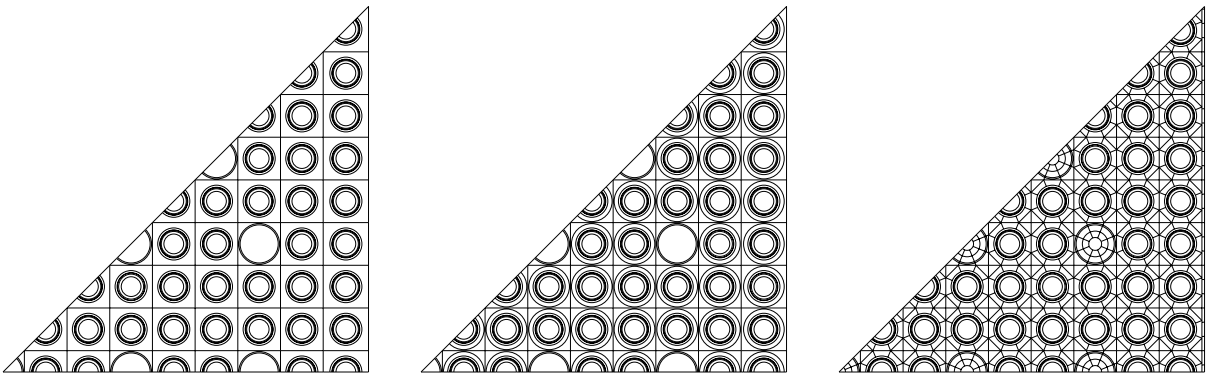

Figure 3.3 Overview of the geometries employed in the different step of the two-level scheme.

Single Level Scheme

The single level scheme is performed without an intermediate flux calculation to compute the weighting-flux for the condensation to a coarser energy mesh. Following the resonance self-shielding calculation, a direct MOC calculation on a fine spatial mesh is conducted using the 295 energy groups self-shielded library. The same windmill-type discretization employed for the MOC calculation of the two-level scheme is adopted. Although similar, it should be remarked that few modifications have been applied with respect to the previous scheme. Since the expansion of the media is not performed after the intermediate energy condensation, the same number of media is employed both for the self-shielding and the main flux calculation. As in the original Canbakan single level scheme, a third-order Legendre polynomial expansion accounts for the scattering anisotropy. Furthermore, we decided to tighten the trajectories for the MOC calculation and to increase the number of the angular quadrature parameter, as considered in previous reference calculations.

3.2.2 *DRAGOR-V1* Scheme

The lattice scheme currently in use at IRSN in the frame of the ORION project, called *DRAGOR-V1*, was designed for the 172-groupoup European XMAS library based on the *Jeff 2.2* evaluation, as suggested in the CEA-97 scheme recommendation[23]. However, the scheme has been adapted such that the SHEM295 library based on the *Jeff 3.1.1* evaluation is considered both for the flux and the self-shielding calculation. The spatial mesh is characterized by a simple discretization, without any subdivision of the moderator in the pin cell.

The resonance self-shielding calculation is performed using the statistical subgroup approach implemented in the module `USS:`, as presented in [16]. This model makes use of physical probability tables for the whole energy domain, activated with the keyword `SUBG`. As in the Canbakan's scheme, the subgroup equations are solved using a double P_1 IC method. The spatial discretization adopted for the self-shielding retrace the method adopted for the Canbakan's schemes. However, no particular discretization is considered for the control rods, and a different grouping of physical cells is considered. For the UOX assembly, the Dancoff effect, originated by the vicinity of the fuel pins with the guide tubes, is taken into account defining three types of physical cells. The guide tubes are considered separately, and an additional physical cell has been designed for the control rods. For the MOX case, six physical cells are defined to follow the three-zone enrichment disposition. Also in this case, due to the low number of physical cells involved, the self-shielding calculation is performed using an iterative procedure (keyword `ARM`) to save computational time. The flux calculation is finally performed on the self-shielded cross sections using a double P_1 IC method, activated through

the keyword DP01; it makes use of a linear anisotropic approach, as recommended by CEA-97. The spatial discretization for the pins is the same adopted for self-shielded calculation, while no grouping is applied, and each pin is treated separately.

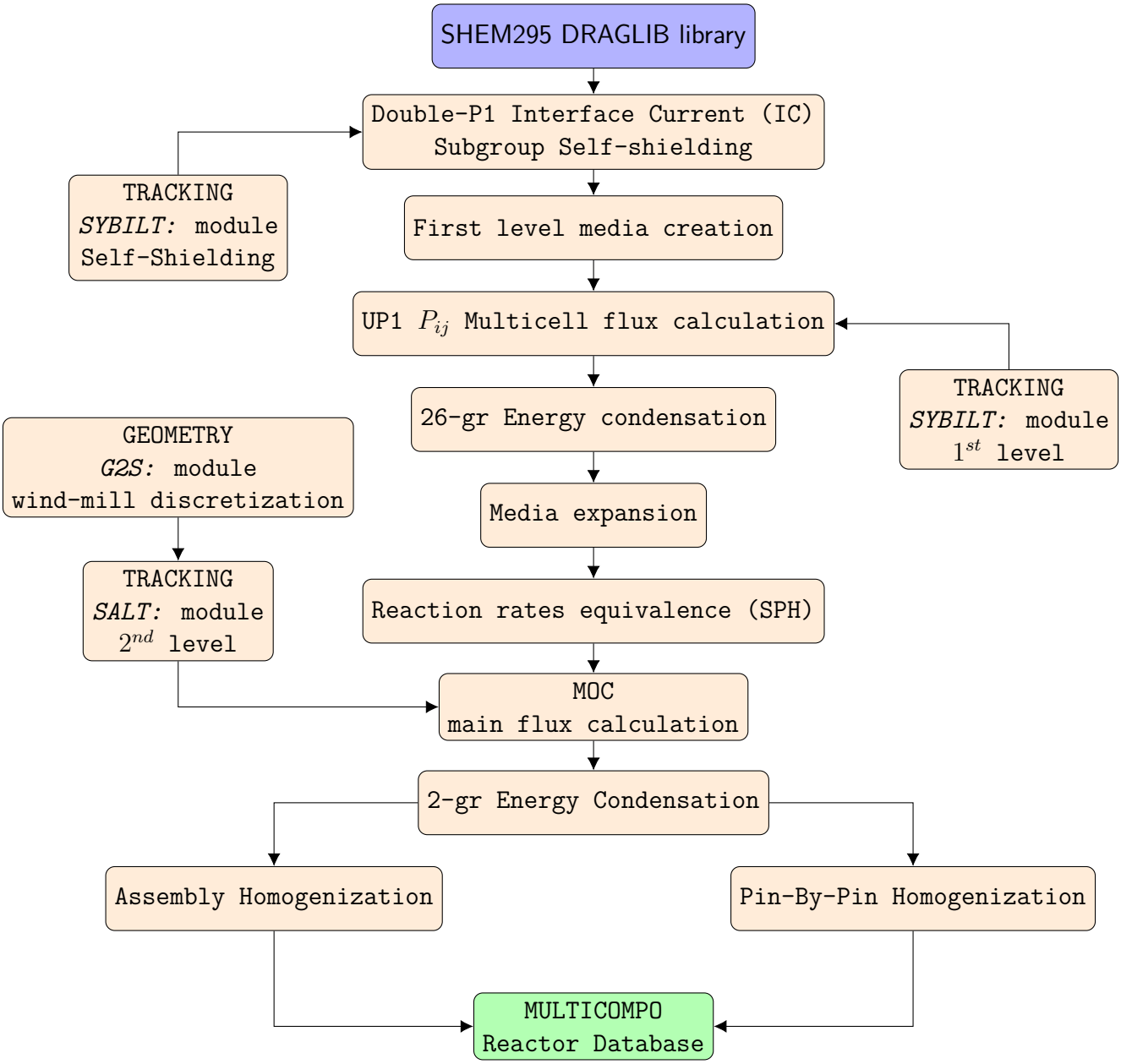

Figure 3.4 Representation of the two-level Canbakan scheme.

3.2.3 Reference Calculation

Regarding the SERPENT2 input file, the cross section library adopted is a continuous-energy ACE format data library based on the *Jeff 3.1.1* nuclear data evaluation. We opted to design the assembly geometry using the lattice option card `lat`, to facilitate the definition of the detectors, hence the assessment of the quantities employed for the comparison and to save computational time. Indeed, the detectors are scored inside each cell of the lattice for each defined material. Furthermore, the water gap surrounding the assembly is explicitly designed through rectangular and square cells, to account for the different compositions of the moderator due to the grid dilution (Figure 3.1). The simulations with SERPENT2 have been performed with 2000 cycles of 1500000 source neutron each.

3.3 Validation

In this paragraph, we present the method that we adopted for the validation and the analysis of the lattice schemes previously presented.

3.3.1 Canbakan's Validation

The validation process is based on the comparison between the lattice code DRAGON5 and the stochastic reference SERPENT2. To investigate the accuracy of the assembly calculation we consider the so-called Canbakan validation process, an academic exercise proposed in [10] and [25] to verify the accuracy of a DRAGON5 lattice scheme. The comparisons are performed by considering no leakage model. The Canbakan's validation relies on several variables that allow the study of the system from a macroscopic and microscopic perspective.

Reactivity

The multiplication factor is defined as the ratio between the production rate of new fission neutrons over the sum of absorption and leakage rates; it provides an estimate of the evolution of the neutron population between two generation of neutrons and allows the evaluation of the deviation from critical conditions.

For each type of fuel assembly, and for each lattice scheme, we first compare the effective multiplication factor and the difference in reactivity (in *pcm*), evaluated as:

$$\Delta\rho = \left(\frac{1}{k_{eff}(S2)} - \frac{1}{k_{eff}(D5)}\right) \cdot 10^5 \tag{3.1}$$

where $k_{eff}(S2)$ and $k_{eff}(D5)$ are the effective multiplication factors of SERPENT2 and DRAGON5.

Reaction Rate

For each type of nuclear reaction x, the group reaction rate can be evaluated as the number of interactions per unit of time and energy group g in a region i of the spatial domain. It can be defined as the product of the group macroscopic cross section $\Sigma^g_{x,i}$, measured in cm^{-1}, and the group volume-integrated flux ϕ^g_i, measured in $\mathrm{cm\,s}^{-1}$. It follows that the total reaction rate is the sum of the group reaction rate for all energy group g and for all the region i that compose the domain. For each energy group g and region i , the group reaction rate for nuclear reaction of type x is defined as:

$$\mathcal{T}^g_i = \Sigma^g_{x,i}\phi^g_i \tag{3.2}$$

In the Canbakan's validation, two nuclear reactions are considered of particular relevance in the analysis of the accuracy: the isotopic group absorption (fission+capture) reaction rate and the total pin fission reaction rate. To conduct the comparison, both of these quantities are normalized to the total fission rate of DRAGON5 so that the relative and absolute differences are estimated as:

$$\Delta r = \left(\frac{\tau_{D5} - \tau_{S2}}{\tau_{S2}}\right) \cdot 100 \tag{3.3}$$

$$\Delta a = (\tau_{D5} - \tau_{S2}) \cdot 10^5 \tag{3.4}$$

where τ_{D5} and τ_{S2} are the integrated reaction rate obtained with DRAGON5 and SERPENT2.

Regarding the absorption rate, the approach is to analyze the isotopic group absorption rate inside the fuel for the whole assembly. Particularly, in our study, we decide to present only the isotopes ^{235}U and ^{238}U for the UOX and UA case, while we add the three principal isotopes of Pu for the MOX one. For a general comparison of all the lattice schemes implemented, a 2-group energy discretization is adopted. However, when single level designs are employed is it possible and more accurate to consider a 13-group energy discretization for the validation process, as presented by Canbakan [25].

The limitation of using a more detail discretization rely on the fact that the 26-group energy mesh does not fit the 13-group structure proposed by Canbakan since several groups are merged during the intermediary condensation procedure. Furthermore, an attempt we made to define a compatible 9-group structure has proved unsuccessful and was abandoned due to the large discrepancies that arose in the 2-level schemes. The fission rate is instead characterized

by its evaluation over each pin and by the sum of the contribution to each group. An eight of assembly chart is presented containing the relative total pin fission rate discrepancies between DRAGON5 and SERPENT2. This representation is appealing because it allows an initial evaluation of the GFFs, required for the pin power reconstruction.

3.3.2 DRAGON5-SERPENT2

The validation is conducted by evaluating separately the result of the lattice schemes proposed for each fuel assembly. A unique table containing the reactivity accuracy is presented for all the cases while for the isotopic absorption rate and the fission reaction map, a separate table is considered for each distinct case. Before moving forward, it should be remarked that the prime objective of our lattice validation has been to test our calculation scheme by trying to reproduce the results presented by Canbakan in his validation effort[10]. We should mention that except few pathological values a good agreement has been observed for the configurations assessed in his work. We did not investigate the observed discrepancies beyond the scope of this study.

UX

Starting from the analysis of the accuracy in reactivity displayed in Table 3.2, small differences are observed in both the Canbakan's schemes with respect to the reference value, even though of opposite sign. The scheme from Orion project behaves slightly worst and presents a gap around 150 *pcm* compared to the SERPENT2 computation.

Table 3.2 k_{eff} and reactivity [*pcm*] for the different fuel assemblies. In parentheses the associated relative statistical error from the Monte Carlo calculation.

	UX		**UA**		**MX**	
	k_∞	$\Delta\rho$	k_∞	$\Delta\rho$	k_∞	$\Delta\rho$
Serpent2	1.38206	(±3)	0.92482	(±4)	1.16319	(±3)
Canb 2-lvl SPH	1.38128	-41	0.92639	183	1.16115	-151
Canb 1-lvl	1.38294	46	0.92808	380	1.16467	109
DRAGOR-V1 1lvl	1.38489	148	0.92249	-274	1.16649	243

The isotopic absorption rate is then presented in Table 3.3. The *DRAGOR-V1* scheme shows the closest result for ^{235}U, due to a balanced compensation of effects between the two groups, while it manifests the absolute highest discrepancy for ^{238}U, almost completely in the fast domain. On the other hand, despite a close agreement in the thermal domain, the two designs introduced by Canbakan differ significantly with regard to the fast absorption rate; the single level scheme displays significantly high deviations, particularly for the ^{238}U (above 150 *pcm*).

Table 3.3 Absorption rate accuracy for UX assembly.

		U235		U238	
	Group	**Δr**	**Δa**	**Δr**	**Δa**
Canb 2-lvl SPH	*1*	0.1	11.4	-0.3	-70.1
	2	0.1	59.2	0.1	3.4
	tot		70.7		-66.7
Canb 1-lvl	*1*	-0.3	-30.4	-0.7	-157.1
	2	0.1	65.1	0.1	3.8
	tot		34.8		-153.3
DRAGOR-V1 1lvl	*1*	-0.4	-53.7	-0.8	-185.5
	2	0.1	44.6	0.0	0.0
	tot		-9.1		-185.5

Finally, the fission rate map (Figure 3.5) outline a significant duality in the lattice schemes proposed. The Canbakan schemes, both single and double level, exhibit an evident closeness, with identical root mean square errors and a slight variation in the maximum deviance. The option from IRSN displays a remarkable gap with respect to the other calculation options, with several pins that present a discrepancy in fission rate above 1%. Particularly, the higher errors are located in the corner region of the assembly.

UA

For the UOX assembly with AIC control rods, the first element that stands out from the validation is the significant degradation in the fission reaction map (Figure 3.6) for the *DRAGOR-V1* scheme; it gains supplementary relevance if compared to the other options for the lattice calculation. In fact, the fission rate exceeds 4% of deviance from the reference solution for several pins, and the root mean square error almost reach 2%.

A particular mention should be made of the fact that the pins presenting the highest discrepancies in the fission map are located close to the control rods and in the corner of the assembly. The Canbakan schemes display large improvements, with root mean square errors around 0.21%, and maximum error below 0.6%. The single level behaves slightly better with respect to the two-level scheme.

The table presenting the inaccuracy in reactivity (Table 3.2) does not reflect what observed in the fission reaction map, where the Canbakan single level scheme exhibits the absolute higher difference with respect to SERPENT2.

The same unexpected assessment can be made for the isotopic absorption rates of Table 3.4. Despite the previously observed imprecision, the *DRAGOR-V1* scheme displays the lower

	max	min	rms	δ
Canb 2-lvl	0.38	-0.25	0.11	0.63
Canb 1-lvl	0.25	-0.21	0.11	0.46
Orion 1-lvl	1.20	-1.11	0.42	2.31

							0.02 0.08 -0.87
						-0.07 -0.05 1.20	-0.19 -0.11 0.05
					-0.02 -0.08 0.23	-0.08 0.00 1.12	0.02 0.02 0.12
					0.00 -0.15 -0.22	-0.13 -0.02 0.92	0.17 0.21 0.26
				0.21 0.25 -0.68	-0.09 -0.08 -1.11	0.04 -0.03 -0.80	0.09 0.05 0.21	-0.06 0.06 -0.03
				-0.03 -0.07 -0.37	-0.01 -0.10 -0.36		0.12 -0.05 0.03	-0.05 0.06 -0.01
		0.03 0.06 0.11	-0.06 -0.13 -0.19	0.04 0.10 0.07	0.05 0.08 0.00	-0.09 -0.17 -0.19	0.22 0.19 0.46	0.07 0.15 0.10
	0.11 0.14 0.19	0.02 0.07 0.12	-0.02 -0.07 -0.08	0.03 0.07 0.07	-0.02 0.03 0.01	-0.14 -0.21 -0.19	0.14 0.16 0.41	-0.08 0.04 0.02
	-0.05 -0.11 -0.07	-0.11 -0.16 -0.16		-0.12 -0.21 -0.23	-0.08 -0.08 -0.14		0.38 0.17 0.34	-0.25 -0.10 -0.13

Figure 3.5 Relative discrepancies in the fission reaction map in the UX assembly.

discrepancies for both isotopes of Uranium, while the Canbakan single-level one turns out to be the most degraded. Furthermore, all the options present greater inaccuracies in the absorption rate of ^{238}U compared to ^{235}U. A remark should be made concerning the behavior of the designs developed at EPM; while both Canbakan schemes exhibit a similar trend in the thermal region, the single-level scheme results particularly degraded in the higher energy group for both ^{235}U and ^{238}U.

MX

Concerning the fission reaction map (Figure 3.7), compared to the previous configuration, an increase in accuracy can be observed for all the lattice schemes, of particular relevance in the

	max	min	rms	δ
Canb 2-lvl	0.58	-0.36	0.21	0.94
Canb 1-lvl	0.55	-0.33	0.17	0.88
Orion 1-lvl	4.61	-4.01	1.93	8.62

							0.25 0.00 **-4.01**
						0.11 -0.04 -1.68	0.06 -0.04 -2.91
					-0.27 -0.12 0.04	-0.01 0.07 -1.11	0.01 0.05 -2.65
					0.00 0.17 0.61	-0.01 0.02 -0.89	-0.01 -0.04 -2.53
				-0.18 -0.14 **4.61**	-0.01 0.18 **4.15**	-0.05 0.18 2.73	-0.25 -0.11 0.52	-0.18 -0.11 -2.20
				0.24 0.27 2.30	0.58 0.55 2.29		0.11 0.06 0.21	0.22 0.13 -2.27
		-0.13 -0.09 1.64	0.40 0.29 1.51	-0.25 -0.15 2.28	-0.05 -0.04 2.36	0.27 0.27 1.25	-0.28 -0.23 0.46	0.01 -0.07 -2.18
	-0.34 -0.21 -1.41	-0.36 -0.31 0.88	0.21 0.06 1.19	-0.20 -0.24 2.11	-0.28 -0.33 2.03	0.15 0.13 1.11	-0.20 -0.13 0.59	-0.03 -0.10 -2.21
	-0.19 -0.06 -2.06	-0.10 -0.16 0.35		0.28 0.06 1.66	0.25 0.12 1.68		0.12 -0.08 0.11	0.30 0.16 -2.35

Figure 3.6 Relative discrepancies in the fission reaction map in the UA assembly.

DRAGOR-V1 scheme; the root means square drops widely and approaches 1% of deviation. However, the latter design still display high errors accumulated in the corner pin (negative peak of 4.65%), where in this case the Pu concentration is lower. The Canbakan schemes exhibit once more an almost identical behavior, with a root mean square below 0.2% and an absolute maximum error that does not exceed 0.4%.

As previously mentioned, in the Table 3.5 containing the isotopic absorption rates, the main isotopes of Plutonium are analyzed. It is interesting to observe the dual behavior of the Canbakan's schemes concerning the different isotopes. While the single level option keeps manifesting a significative degradation in the fast energy domain for both isotopes of Uranium, the two-level scheme shows the most unfavorable outcome in the same domain for ^{239}Pu, ^{240}Pu, and ^{241}Pu. In this configuration, the Orion's design displays the worst result, and

Table 3.4 Absorption rate accuracy for UA assembly.

		U235		U238	
	Group	**Δr**	**Δa**	**Δr**	**Δa**
Canb 2-lvl SPH	*1*	-0.2	-22.1	-0.6	-147.0
	2	0.3	92.8	0.2	8.2
	tot		70.6		-138.7
Canb 1-lvl	*1*	-0.7	-77.6	-1.2	-261.8
	2	0.3	109.1	0.3	9.8
	tot		31.5		-252.0
DRAGOR-V1 1lvl	*1*	0.0	1.2	-0.4	-82.4
	2	0.0	-14.0	-0.1	-4.0
	tot		-12.7		-86.4

particular attention should be given to the absorption rate of ^{238}U and ^{240}Pu in the fast region.

Finally, the reactivity exhibits a similar trend for the Canbakan's schemes, as observed for the UOX case. At the same time, the *DRAGOR-V1* scheme reveals again the most degraded result.

Table 3.5 Absorption rate accuracy for MX assembly.

		U235		U238		Pu239		Pu240		Pu241	
	Group	**Δr**	**Δa**	**Δr**	**Δa**	**Δr**	**Δa**	**Δr**	**Δa**	**Δr**	**Δa**
Canb 2-lvl SPH	*1*	0.1	0.3	-0.1	-20.5	0.5	67.0	0.7	25.8	0.7	25.8
	2	0.8	3.5	0.6	5.5	-0.1	-28.9	0.1	4.3	0.1	4.3
	tot		3.8		-15.0		38.1		30.1		30.1
Canb 1-lvl	*1*	-0.7	-3.8	-0.8	-156.8	-0.1	-12.0	0.0	-0.5	0.0	-0.5
	2	1.2	5.8	1.0	9.5	0.1	21.3	0.5	21.8	0.5	21.8
	tot		1.9		-147.3		9.3		21.3		21.3
Orion 1-lvl	*1*	-0.9	-5.0	-0.9	-183.8	-0.5	-60.4	-0.8	-93.3	-0.2	-6.8
	2	0.8	3.9	0.6	5.5	0.0	16.7	0.4	11.2	0.5	21.2
	tot		-1.1		-178.2		-43.7		-82.2		14.4

3.4 Sensitivity Study

To have a better understanding of the discrepancies previously observed, a deeper study of several elements of the calculation schemes has been conducted. Not to burden the discussion concerning the calculation options, we opted to avoid the representation of explicit fission reaction map, and to condensed the outcome in a summary table (Table 3.7) composed mainly of the root mean square error and the absolute maximum gap with respect to the SERPENT2 reference. Furthermore, we include several results in the appendices, which go beyond the actual objectives of this chapter.

	max	min	rms	δ
Canb 2-lvl	0.33	-0.37	0.17	0.70
Canb 1-lvl	0.34	-0.38	0.18	0.73
Orion 1-lvl	2.28	-4.65	1.07	6.94

							-0.09 -0.09 **-4.65**
						-0.18 -0.32 0.71	-0.28 -0.15 -2.21
					-0.03 0.08 0.76	-0.37 -0.16 1.66	-0.20 -0.02 -1.23
					0.20 -0.04 1.24	-0.05 -0.07 2.28	0.06 0.06 -0.37
				0.15 0.30 -1.66	-0.04 0.13 -0.98	-0.15 -0.12 -1.11	-0.09 0.12 -0.10	0.14 0.29 -0.88
				0.11 -0.04 0.58	-0.13 -0.38 0.74		0.06 -0.10 0.29	-0.29 -0.24 -1.00
		0.33 0.29 0.02	0.00 -0.21 0.53	0.12 0.26 0.20	0.19 0.20 0.14	-0.01 -0.09 0.74	0.11 0.16 0.03	-0.08 0.00 -1.00
	0.31 0.34 -0.09	0.07 0.14 -0.19	0.09 -0.08 0.59	0.18 0.22 0.03	0.30 0.32 0.19	-0.15 -0.29 0.57	-0.19 0.06 -0.23	0.10 0.21 -0.77
	-0.04 -0.28 0.35	0.20 0.01 0.55		0.05 -0.14 0.61	-0.26 -0.24 0.57		0.20 -0.10 0.10	-0.25 -0.11 -0.95

Figure 3.7 Relative discrepancies in the fission reaction map in the MX assembly.

The analysis of the nuclear data evaluation adopted for the calculation is firstly examined as a possibile explanation for the deterioration of the fission reaction map of the *DRAGOR-V1* scheme. It must be emphasised that an exhaustive research of the source of discrepancies goes beyond the scope of this work. Nevertheless, during the initial stage of this research project, the spatial discretization had been pointed out as the primary source of inaccuracies. A conclusion from a report at IRSN was that the absence of a refined spatial mesh leads to a wrong evaluation of the flux distribution inside the moderator of the fuel pins. In fact, it can be assumed that the sectoritation of the moderator reproduce the correct non-uniform distribution of flux while a single zone discretization depicts a homogenized distribution surrounding the fuel rod, with a complete loss of the orientation. As an example, this phenomenon should be amplified by the presence of a strong absorber, as the AIC rods, since

it can be expected that higher values of the thermal flux are localized as far as possible from the absorber. More specifically, a higher value of the thermal population is facing the interface between the fuel pin and the absorber, and as a consequence, a higher value of neutrons is moving towards the absorber with respect to the reference value (following the idea that the flux is smaller in the central part of the assembly where the control rods are, and increases towards the sides). Since the absorption is higher, a lower value of multiplication factor is observed. The windmill type spatial mesh has been built to shape better the behavior of the flux in the fuel pin.

Other options that we examined are evaluated only for the Canbakan two-level scheme. It is the most promising tool for the industrial application, and it represents a good compromise between accuracy and required CPU time. Notably, two choices have been evaluated regarding the 26-group equivalence and the tracking option employed at the boundary of the assembly; we considered them as of primary influence in the computation of the homogenized parameters.

Finally, even if we dedicated the majority of the project in the implementation of the Vallerent calculation scheme[9], we decide to avoid the description of a design that appears quite obsolete in comparison to the Canbakan's scheme, because of a not optimized spatial discretization of the moderator in the fuel pins, that affect the computational time strongly. We should mention that the significant degradation of the fission reaction map has been observed for the rodded case with the spatial discretization of the moderator implemented by Vallerent.

3.4.1 Nuclear Data Evaluation

As described in the Orion scheme we decided to employ the draglib SHEM295 based on the *Jeff 3.1.1* evaluation instead of the suggested Cea93v7. The latter is an APOLIB format library based on the *Jeff 2.2* evaluation and designed for the 172-group European XMAS energy mesh. Looking for an improved understanding of the discrepancies observed in the scheme employed by IRSN, we decided to test the draglib XMAS172 based on the *Jeff 3.1.1* evaluation, since it adopts an equivalent energy mesh compared to the Cea93v7.

It should be remarked that for the APOLIB developed by CEA a lack of compatibility would be generated in this test case. In fact, the DRAGON5 procedure developed by IRSN, make use of the information stored in each library implemented in the computation. In particular, the metal mixture adopted for the neutronic simulation are computed using unique values for the mass fraction, while the average atomic masses are estimated using the isotopic masses that are extracted from the nuclear data library. As a consequence, the isotopic concentrations would slightly differ according to the library implemented. This problem is avoided by the use of the same nuclear data evaluation (*Jeff 3.1.1*) with a different energy

mesh structure (XMAS172). Furthermore, an additional compatibility issue would be to recover the continuous-energy ACE format data library correspondent for the Cea93v7, since it derives from the modification of the available *Jeff 2.2* evaluation.

Starting from the comparison of the reactivities (Table 3.6), with respect to the SHEM295, the XMAS172 energy mesh provokes a significative amelioration of the UX and MX accuracy (-80 *pcm* and -200 *pcm* respectively), countered though by a substantial degradation of the rodded assembly ($+200$ *pcm* of absolute difference).

Thereafter, the fission reaction comparison (Table 3.7) exhibits a negligible improvement with the change of library and the huge gap compared to the Canbakan's schemes is barely narrowed. Finally we compared the isotopic absorption discrepancies compared to the SERPENT2 reference. Since the use of a single level approach allows the use of a more detailed group representation of the isotopic absorption rate, it is interesting to juxtapose the 2-group representation (Tables 3.8 and 3.9) with a 13-group one and to analyzed the two variants implemented in the Orion's design with the single level Canbakan scheme. To lighten the presentation the 13-group tables are included in the appendices together with the 13-group energy mesh considered (Appendix A). Taking into account the outcome from the two energy representations, the central element that emerges is the significative compensation of effects displayed by the XMAS energy mesh library along the 13-group structure. While with the 2-group representation an overall improvement compared to the SHEM295 seems to be asserted, the detailed 13-group isotopic absorption rates exhibit the profound discrepancies that occur for certain isotopes and group; the final balance derives from the mutual adjusting of large gaps among energy group. These differences can exceed 200 *pcm*.

Concerning the 13-group structure, a more detailed analysis of the discrepancies should be performed but is way beyond the purpose of this chapter and the study. However, even if it is not possible to point out a clear source of errors, the easiest remark is to relate this phenomenon to the particular choice of the energy mesh employed for the lattice calculation. In conclusion, there in no advantage to consider a change of library to account for the large degradation observed in the previous validation process.

3.4.2 SPH

In the REL2005 recommendations, it has been observed that the SPH equivalence performed after the 26-group condensation in the two-level scheme leads to an improvement of the reactivity but at the same time to a deterioration of the spatial reaction rates; they consequently modified the final group energy structure to avoid any equivalence procedure. However, both in the works of Vallerent and Canbakan, the conclusion is that an equivalence SPH correction

is strongly supported by a general improvement of the results.

The comparison of the multiplication factors (Table 3.6) shows a worsening of the result with respect to the reference calculation. The general trend is an underestimation of the reactivity for all the cases, becoming significantly relevant in the configuration of UOX with AIC rods inserted (almost 400 *pcm* compared to the Monte Carlo reference and an absolute difference of 600 *pcm* from the two-level scheme with equivalence). Furthermore, the isotopic absorption rates (Tables 3.8 and 3.9) exhibit an overall degradation generated by the equivalence procedure, except occurrences were the outcome clearly improved, like the absorption of ^{238}U for the rodded assembly. It should be remarked that the SPH equivalence induces a considerable reduction of the absorption rate of ^{238}U. Regarding the fission reaction rates (Table 3.7), from the summary table, a general improvement is observed when the equivalence is performed; only the δ between maximum and minimum is marginally decreased for the UX case.

3.4.3 Tracking MOC

To evaluate the calculation options that can affect the computation of the homogenized parameters, two options for the tracking in the MOC calculation have been considered. The reflective boundary condition can be implemented considering two options in the tracking modules of DRAGON5: reflective specular (`TSPC`) and white (`TISO`). The first case represents a neutron traveling towards the border that when reaches the boundary surface it is sent back as if by a perfect mirror. The latter assumes that the neutron is sent back with an isotropic angular distribution. It should be remarked that in order to activate the `TISO` option in the tracking calculation with DRAGON5, the boundary condition in the geometry module has to be set as `ALBS` card equal to 1.0, since the `REFL` parameter is not working with `SALT:` tracking module.

The specular reflective condition represents the closest representation of the reality of a neutron that strikes the boundary of a 2-D assembly; the white reflection condition is used to save computational time, and it affects mostly the flux calculation in the outer region of the assembly. As a consequence, we assume direct impact on the calculation of the homogenized parameters of interest.

An overall comparison can be made observing the results presented for the sensitivity study (Tables 3.6, 3.7, 3.8 and 3.9). Concerning the outcome of the validation process, it is useful to highlight the two prevailing elements that are peculiar in the comparison between isotropic and specular: the differences in trends between fast and thermal domain concerning the isotopic absorption rate and the distinctive degradation of the rodded fuel assembly when the

TISO card is implemented.

The first remark can be highlight by the analysis of the relative and absolute discrepancies between the two tracking options in the isotopic absorption rate tables (Tables 3.8 and 3.9) with respect to the stochastic reference solution. For nearly all the configurations, the isotropic angular case displays a consistent underestimation of the absorption rate in the fast energy domain that is contrasted by an overestimation in the thermal one. The latter is exposed in the deterioration of the fission reaction map (Table 3.7) for the rodded case, where the root mean square error rise from 0.21 % to more than 0.4 %. A possible interpretation can be found in the relative difference in the flux distribution between the tracking options (Figure 3.8); it derives from the nature of the isotropic angular distribution approximation as regards to the neutron that comes back from the border. As previously suggested by Vallerent[9], the TISO option can be represented ideally by the substitution of all the cylindrical fuel pins of the outer row with an infinite slab of fuels that face the border of the assembly. In this way, the isotropic angular distribution would be an accurate approximation, but a larger amount of fuel would be theoretically assumed in the lateral part of the assembly. Besides, since the isotropic approximation ideally represents a higher volume of fuel and less moderator, the neutron population is slow down less at the border of the assembly.

The effect is displayed in the flux distribution, where the outer pin row presents a marked overestimation of the fast flux, which is compensated by a remarkable underestimation of the thermal flux in the interior region of the assembly. It should be noted that each fuel assembly presents a distinctive behavior: in the UX case, the effect is clearly delineated, while in the other configuration other variables affect this trend. For the rodded case, a peculiar overestimation of the flux can be observed both in the fast and thermal distribution; from the outer control rod towards the corner of the assembly. It can be hypothesised that if the fast flux increases in the peripheral region compared to the specular configuration (Figure 3.8) and a balance distribution is establish in the assembly between the two groups, a smaller portion of the domain is subject to this incrementation with respect to the complementary region, that is facing a higher thermal flux, always with respect to TSPC. As a consequence, an augmentation of the absorption rate should be observed in the thermal domain, compensated by a contraction in the fast energy group.

Regarding the degradation of the rodded case, a possible interpretation could be related to the high absorption that takes place in the central part of the assembly, and the intense neutron currents that are established inside the assembly toward the outermost region from the absorbers. Internal neutron current might be generated with the effect of redistributed the flux in the assembly. However, a proper explanation needs to be found and required a

deeper analysis.

Table 3.6 k_{eff} and reactivity [pcm] for the different fuel assemblies (sensitivity study).

	UX		**UA**		**MX**	
	$\boldsymbol{k_\infty}$	$\boldsymbol{\Delta\rho}$	$\boldsymbol{k_\infty}$	$\boldsymbol{\Delta\rho}$	$\boldsymbol{k_\infty}$	$\boldsymbol{\Delta\rho}$
DRAGOR-V1 1lvl SHEM295	1.38489	148	0.92249	-274	1.16649	243
DRAGOR-V1 1lvl XMAS172	1.38338	69	0.92092	-458	1.16375	41
Canb 2-lvl SPH	1.38128	-41	0.92639	183	1.16115	-151
Canb 2-lvl w/o SPH	1.37907	-157	0.92143	-398	1.15960	-266
Canb 2-lvl SPH TISO	1.38193	-7	0.92721	279	1.16265	-40

Table 3.7 Summary comparison of the fission reaction map (sensitivity study).

	UX			**UA**			**MX**		
	max	***min***	***rms***	***max***	***min***	***rms***	***max***	***min***	***rms***
DRAGOR-V1 1lvl SHEM295	1.20	-1.11	0.42	4.61	-4.01	1.93	2.28	-4.65	1.07
DRAGOR-V1 1lvl XMAS172	1.18	-1.11	0.42	4.60	-3.98	1.92	2.29	-4.75	1.09
Canb 2-lvl SPH	0.38	-0.25	0.11	0.58	-0.36	0.21	0.33	-0.37	0.17
Canb 2-lvl w/o SPH	0.24	-0.21	0.12	0.50	-0.50	0.22	0.37	-0.46	0.18
Canb 2-lvl SPH TISO	0.40	-0.27	0.13	1.13	-0.74	0.42	0.58	-0.63	0.26

Table 3.8 2-gr absorption rate accuracy for UX and UA assemblies (sensitivity study).

		U235		**U238**		**U235**		**U238**	
	Group	$\boldsymbol{\Delta r}$	$\boldsymbol{\Delta a}$	$\boldsymbol{\Delta r}$	$\boldsymbol{\Delta a}$	$\boldsymbol{\Delta r}$	$\boldsymbol{\Delta a}$	$\boldsymbol{\Delta r}$	$\boldsymbol{\Delta a}$
DRAGOR-V1 1lvl SHEM295	*1*	-0.4	-53.7	-0.8	-185.5	0.0	1.2	-0.4	-82.4
	2	0.1	44.6	0.0	0.0	0.0	-14.0	-0.1	-4.0
	tot		-9.1		-185.5		-12.7		-86.4
DRAGOR-V1 1lvl XMAS172	*1*	0.4	46.6	-0.5	-121.8	0.9	98.6	-0.1	-12.0
	2	0.0	1.9	-0.1	-5.0	-0.2	-59.8	-0.3	-9.3
	tot		48.4		-126.8		38.8		-21.3
Canb 2-lvl SPH	*1*	0.1	11.4	-0.3	-70.1	-0.2	-22.1	-0.6	-147.0
	2	0.1	59.2	0.1	3.4	0.3	92.8	0.2	8.2
	tot		70.7		-66.7		70.6		-138.7
Canb 2-lvl w/o SPH	*1*	0.9	105.1	0.4	86.0	0.8	89.3	0.3	66.2
	2	0.0	-12.8	-0.1	-4.8	0.0	-6.3	-0.1	-2.9
	tot		92.2		81.2		83.0		63.3
Canb 2-lvl SPH TISO	*1*	-0.1	-16.4	-0.4	-99.9	-0.5	-58.2	-0.8	-186.4
	2	0.1	66.9	0.1	3.9	0.3	103.7	0.3	9.1
	tot		50.5		-96.0		45.6		-177.3

Table 3.9 2-gr absorption rate accuracy for MX assembly (sensitivity study).

		U235		U238		Pu239		Pu240		Pu241	
	Group	**Δr**	**Δa**	**Δr**	**Δa**	**Δr**	**Δa**	**Δr**	**Δa**	**Δr**	**Δa**
DRAGOR-V1 1lvl SHEM295	*1*	-0.9	-5.0	-0.9	-183.8	-0.5	-60.4	-0.8	-93.3	-0.2	-6.8
	2	0.8	3.9	0.6	5.5	0.0	16.7	0.4	11.2	0.5	21.2
	tot		-1.1		-178.2		-43.7		-82.2		14.4
DRAGOR-V1 1lvl XMAS172	*1*	-0.9	-5.1	-0.3	-61.3	0.2	22.1	0.2	30.8	1.3	44.3
	2	0.3	1.2	0.0	0.3	-0.3	-95.6	-0.2	-5.4	0.0	1.3
	tot		-3.9		-61.0		-73.6		25.4		45.6
Canb 2-lvl SPH	*1*	0.1	0.3	-0.1	-20.5	0.5	67.0	0.3	33.4	0.7	25.8
	2	0.8	3.5	0.6	5.5	-0.1	-28.9	0.2	7.2	0.1	4.3
	tot		3.8		-15.0		38.1		40.6		30.1
Canb 2-lvl w/o SPH	*1*	0.9	5.3	0.5	106.4	1.4	177.9	0.4	48.3	1.8	62.6
	2	0.3	1.4	0.2	1.5	-0.5	-153.1	-0.1	-2.6	-0.4	-16.2
	tot		6.6		107.9		24.7		45.8		46.4
Canb 2-lvl SPH TISO	*1*	-0.3	-2.0	-0.4	-74.3	0.1	15.5	-0.2	-23.3	0.3	10.2
	2	1.0	4.5	0.8	7.2	0.0	12.8	0.3	10.1	0.3	14.7
	tot		2.5		-67.1		28.4		-13.1		24.9

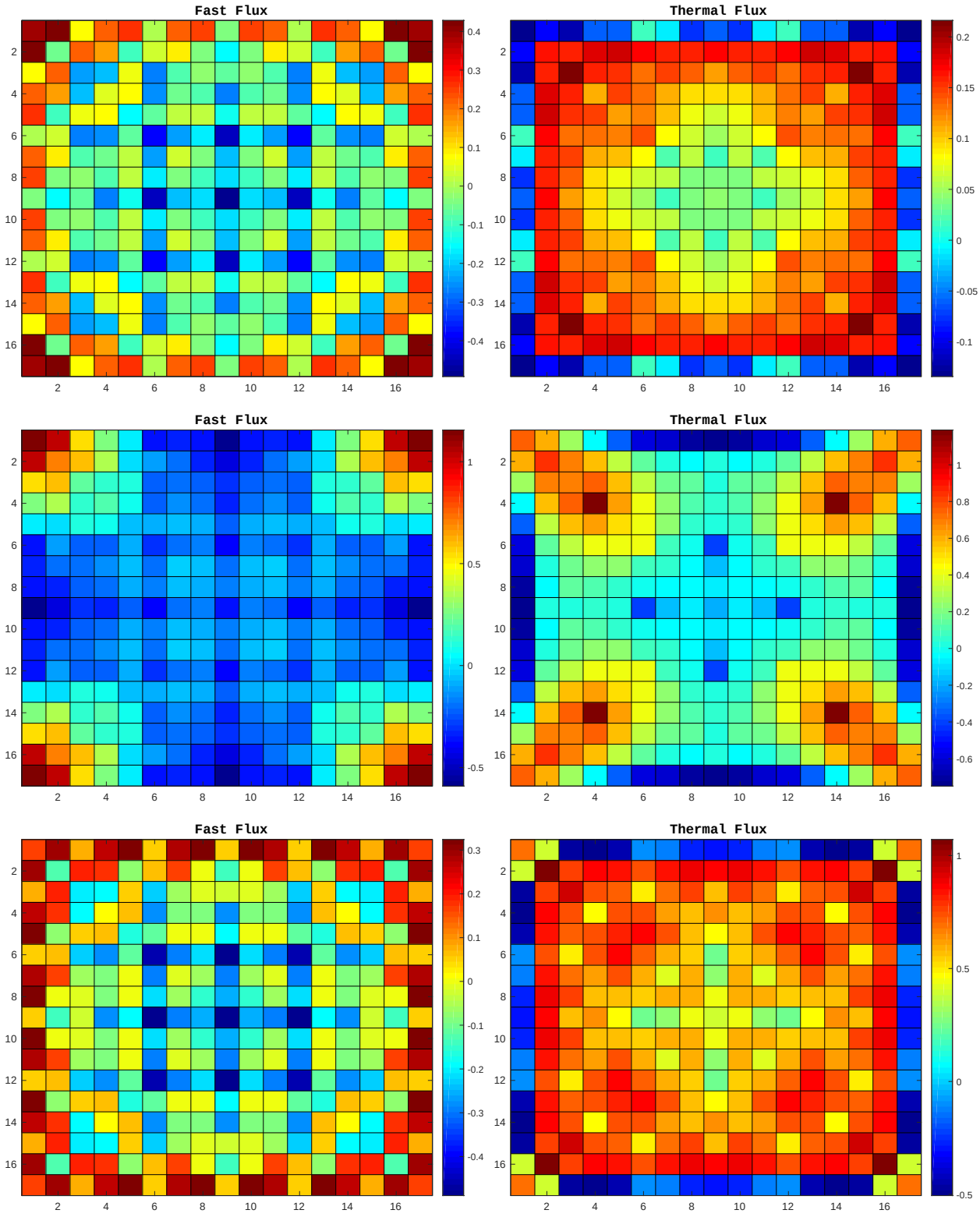

Figure 3.8 TSPC-TISO discrepancies observed on fast and thermal fluxes for UX (first row), UA (second row) and MX (third row) assemblies. All calculations correspond to a Canbakan 2-lvl SPH scheme with B_1 leakage model.

3.5 Computation of ADF, CDF and GFF

After the main flux calculation had been performed, the resulting weighting-flux is employed for the computation of the homogenized cross section and the diffusion coefficients that are going to be stored in the MULTICOMPO database before being implemented for the diffusion calculation with PARCS. At this stage, the information concerning surface and corner fluxes, plus pin-wise homogeneous parameter need to be defined for the subsequent computation of ADF, CDF, and GFF. As introduced previously, the ADF are required to increase the accuracy of the nodal calculation while CDF and GFF are only related to the pin power reconstruction routine utilized by PARCS. In this section, only an explanation will be given regarding the procedure that needs to be implemented in DRAGON5 at the conclusion of the lattice calculation.

Two separate algorithms for storing the information need to be applied according to the case. Concerning the ADF and CDF, only the information regarding the surface and corner fluxes need to be provided, while for the GFF a distinct separate condensation and homogenization need to be implemented to generate the pin-wise homogenized parameters. To give a rough idea about the magnitude of these additional homogenized parameters, a representation of the fast and thermal flux distribution obtained for the Canbakan two level scheme is presented in Figure 3.14. Both flux distributions are normalized with respect to the averaged assembly flux.

After the initialization of the `MULTICOMPO` database, the general algorithm is composed in 3 step:

1. Complete assembly homogenization. Extraction of surface and corner fluxes;
2. Pin-by-Pin homogenization;
3. Feed the `MULTICOMPO`.

The first two steps are accomplished through the `EDI:` module of DRAGON5, dedicated to the coarse energy group condensation and the spatial homogenization. Concerning the computation of the averaged fluxes in selected regions, the card `ADF` needs to be activated, and the number of regions or mixtures are inserted to identify the selected volume. For the pin-by-pin homogenization, since the geometry considered is an eight of assembly, the definition of the unfold geometry is required to identify the correct position of the GFFs. In the last stage, the `COMPO:` module is used to recover the output of the `EDI` module and store the results in the database. The card `GFF` need to be activated, to combine the outcomes

of the homogenizations simultaneously, and recover the group form factor information from the Pin-by-Pin one. We should recall that the leakage model has a negligible impact on the computation of ADF and CDF.

3.5.1 ADF

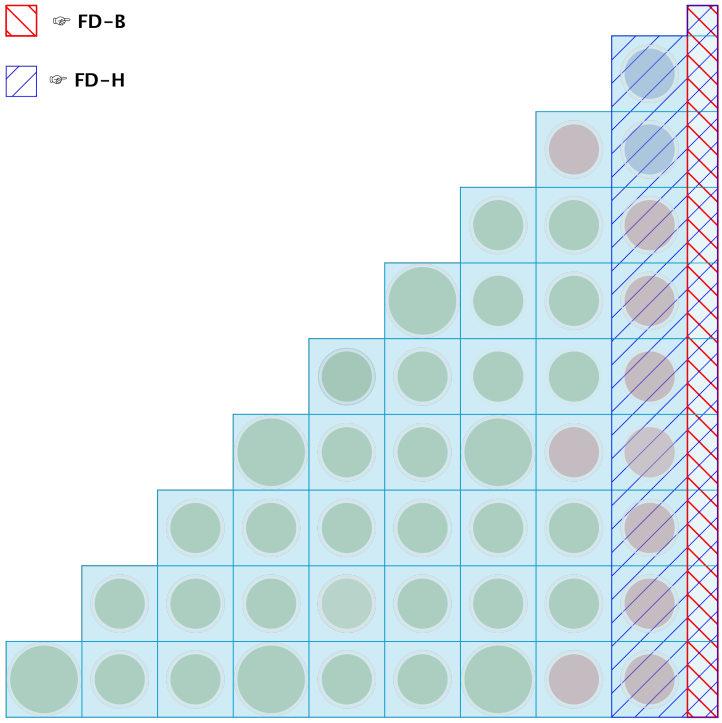

Figure 3.9 Regions where the surface flux is recovered in the thin region method for the computation of ADF. Only when Windmill-type spatial discretization is used.

As mentioned before, the assembly discontinuity factors are defined as the ratio of the surface average heterogeneous flux over the average heterogeneous flux over the whole assembly:

$$\mathrm{adf}_{g,j} = \frac{\phi^*_{g,j}}{\bar{\phi}_{g,j}} \tag{3.5}$$

Different evaluations can be done to generate the surface flux required to compute the ADFs. Indeed, usually two methods are used to recover the surface flux[29]:

- direct interface current (IC) method;
- thin regions method.

In the direct IC method, the surface flux is obtained by direct homogenization of the interface currents of the pins corresponding to the outer row. Once the outgoing current is computed, the following relation is employed to calculate the surface flux:

$$\phi_{surf} = \frac{4J_{out}}{S} \tag{3.6}$$

where ϕ_{surf} is the boundary flux, J_{out} is the outgoing interface current and S the correspondant surface. This method is available only when the IC method is used to perform the flux calculation.

The thin regions approach instead consists of defining a thin outer region close to the external surface of the assembly and assuming that the volumic flux in this small region is equivalent to a corresponding surface flux. In this work, two options of the volume have been studied for the computation of the surface flux (Figure 3.9):

- The water gap (case `FD_B`);
- The outer pin row facing the side of the assembly and its surrounding water gap (case `FD_H`).

For all the lattice schemes where the MOC flux calculation is performed considering the windmill-type geometry, only the thin region method has been contemplated. However, in the Orion scheme is not possible to apply the same methodology because the water gap region is not explicitly discretized. Instead, the direct IC method has been adopted, and we are going to refer to it as `FD_B`. The modification has been performed directly during the lattice calculation taking advantage of the utility modules of DRAGON5.

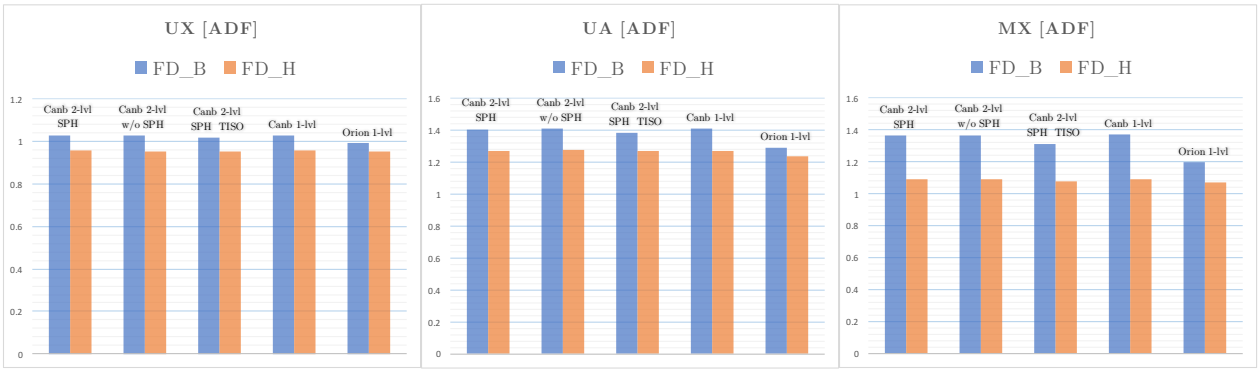

Figure 3.10 Comparison of thermal ADF computation. B_1 leakage model.

In Figure 3.10, a comparison of the thermal ADF computed for the different lattice schemes, is displayed.

As expected, the ADF computed for the UOX configuration have values close to the unity, and a flat behavior is observed through all the cases. For both UA and MX, the thermal ADF diverge notably from unity, and due to the flux distribution along the assembly, the impact of the methodology adopted becomes relevant. As an example, passing between the `FD_B` case to the `FD_H` display a strong variation of thermal flux that occurs inside the outer row of the assembly.

It is interesting to remark the impact of white boundary condition at the border of the assembly. As previously discussed, the isotropic angular distribution approximation generates an overestimation of the fast flux and an underestimation of the thermal flux in the outer pin row of the assembly. This effect is recognized in the comparison of the ADF: the `TISO` case presents a higher value of fast factor but a lower value of the thermal one, particularly relevant for the `FD_B` case.

3.5.2 CDF

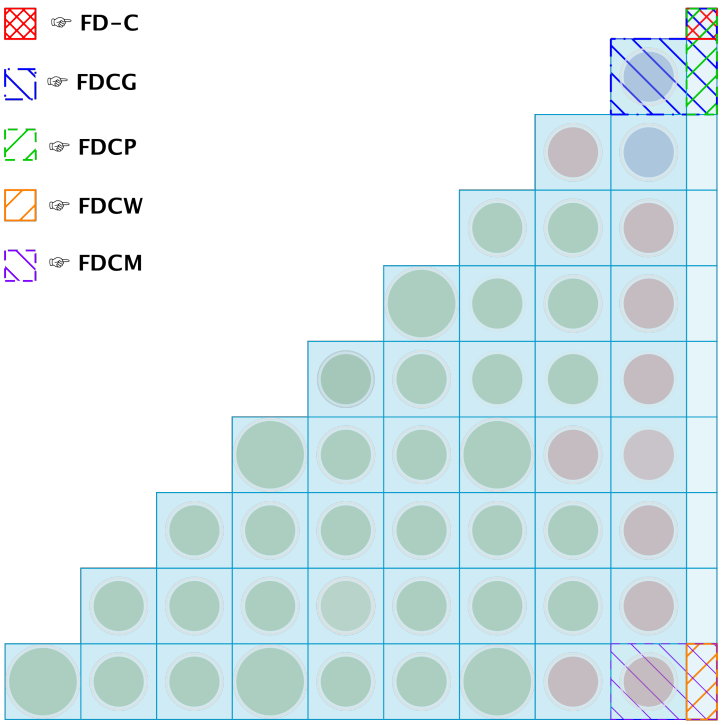

Figure 3.11 Regions where the surface flux is recovered in the thin region method for the computation of CDF and MDF. Only when Windmill-type spatial discretization is used.

Regarding the CDF, they are defined similarly to the ADF, with the surface average heterogeneous flux that is replaced by the average heterogeneous flux in the corner region of the

assembly:

$$\mathrm{cdf}_{g,j} = \frac{\phi^*_{g,j,corner}}{\bar{\phi}_{g,j}} \tag{3.7}$$

The CDF are required to increase the accuracy in the pin power reconstruction process.

Following the sensitivity study that has been conducted for the ADF computation, different regions have been considered for the calculation of the corner surface flux (Figure 3.11):

- the square water gap region in the corner of the assembly (case `FD_C`);
- the corner water gap region plus the water gap adjacent to the corner pin (case `FDCP`);
- the corner pin cell and its surrounding water gap (case `FDCG`).

Regarding the Orion scheme, due to the spatial discretization, only the former case is available.

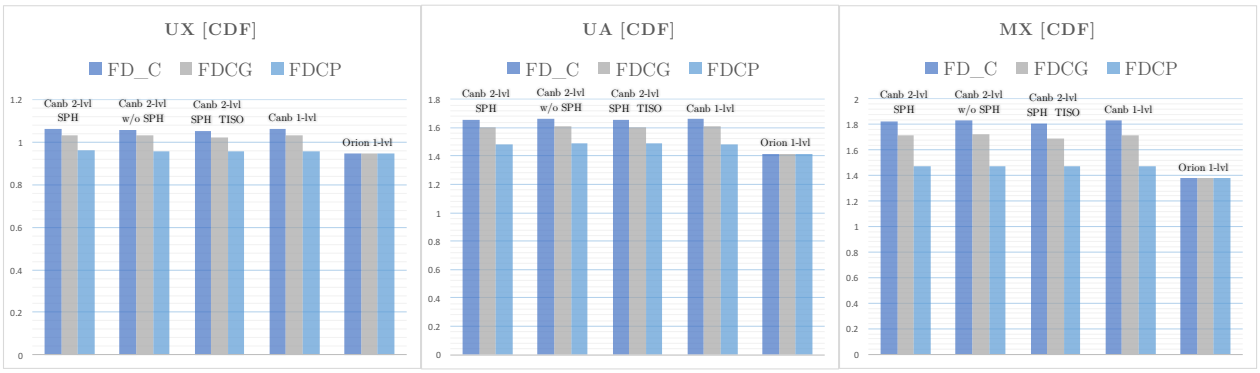

Figure 3.12 Comparison of thermal CDF computation. B_1 leakage model.

An additional parameter, corresponding to a CDF for the mid lateral side of the assembly is then introduced. In the chapter dedicated to the validation of the PARCS calculation, the necessity of defining an additional homogenized parameter will be highlighted when a 2x2 mesh is considered. For simplicity, we are going to refer to it as middle CDF, or MDF. Two different options for the heterogneous flux has been evaluated (Figure 3.11):

- the water gap region adjacent to the outer pin of the first row (case `FDCW`);
- the outer pin of the first row and its adjacent water gap (case `FDCM`).

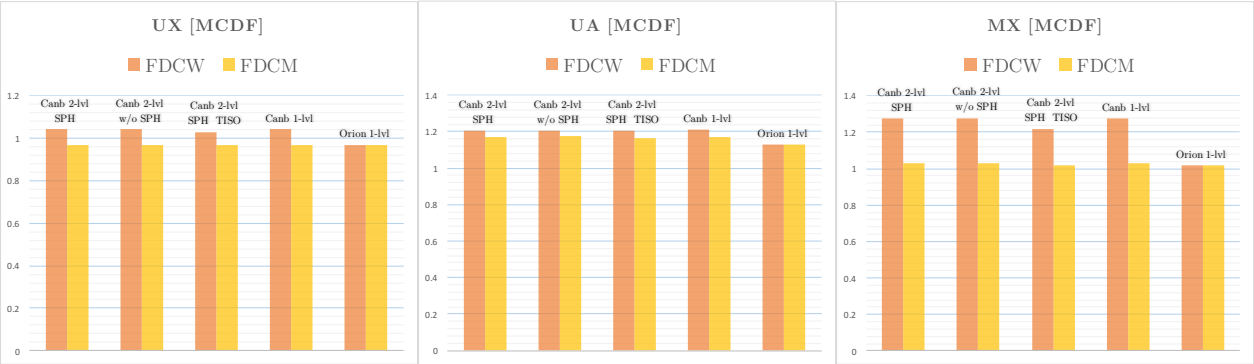

Figure 3.13 Comparison of thermal MDF computation. B_1 leakage model.

In figure 3.12 and 3.13 a comparison of the thermal CDF and MDF computed for the different lattice schemes is presented.

3.5.3 GFF

Regarding the computation of the GFFs, since an automated procedure is not yet implemented for the windmill-type geometry in homogenization module of DRAGON5, the number of regions to be homogenized need to be defined explicitly. As already observed by Chambon[11], it should be highlighted that the group form factors should be computed in the outer pin row without including the water gap. For the Orion case, since the water gap is included in the last row of pins, a volume correction is performed following the pin power reconstruction. Each value in the power map is multiplied by the correspondent ratio between the homogenization volume and the reference volume of the pin cell (fuel, cladding, and moderator); in the case of the Orion scheme, the homogenization volume contains the water gap, and the ratio is greater than one. Lastly, the correct position of the GFF for the PARCS calculation requires the representation of an unfold macro-geometry.

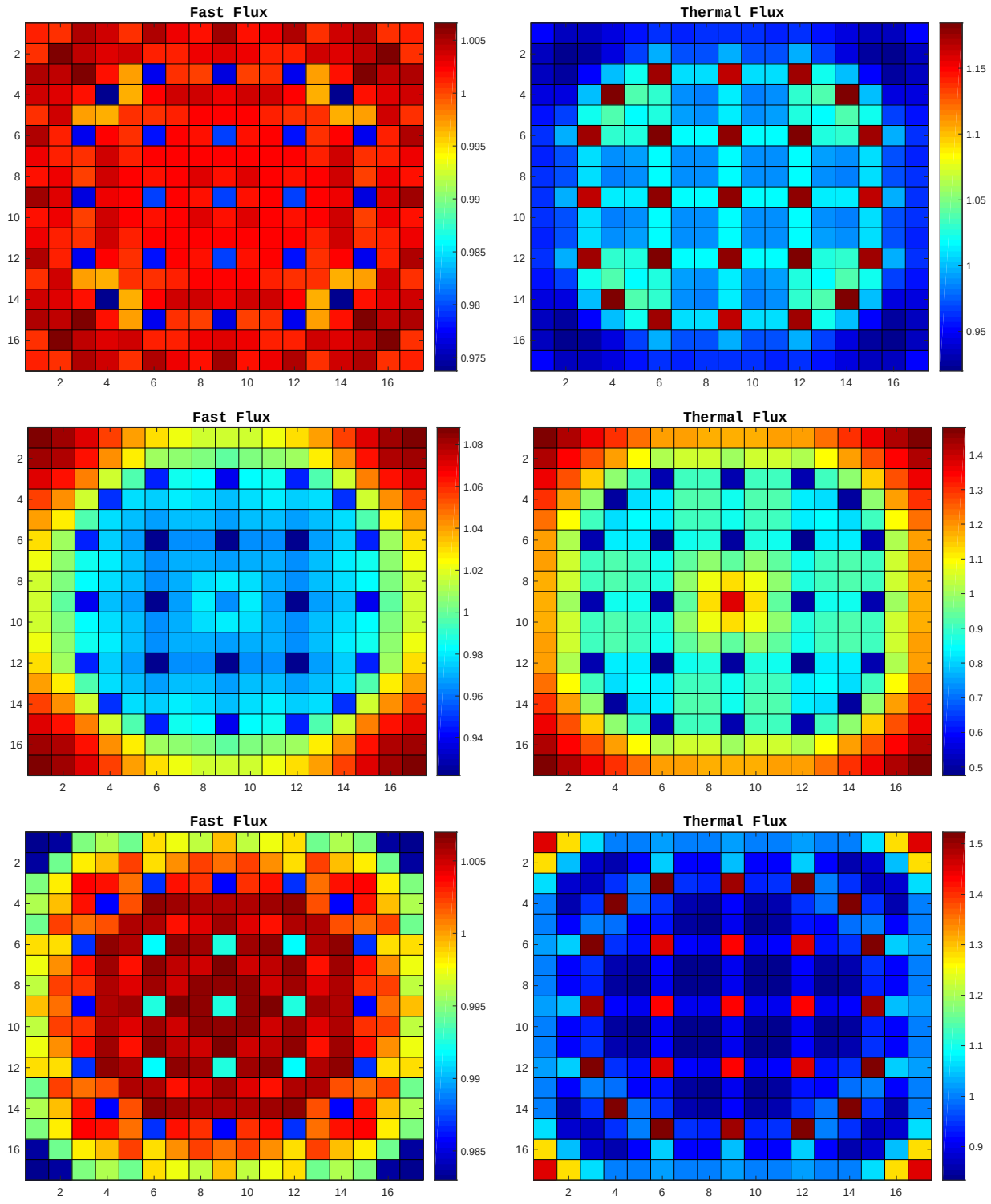

Figure 3.14 Fast and thermal flux distribution of UX, UA and MX fuel assemblies for Canbakan 2-lvl SPH lattice scheme. B_1 leakage model.

3.6 Conclusions

This section has been dedicated to the validation of the lattice schemes used to generate the homogenized parameters for the fuel assemblies, required in the nodal diffusion simulation. These lattice calculations have been performed on a single assembly in infinite lattice approximation considering different leakage models. A comparison of the lattice schemes currently adopted by EPM and IRSN was shown, and a preliminary investigation of the sources of discrepancies have been conducted with respect to a Monte Carlo reference. Furthermore, the methodology adopted for the computation of ADF, CDF, and GFF has been presented.

3.6.1 Orion Lattice Scheme

The primary interest in this chapter was to maintain consistency with the work currently performed both for the ORION project and at École Polytechnique de Montréal. Hence, besides investigating the possible sources of discrepancies to be expected in the diffusion calculation, interest has been shown by IRSN for a first verification of their calculation scheme by the comparison with an up to date design, such as the one proposed by Canbakan.

Actually, the *DRAGOR-V1* is a lattice scheme that has been developed based on the standard tools currently employed for industrial application in French PWR. On the other hand, the two-level scheme employing the windmill spatial discretization represent a state of art design in the domain of lattice calculation. The definitive interest of IRSN is to acquire all the possible information to include this capability in their next future standard calculation routine. That being said the discrepancies displayed by the *DRAGOR-V1* scheme are significant and starting from the lattice validation, this option appears quite inadequate to be implemented for a nodal diffusion calculation.

All the investigated elements display a net degradation. Notably, a large inaccuracy stands out in the fission reaction map: several peaks above 4.0% feature both the MOX and the UOX assemblies with control rods inserted. Besides the **rms** value is largely above what observed for the EPM's designs. In our opinion, the explanation should be sought in the poor spatial discretization of the pin cells and in the fact that the water gap is included in the outer pins, in a manner that affects the computed fission reaction rate.

Due to the direct interest of IRSN, for the purpose of this study, it has been then decided to present the *DRAGOR-V1* through the entire cluster validation. It will be considered as a touchstone for the Canbakan's scheme, and as a frame of reference for the applicability of this standard design for nodal diffusion calculations.

3.6.2 Canbakan's Scheme

The results obtained in the validation process are overall in accordance with the observations made by Canbakan[10].

Therefore, due to the overall positive results display throughout the validation exercise, starting from now on, the two-level Canbakan scheme with 26-group SPH equivalence will be considered as the most likely design to be applied as a standard for our lattice calculation. All the sensitivity studies for the cluster validation will be performed considering only this possibility, as well as the validation on the simplified core.

The choice of also considering the single level scheme lies on the work initially performed for this study and also as an opportunity to ensure and extend the work previously initiated by Canbakan. Indeed, before considering the Monte Carlo validation, the verification of the assembly calculation was performed by comparison to a detailed single-level scheme. It was in our interest to assess and re-interpret the earlier obtained results. The outcome of this validation exercise is that there is no interest to increase the computational time and employ this option. On the contrary, excluding the fission reaction map, the result displayed are generally degraded with respect to the two-level scheme. It should also be remarked that a peculiar inaccuracy is observed in the fission abortion rate of different isotopes.

The sensitivity study has been conducted to highlight calculation option that could have been relevant in the creation of a reactor database for nodal diffusion calculation. It further allowed to broaden the range of information for a better understanding of the problematic. The results from this basic analysis suggest a possible interest from the SPH equivalence. In fact, concerning the `TISO` option, the slight advantage gained in computational time is compensated by an overall degradation of the results. There is no clear convenience to opt for this choice. The outcome from the Canbakan's scheme performed without 26-group SPH equivalence is more challenging for a precise comprehension. Compared to the two-level reference scheme, both amelioration and several deterioration are observed. While the outcome from `TISO` option display just a slight degradation, concerning the SPH choice, the nature of the observed discrepancies may be interesting to assess during the diffusion calculation.

3.6.3 Final Remarks

In conclusion, the reactor database has been generated for all the options investigated during the lattice validation, and five paths have been established to adapt the calculation scheme to each different lattice design.

In summary, these separate DRAGON5 runs have been performed and validated:

1. *Canb 2lvl SPH*
2. *Canb 2lvl w/o SPH*
3. *Canb 2lvl SPH TISO*
4. *Canb 1lvl*
5. *DRAGOR-V1 1lvl*

However, for the following step we opted only to present the design of major interest for IRSN explicitly: the Canbakan's two-level scheme with 26-group SPH equivalence and the *DRAGOR-V1* one. The outcome of the other lattice choices has been included in the appendices, such that few remarks can be made during the validation when it is interesting to mention findings of particular interest.

CHAPTER 4 VALIDATION OF ADF ON A CLUSTER GEOMETRY

This chapter is devoted to the presentation of the methodology implemented for the coupling between DRAGON5 and PARCS, and the validation on simplified core configurations through the comparison to a Monte Carlo reference obtained with SERPENT2. The geometries considered are a 2x2 and a 3x3 PWR clusters computed with reflective boundary conditions.

4.1 Cross Section Preparation

The macroscopic cross section data generated by the lattice calculation with DRAGON5 are stored in a `MULTICOMPO` data structure and subsequently are reprocessed to build an input file for the nodal code PARCS. Since the GenPMAXS utility is not able to read a `MULTICOMPO` data structure as produced by DRAGON5, a procedure has been developed to transform the `MULTICOMPO` object into an HELIOS-like data file, before calling the GenPMAXS utility. The `NCR:` and `D2P:` modules of DONJON5 allow to interpolate the values of the `MULTICOMPO`, compute the ADF and reformats the reactor database into an input file readable by the GENPMAXS utility which in turn will create a PMAX file, the input file for PARCS simulation. The flow of information is presented in Figure 4.1.

4.1.1 `D2P:` Module

Starting from a reactor database (`MULTICOMPO` or `SAPHYB`) generated by DRAGON5, the aim of the `D2P:` module is to compute and reformat the homogenized parameters, such that the output file is readable by the GenPMAXS utility software. Particularly, during the development of the module, the HELIOS format has been selected as the most suitable output already accepted by GenPMAXS.

Through the `D2P:` module, the cross sections and other homogenized information are extracted from the microlib embedded in the considered reactor database. At the end of the procedure two files are generated:

- an input file needed by GenPMAXS to produce a PMAXS (extention ".inp")
- a file containing data cross sections in HELIOS-like format (extention ".dra")

These are the input files to run GenPMAXS code.

For our calculation, this task is performed in three different stages:

i) Phase 1: Recover information form MULTICOMPO reactor database and from the input file DONJON (keycards of `D2P:` module) to generate the GenPMAXS input file (".inp").

ii) Phase 2: The cross section are interpolated via `NCR:` module and stored in memory;

iii) Phase 3: The cross sections are stored in the HELIOS .dra output file.

For further details, a long description of the module is presented in the DONJON manual[31].

4.1.2 `PMAXS` Format

Since in our case, no depletion calculation is performed, and only one elementary calculation is originally stored in the `MULTICOMPO`, it is of no interest to give a detailed description of the PMAX format used by PARCS. However, a more comprehensive description can be found in the GenPMAXS manual[32].

Without going into too much detail, the characteristic PMAXS structure has been created to fit the PARCS depletion routine. The cross sections are represented as a function of several global and local parameters (burnup, presence of control rods, density, and temperature of coolant, temperature of fuel, etc.) and provided in a hierarchical system. Each combination of parameters defines a branch of information that contains the reference cross sections (same as the input file), and the partial derivatives of the cross section respect to the reference branch.

In the PMAX files generated during this study, only one branch is considered because, as mentioned before, no depletion calculation is conducted and only one reference set of cross sections for nominal parameters is employed.

4.2 Core Calculation

There is no interest to assess a core configuration composed of identical assemblies since the implementation of the ADF is irrelevant, and the calculation options have a negligible influence. Hence, the reactor database generated with the lattice calculation is evaluated for two configurations of each 2x2 and 3x3 motifs (Figure 4.2): with an AIC assembly (UA-UX) and with a MOX assembly (MX-UX). In the first case a checkerboard is defined where UX and UA/MX are alternated; for the 3x3, the UA/MX assembly at the center of the motif is surrounded by eight UX assemblies.

We recall that it was not possible to simulate a 2x2 colorset with periodic boundary conditions due to a limitation in the pin power reconstruction procedure in PARCS. The main problematic

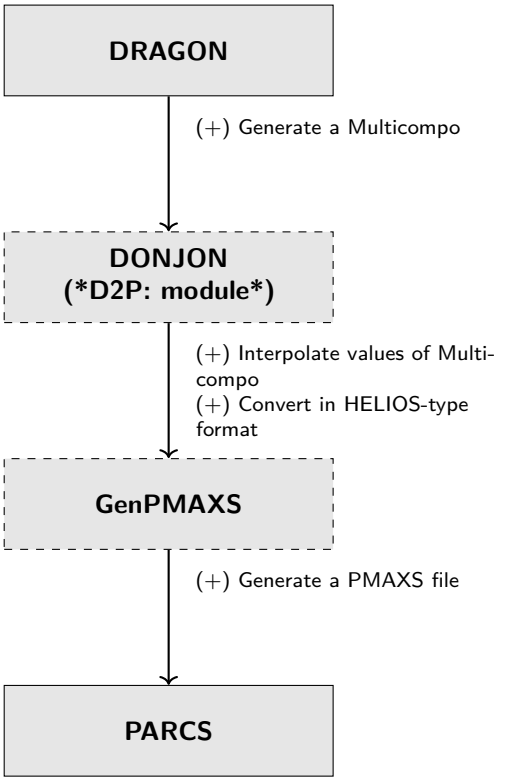

Figure 4.1 Interfacing DRAGON with PARCS.

concerns the periodic boundary conditions options, that was not working at the time that this research project has been carried out (PARCS version *v32m20*). Actually, even if we were able to perform the diffusion calculation for the colorset using a quarter of assembly nodes instead of a full-node assembly, PARCS was not able to reconstruct the pin power values correctly.

In order to be consistent with the lattice calculation, the boron concentration has been maintained equal to zero. It should also be remarked that the colorset configuration has been chosen not to have a quasi-critical cluster and not to obtain a core critical configuration. The impact of leakage model of the lattice calculation is relevant for the evaluation of the results. These configurations have been preferred since a sharp gradient of flux is generated at the interface of the assemblies in both cases, and represents a challenge for nodal calculations with assembly homogenization. Indeed, the impact of ADF is supposed to be of primary importance.

Several calculation options available from the lattice calculations will be assessed during the validation. These choices, partially presented in the previous chapter, concern:

Leakage Model: B_1, P_1 and no leakage ;

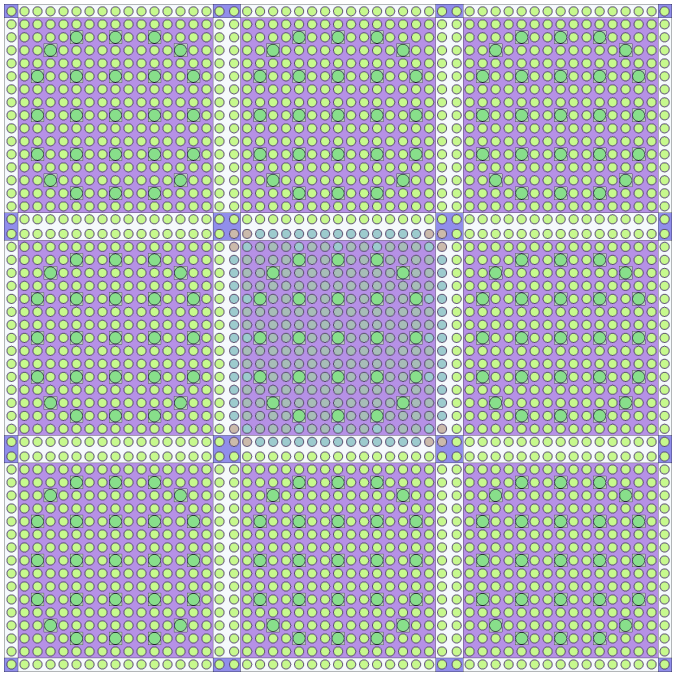

Figure 4.2 3x3 PWR motif. Center MOX fuel assembly surrounded by eight UOX fuel assemblies (geometry output from SERPENT2 computation).

ADF: `FD_B`, `FD_H` and `NO ADF` ;

CDF: `FD_C`, `FDCG`,`FDCP` and `NO CDF` ;

MDF: `FDCW`, `FDCM` and `NO MDF`.

It should be recalled that the options `NO ADF`, `NO CDF` and `NO MDF` correspond to a diffusion calculation with PARCS run with unity values for these homogenized parameters.

The remainder of the chapter will be divided into two parts. First, a sensitivity study is considered to assess the combination of calculation options that guarantees the best accuracy for each motif; afterward, the results for the two configurations selected are presented for the various lattice schemes proposed.

4.2.1 PARCS Calculation

The PARCS input system is based on card names. Since a transient is not taken into account, only the steady-state reactor was considered. The 3-D geometric representation is reduced to a 2-D one assuming an infinite approximation on the axial direction (zero current at the top and the bottom of the plane); also radially the cluster is closed similarly by reflective boundary conditions.

The dimension of each separate node correspond to a lattice pitch in the radial plane; an additional sub mesh can be applied in each Cartesian dimension. The simulation can be performed with different nodal solver for which default values are considered for the steady-state convergence criteria (`CONV_SS` card); as suggested in the technical report IGE-349 [11], larger convergence criteria are not affecting the results.

The printing of the power distributions is actuated in the `print_opt`. The assembly power is then extracted from the ".rlp" output of the PARCS calculation while the pin power maps are instead obtained from the ".pin" output generated for each separate node. The `PIN POWER` option needs to be set to `true` and the position where the information are extracted need to be defined by `PINCAL_LOC`.

It should be noted that starting from version *v32m20*, the pin powers are scaled to the assembly power, and there is no need for multiplication with respect to a normalization factor, in order to account for the assembly power distribution. For good measure, during the reprocessing of the results, the nodal powers from the assembly and the pin power outputs are confronted.

4.2.2 Reference Calculation

The reference computation employs the same methodology adopted for the single assembly calculation. Actually, the input file of each single assembly are nested together and arranged to depict the desired simple core configuration. The clusters are defined through the lattice option card `lat`, where each cell corresponds to an entire assembly.

The assembly and the pin-wise power distributions are generated by setting a value of 2 for the card `cpd` (a "_core0.m" file is generated). The appealing feature is that SERPENT2 evaluates these integral power values inside nested lattice structures, simplifying the collection of results considerably. Only non-zero values are displayed.

4.2.3 Method of Validation

The reactivity is evaluated in the same fashion as in Eq. 3.1. Regarding the assembly power and the pin power maps, the results of SERPENT2 are normalized with respect to the total power computed from the PARCS estimate. The percentage relative difference between the diffusion and the stochastic calculation is used as an estimation of accuracy. Taking advantage of the symmetry of the problem, in the 3x3 configuration, only three representative assemblies (Corner, Center, and Side) are considered in the assessment of the assembly power, while the N-E quadrant is depicted just for the pin power validation. Furthermore, four quantities

are displayed for the evaluation of the pin power accuracy: the maximum (**max**), minimum (**min**), the absolute difference between these two peak values ($\boldsymbol{\delta}$) and the root mean square error (**rms**).

4.3 Sensitivity Studies

In this paragraph, we have focused on the options that can affect the diffusion calculation, and we have tried to assess the most suited combination to be applied for the validation.

It should be noted that only the two-level scheme proposed by Canbakan has been evaluated in the sensitivity study to reduce the amount of values available; as already explained, it represents the most suitable design for industrial applications.

Regarding the other computation option, we choose to maintain the following choices during this excercise:

Leakage Model: B_1 ;

ADF: `FD_B` ;

CDF: `FD_C` ;

MDF: `FDCM` ;

Nodal Solver: ANM with 2x2 meshes (`A2`).

Only if explicit mentioned a different choice will be considered.

4.3.1 GFF Calculation

The importance of activating the option for recovering the GFF from lattice calculation, instead of using unity values, can be easily assessed in Figure 4.3. The same trend is noted for all the configuration and all the calculation options.

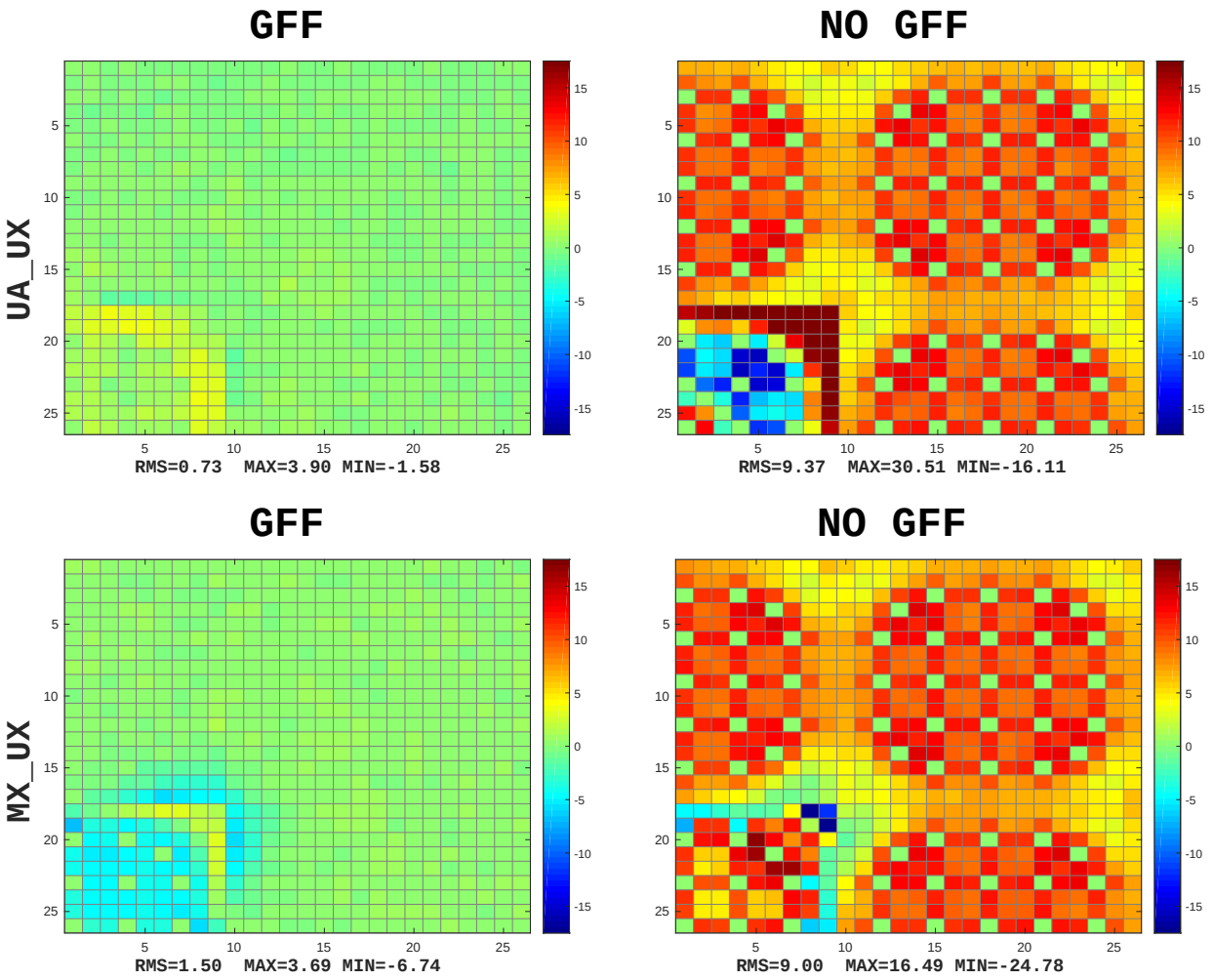

Figure 4.3 Comparison of pin power (% difference) error maps with or without GFF, for configurations UA-UX and MX-UX of 3x3 PWR motif.

The use of unity GFF values enhances the deterioration of the results throughout the motif, with the **rms** that presents discrepancies close to 10%. Furthermore, the $\boldsymbol{\delta}$ between the maximum and minimum differences exceeds 50% in several cases. In conclusion, the GFF keyword should always be activated.

4.3.2 Higher-order Nodal Method

The two-group diffusion equation in PARCS is primarily solved via a Coarse Mesh Finite Difference (CMFD) formulation; then an higher-order solution kernel is evaluated with the purpose of improving the coupling coefficient at the interfaces of each node, through the resolution of a 2-node problem.

For the latter case, several nodal methods were implemented, and have been tested[6]. The Analytic Nodal Method (ANM) and Nodal Expansion Method (NEM) are widely applied for PWR simulation. In addition, a so-called hybrid ANM-NEM method can be used (HYBRID): it employs the ANM method principally, but it switches to NEM for near critical node problem where the first kernel may suffer the absence of intranodal leakage. However, in our simulations, the hybrid method is equivalent to ANM, since our configuration are far from criticality. Furthermore, a fine mesh finite difference (FMFD) solver can be employed.

It should be noted that for the NEM method, we observed a limitation in the verification of the default convergence criteria. We tried to assess the spectrum of these parameters, and we noticed that it is hard to obtain a proper convergence both due to inner and outer iteration threshold values. Even by reducing the magnitude of this criteria and increasing the maximum number of iteration, the convergence is still hardly achieved. We also observed that despite the several attempts to obtain a complete convergence, the outcome of the computation was not affected and the nodal solution was maintained unaltered. However even if compelling results were generated performing the run with default convergence parameters and interrupting the computation after 500 outer iterations, the lack of a proper convergence does not allow us to rely on them. We only present the outcome in this paragraph with a grain of salt, since the calculations are not reliable.

For the diffusion calculation, each node can then be subdivided according to a Cartesian mesh in the x and y direction (2-D problem). Two possibilities are considered: a single mesh per node (1x1) and four meshes (2x2) per node, where each direction is discretized in 2 identical sub meshes. Higher discretizations have been tested but the outcome is not displayed because a null pin power matrix was generated for each node.

A comparison of the available nodal methods is presented in Tables 4.1.

Table 4.1 Comparison of *nodal kernel* options for configurations UA-UX and MX-UX of 3x3 PWR motif.

		REACTIVITY		ASSEMBLY POWER			PIN POWER		
	Kernel	k_{eff}	$\Delta\rho$	**Crn**	**Ctr**	**Side**	**max**	**min**	**rms**
UA-UX	A1	1.34096	-81	-0.20	0.56	0.13	4.87	-3.52	0.97
	A2	1.34080	-90	-0.06	0.98	-0.07	3.90	-1.58	0.73
	N2	1.34077	-91	-0.03	0.58	-0.05	4.25	-2.06	0.84
	F1	1.34862	343	2.54	-19.39	-0.03	28.83	-7.46	7.33
	F2	1.34214	-15	0.50	-2.49	-0.19	7.31	-1.83	1.78
MX-UX	A1	1.35704	-26	-0.50	2.20	0.10	3.53	-6.34	1.57
	A2	1.35698	-29	-0.43	2.46	-0.04	3.69	-6.74	1.50
	N2	1.35696	-30	-0.19	-0.31	0.26	7.63	-11.29	2.38
	F1	1.36062	168	1.68	-18.37	1.91	36.71	-29.30	7.69
	F2	1.35827	41	0.03	-7.56	1.50	24.95	-24.43	4.71

The Finite Difference kernel with 1x1 mesh (F1) does not seem appropriate to be applied for the refinement of the coupling coefficients in the two-node problem: starting from the reactivity, the overall highest variances observed are produced with this kernel for all the quantities examined in the validation.

A net improvement is achieved by doubling the number of meshes (option F2, mesh 2x2), and a good accuracy is obtained for both 2x2 and 3x3 motifs when the configuration contains a UA assembly. Compared to the Monte Carlo solution, it generates the best result concerning the reactivity. However, the assembly power displays huge gaps when confronted with the other alternatives, and more importantly the pin power values can be notably degraded.

Concerning the Analytic Nodal Method solution (ANM) the choice of using one or four nodes per assembly depends on the configuration chosen and slightly on the calculation options adopted. For all the computations an increased accuracy is observed for the reactivity and the assembly power when a single 1x1 mesh is employed, while the reconstruction process is generally more refined in the 2x2 case. It should be remarked that for the former mesh, the MDF has a not negligible impact on the reconstructed pin power values.

Lastly, the performance of the NEM kernel (2x2 mesh) is usually close to the ANM, with significant differences that can arise in the MX-UX case. We did not present the 1x1 mesh since it was not possible to generate a pin power matrix and it was of no interest in our validation.

The results that have been presented belong to a selection of a combination of the different configurations and calculation options implemented. We observed that, excluding very

particular cases, Table 4.1 is representative of the general trend. In the results presented from now on, only the ANM with 1x1 and with 2x2 meshes will be analyzed; they result as the most accurate of an overall comparison of all the quantities investigated for the validation.

4.3.3 CDF & MDF

The computation of CDF and MDF has been presented in the previous chapter. They have a strong impact on the pin power reconstruction process and various combination of CDF and MDF should be assessed to increase the accuracy of the diffusion calculation. It should be remarked that due to the methodology adopted in the dehomogenisation, the MDF has no impact when a single node per assembly is defined.

We observed that the 2x2 mesh option almost reproduces the discrepancies found for the 1x1 mesh if the same calculation option is employed. If a certain difference is observed with the former case, almost in every case a similar discrepancy can be assessed when 4 nodes per assembly are defined. To reduce the number of possible combinations, we opted to assume that in a first approximation the effect of the MDF can be separate from the choice of CDF. The sensitivity of the CDF is then evaluated by the comparison of computations performed by the ANM kernel with a 1x1 mesh.

The comparion of CDF is displayed in Table 4.2 for the cluster 2x2. A similar outcome can be observed in the 3x3 case.

Table 4.2 Comparison of CDF options for configurations UA-UX and MX-UX of 2x2 PWR motif. *Nodal kernel*=`H1` employed.

	UA-UX			MX-UX		
CDF	**max**	**min**	**rms**	**max**	**min**	**rms**
`FD_C`	6.35	-3.28	1.97	4.98	-9.90	2.36
`FDCG`	6.39	-3.32	1.98	5.08	-9.11	2.33
`FDCP`	6.41	-3.33	1.98	5.31	-7.65	2.25
`NO CDF`	10.59	-12.47	3.04	7.60	-12.13	2.47

The first result that stands out is the necessity of recovering a proper value of CDF to notably enhance the accuracy of the reconstruction method; if a unity value is employed (`NO CDF` option), large discrepancies can be observed in every case. Concerning the choice where to recover the surface flux, a slight deviation is perceived between the different options; depending on the configuration, it seems that `FD_C` is better suited for rodded configurations, while `FDCP` for MOX ones. For the latter case, we can hypothesize that the surface flux in the

corner water gap, computed in infinite lattice approximation, may not be representative as the actual environmental case. The same assessment should also be done for the ADF.

An explicit comparison between the different option is presented for the MX-UX configuration of the cluster 3x3 (Figure 4.4).

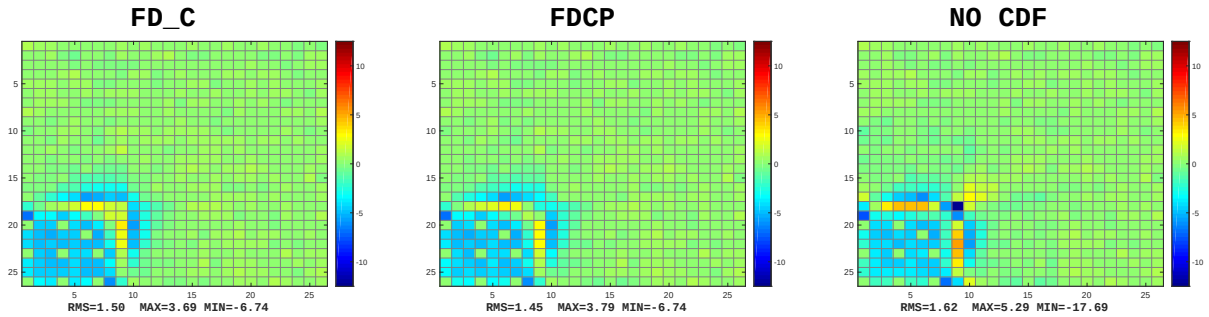

Figure 4.4 Comparison of CDF options for configuration MX-UX of 3x3 PWR motif. Pin power (% difference) error map.

It should also be noted that we chose a configuration where significant discrepancies stand out along the interface between the assemblies; by comparison with the `NO ADF` option, an inappropriate evaluation of the ADF should be pointed out as a possible source of degradation. We are going to discuss this problematic along the chapter. In any case, the impact of the CDF can be assessed through the comparison of the discrepancies around the point of contact between the assemblies: with the `FDCP` option, the magnitude of the differences tends to decrease, affecting 3-4 rows around the corner.

Following the CDF, also the sensitivity of MDF should be assessed based on the different options available. For the same reason exploited before, it is not possible to evaluate all the possible combinations between the calculation options, and some choices for the presentation of the results has to be made. During the assessment of the results for all the possible computations, arose the issue of defining an appropriate option based on the most plausible procedure that should be adopted. To be more clear, it should be more consistent to recover the heterogeneous flux in a similar region for all the three factors: hence, when `FD_B` is chosen, the ideal option should be to recover CDF and MDF from the same water gap region, namely `FD_C` or `FDCG` and `FDCW` respectively.

The comparison of CDF and MDF, is presented in Table 4.3. Due to a lack of usefulness we excluded the combination `NO CDF` with `NO MDF`.

Table 4.3 Comparison of CDF and MDF options for configurations UA-UX and MX-UX of 3x3 PWR motif.

		FD_C			FDCG			FDCP		
	MDF	**max**	**min**	**rms**	**max**	**min**	**rms**	**max**	**min**	**rms**
UA-UX	FDCW	4.04	-1.69	0.74	4.05	-1.70	0.75	4.07	-1.70	0.75
	FDCM	3.90	-1.58	0.73	3.91	-1.59	0.74	3.93	-1.60	0.74
	NO MDF	6.41	-4.01	0.87	6.41	-4.01	0.87	6.42	-3.99	0.87
MX-UX	FDCW	3.24	-6.06	1.53	3.19	-6.01	1.51	3.34	-5.87	1.49
	FDCM	3.69	-6.74	1.50	3.65	-6.74	1.48	3.79	-6.74	1.45
	NO MDF	3.87	-7.43	1.51	3.83	-7.43	1.49	3.96	-7.43	1.45

When the 3x3 mesh is employed, the use of the MDF is strongly recommended for rodded configurations. A significant correction can be seen in the middle side of the assembly, with a diminishing of the peak values of the gaps. The impact of the different options can also be assessed graphically in Figure 4.5. In the case of MX configurations, the impact of MDF is almost negligible for the FDCM option, while the highest degradation of the **rms** is observed for FDCW. Concerning the two options for MDF, the FDCM seems overall the best solution, with always an improvement of the **rms** and $\boldsymbol{\delta}$ values. Although not obvious, the FDCM should be preferred in the definition of the MDF.

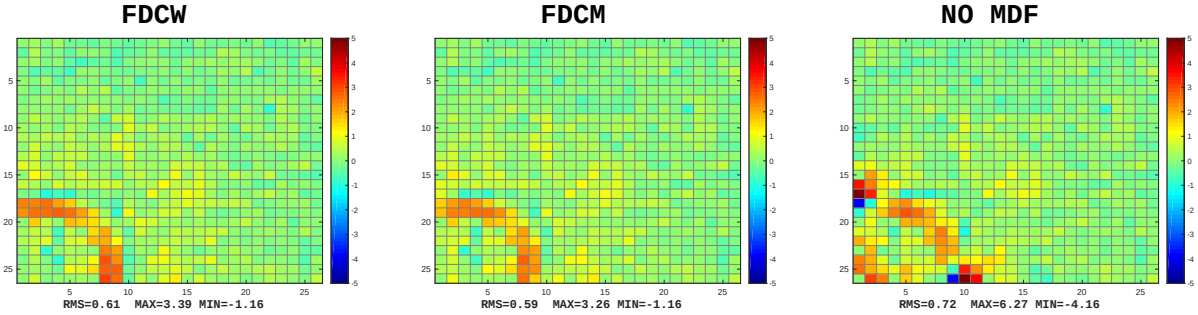

Figure 4.5 Comparison of MDF options for configuration UA-UX of PWR 3x3 PWR motif. Pin power (% difference) error map. ADF=FD_H employed.

4.4 Validation

The results from the diffusion computation are assessed through the comparison between the reactivity, the assembly powers, and the pin power maps generated by PARCS and the values computed with the stochastic calculation with SERPENT2.

For all the lattice schemes, three option will be displayed (B_1, P_1 and no leakage) to highlight

the impact of the leakage model plus other three options (`FD_B`, `FD_H` and `NO ADF`) related to the methodology implied for the computation of the ADFs. It should be recalled that the ADF option `NO ADF` corresponds to a diffusion calculation with PARCS run with ADF equal to unity. The `FD_B` option represents the flux recovered in the water gap region while `FD_H` refers to the area defined by the water gap and the outer pin row.

We chose to present only the overall best combination obtained through the assessment of *Nodal Solver*, CDF and MDF observed for the lattice schemes. The following choices are considered:

CDF: `FD_C` for the UA-UX configuration, while `FDCP` for the MX-UX one ;

MDF: `FDCM` ;

Nodal Solver: ANM with 2x2 meshes (`A2`).

Both the geometries have been validated and the diffusion computations have been performed employing all the lattice scheme and options described in the previous chapter. However, we opted to present in this paragraph only the outcome from the PWR 3x3 motif using the Canbakan two-level scheme with 26-gr SPH equivalence and the Orion design. The primary reason relies on the necessity to reduce the amount of information obtained by all these runs. Furthermore, apart from limited cases, we did not observe any important aspect that would have been of particular interest in this study. Several elements should be investigated, but they go beyond our purpose of validating ADF in a calculation scheme DRAGON5-PARCS.

Few references though will be included when it is worth considering certain results. It should be remarked actually that the outcome from the validation of the PWR Cluster 2x2, and the remaining lattice schemes for the PWR 3x3 motif have been included in the appendices (Appendix B and C).

4.4.1 3x3 PWR motif

The validation is conducted on a PWR Cluster of 3x3 assemblies with reflective boundary conditions. The central UA/MX assembly displays the highest source of error while the surrounding ones exhibit a minor degradation. Compared to the PWR Cluster 2x2, it represents a less challenging test for the ADF, and lower discrepancies are observed.

UA

Starting from the comparison of the reactivities (Table 4.4), an increased accuracy is displayed without implementing any leakage model: the best result is obtained with the two-level Canbakan scheme using `FD_H` option (12 *pcm* of difference). The use of a leakage model leads to an increased of discrepancies, and a modest underestimation of the multiplication factor can be shown both for the B_1 and P_1 approaches. The impact of the ADFs induces a net increase of the multiplication factor between 110 *pcm* and 150 *pcm*, despite the leakage correction (a lower magnitude is observed for the *DRAGOR-V1* scheme compared to the Canbakan design). In particular, for the two-level Canbakan scheme, it translates in a switch between overestimation to underestimation of the reactivity when the simulation is performed without leakage. Overall the `FD_B` option produces the greater magnitude effect, and it results in the best alternative both for B_1 and P_1 methods.

Table 4.4 k_{eff} and reactivity [*pcm*] for the UA-UX 3x3 PWR motif as a function of *leakage model* and *ADF* option.

		FD_B		FD_H		NO ADF	
		k_{eff}	$\Delta\rho$	k_{eff}	$\Delta\rho$	k_{eff}	$\Delta\rho$
Canb 2-lvl SPH	NoL	1.34284	24	1.34262	12	1.34021	-122
	B1	1.34080	-90	1.34055	-103	1.33826	-231
	P1	1.34077	-91	1.34053	-105	1.33822	-233
DRAGOR-V1	NoL	1.34524	157	1.34527	158	1.34316	42
	B1	1.34315	41	1.34314	40	1.34113	-71
	P1	1.34312	40	1.34311	39	1.34109	-73

Moving now towards the assembly power validation (Figure 4.6), the use of ADFs increases the accuracy widely when the fundamental mode is applied, while in the absence of a leakage correction a switch is seen from an overestimation to the underestimation of the power (from approximately 4.5% to -3.5% in the rodded assembly). The impact of the ADF implementation is estimated between 6% and 8% in the center of the motif, and around 1% in the UX side assembly. On the other hand, the corner assembly is barely affected. Therefore, confronting the alternatives for the ADF, the `FD_B` result the most accurate for the B_1 and P_1 methods, while `FD_H` with the `NoL` option.

Similarly to the assembly power, for leakage corrected assemblies, a net amelioration of the pin power accuracy is induced by the ADFs (gain above 1.5% for the **rms** and between 8% and 15% in the $\boldsymbol{\delta}$ between maximum and minimum), while a degraded outcome arises without leakage models (Table 4.5). For the latter case, the variation of the **rms** value is in the range of $0\% - 0.5\%$, while only the **min** value is affected by the ADFs (between 3.5% and 7.5%

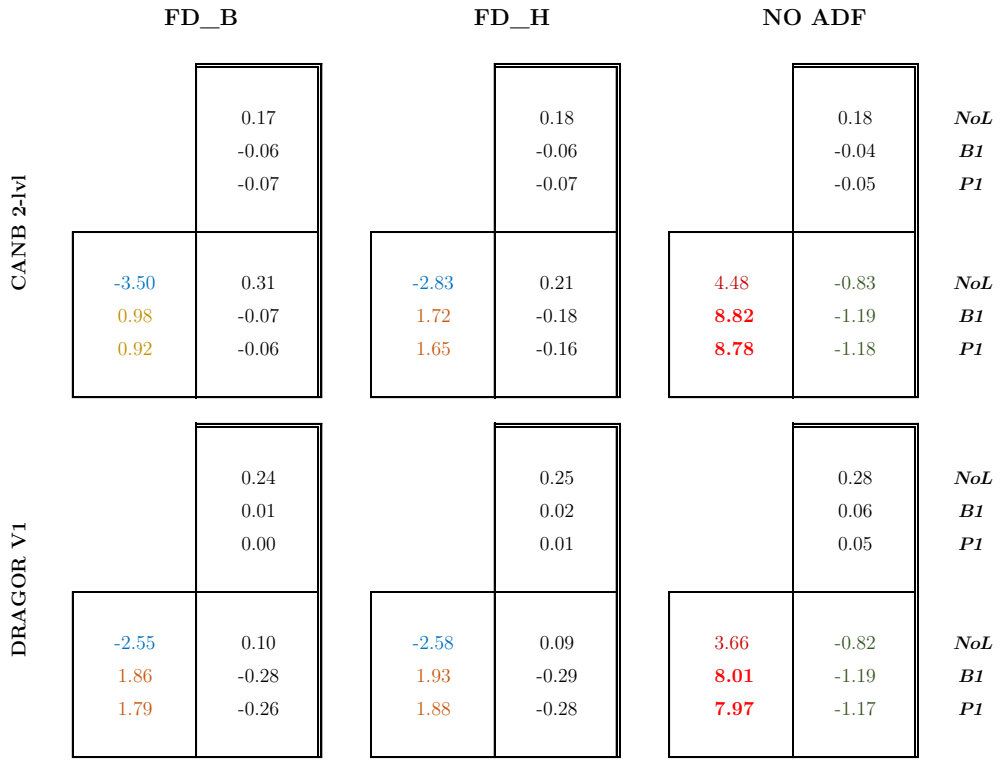

Figure 4.6 Assembly power (% difference) for the UA-UX 3x3 PWR motif as a function of *leakage model* and *ADF* option.

depending on the lattice scheme). It is then interesting to examine the explicit power map (Figure 4.7). Concerning the Canbakan scheme, the net impact induced by the `FD_B` option is particularly remarked along the interfaces of the nodes, if compared to the smoother effect of the `FD_H` one. For the Orion scheme instead, even if the choice of ADF is practically irrelevant, the power map highlights the considerable underestimation of the pin power values in the region surrounding the absorber rods of the central assembly. Bearing in mind the results from the lattice validation, the homogenized cross sections and GFFs may be addressed as a possible source of inaccuracies, since the ADFs can be correlated to a predominant local effect.

In conclusion, a different magnitude concerning the impact of ADF is assessed between the Canbakan design and the *DRAGOR-V1* scheme. The choice of ADF option affects the Canbakan scheme moderately, with a different impact evaluated according to the option. Notably, for B_1 and P_1 models, the `FD_B` choice induces a better effect on the accuracy of the reactivity and the assembly power, while `FD_H` on the reconstructed pin power values. On the other hand, `FD_H` is always the best alternative without leakage.

Table 4.5 Pin power (% difference) for the UA-UX 3x3 PWR motif as a function of *leakage model* and *ADF* option.

		FD_B			FD_H			NO ADF		
		max	**min**	**rms**	**max**	**min**	**rms**	**max**	**min**	**rms**
Canb 2-lvl SPH	NoL	8.14	-1.32	2.06	7.54	-1.32	1.86	8.36	-8.50	1.64
	B1	3.90	-1.58	0.73	3.26	-1.16	0.59	7.98	-11.74	2.40
	P1	3.90	-1.68	0.75	3.24	-1.15	0.59	7.88	-11.88	2.38
DRAGOR-V1	NoL	8.29	-2.30	1.66	8.43	-2.31	1.67	8.55	-5.79	1.58
	B1	4.12	-4.96	0.90	3.90	-4.91	0.89	8.15	-8.96	2.40
	P1	4.02	-4.75	0.87	3.81	-4.71	0.86	8.04	-9.07	2.37

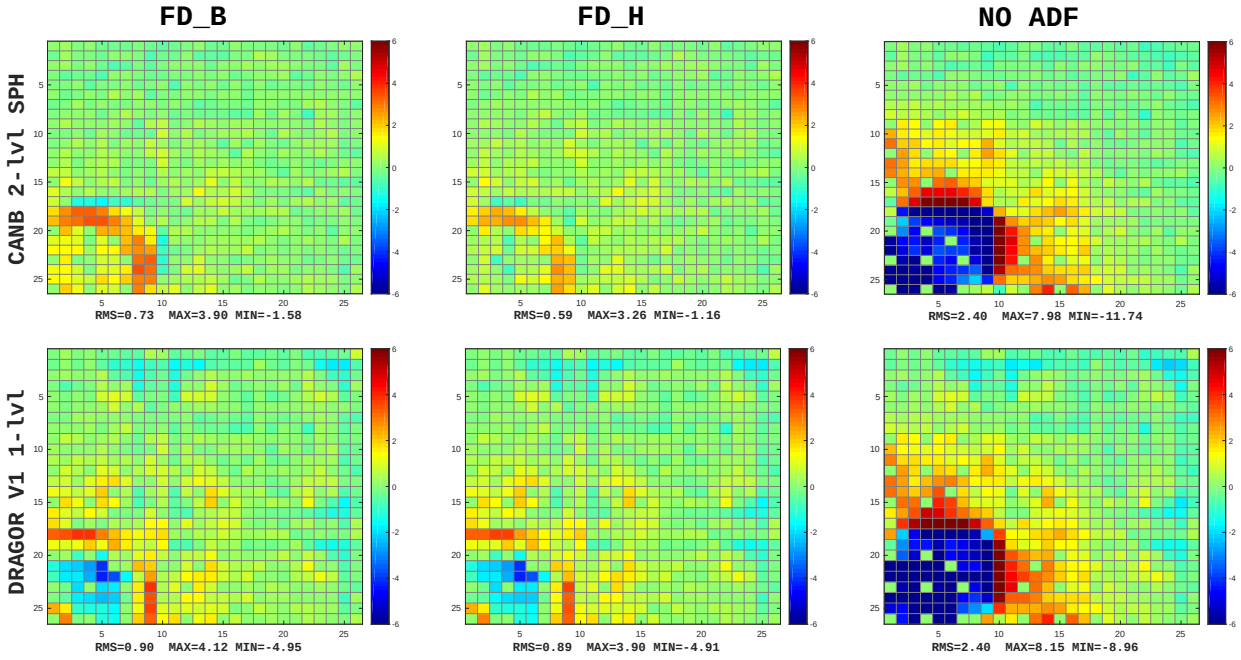

Figure 4.7 Pin power (% difference) error map for the UA-UX 3x3 PWR motif. *Leakage model*=B1.

MX

The second configuration that will be validated is the MX-UX case.

The most precise values for the reactivity are obtained without considering leakage corrections (Table 4.6). Particularly, B_1 and P_1 models induce a decrease in reactivity estimated around 50 *pcm*. The impact of the ADFs is almost negligible for the `FD_H` option (few pcm), while for the `FD_B` case a modest augmentation is observed (around 20 *pcm*). As for the configuration previously presented, the ADF implementation leads to an amelioration of the results when the B_1 or P_1 methods are employed, while it degrades the accuracy on the opposite choice.

Table 4.6 k_{eff} and reactivity [*pcm*] for the MX-UX 3x3 PWR motif as a function of *leakage model* and *ADF* option.

		`FD_B`		`FD_H`		`NO ADF`	
		k_{eff}	$\Delta\rho$	k_{eff}	$\Delta\rho$	k_{eff}	$\Delta\rho$
Canb 2-lvl SPH	`NoL`	1.35781	16	1.35755	2	1.35749	-1
	`B1`	1.35698	-29	1.35670	-44	1.35661	-49
	`P1`	1.35696	-30	1.35668	-45	1.35659	-50
DRAGOR-V1	`NoL`	1.36144	212	1.36126	203	1.36122	201
	`B1`	1.36055	165	1.36036	154	1.36030	151
	`P1`	1.36055	165	1.36036	154	1.36030	151

The assembly power differences are then presented in (Figure 4.8). The magnitude of error in the interior assembly has a high dependence on the leakage model adopted: in the best case, close to 1.0% without leakage, while above 2.4% considering the fundamental mode activated (the *DRAGOR-V1* scheme presents even an higher degradation). The use of the ADFs mostly reduces the discrepancies in the assembly power, regardless of the case considered. Particularly for the MOX assembly, the `FD_H` option leads to an increment in accuracy estimated between 1.0% and 1.4%, while for the `FD_B` case the range is $2.3\% - 3.7\%$. Furthermore, as observed for the UA-UX configuration, only the side UX assembly display a slight refinement (between 0.2% and 0.7%), while the corner one remains nearly unchanged.

Finally, the validation of the reconstructed pin powers values is investigated (Table 4.7). The pin power accuracy reflects the consideration made concerning the assembly power. The absence of leakage correction induces the best overall outcome while the ADF option affects differently the **rms** and the $\boldsymbol{\delta}$ values. Considering first the Canbakan scheme without leakage model implemented, it is worth noting that `FD_B` produces the lower **rms** (=1.10%), while `FD_H` reduces significantly the **max** value compared to the other ADF option (with respect to `NO ADF`, `FD_H` induces an improvement above 3%, while for `FD_B` is lower than 0.5%). This effect can be appreciated in the explicit power map (Figure 4.9), where positive peaks are

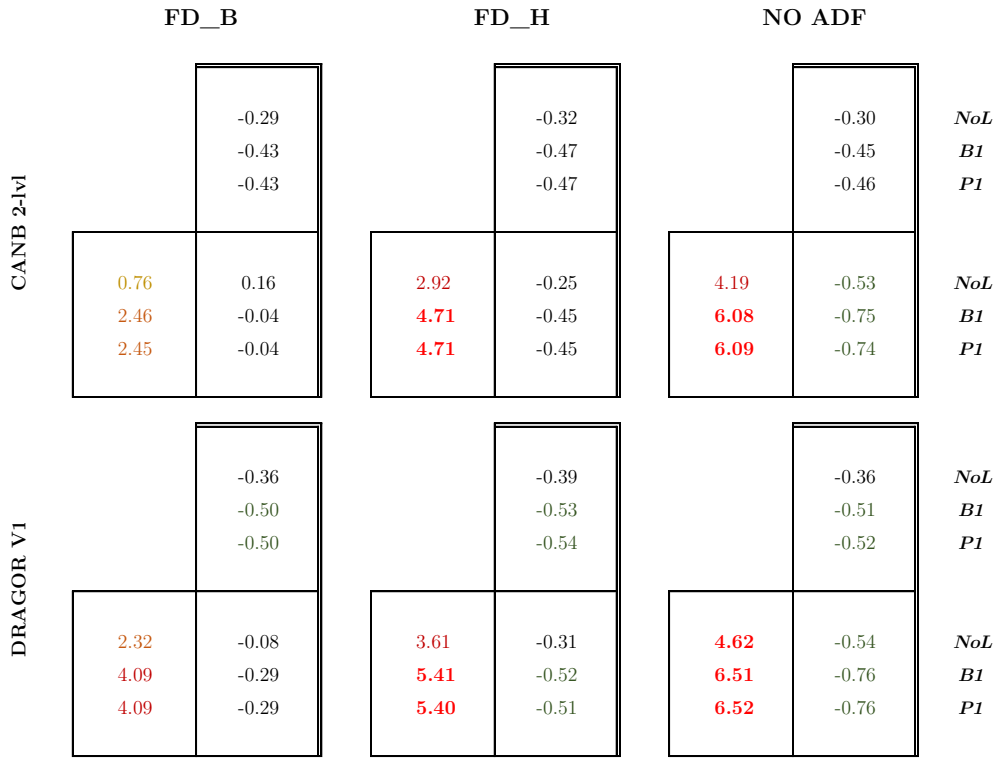

Figure 4.8 Assembly power (% difference) for the MX-UX 3x3 PWR motif as a function of *leakage model* and *ADF* option.

displayed at the interface between the nodes employing the `FD_B` option; it should be noted that instead, `FD_H` induces an extended underestimation of the inner region. For B_1 and P_1 leakage models, the impact of `FD_H` is almost equivalent, while an increased amelioration in the **max** value is observed for the `FD_B` option (around 1.4%). On the other hand, the `FD_B` option represents always the best alternative for the *DRAGOR-V1* design.

In conclusion, as for the UA-UX configuration, the extent of the impact of the ADF varies between the Canbakan and Orion schemes. The impact of the ADFs leads to an amelioration of the **rms** value between 0.4% and 0.7% for the `FD_B` choice, while is reduced between 0.3% and 0.4% for `FD_H` one. On the other hand, the $\boldsymbol{\delta}$ value is usually better represented by the `FD_H` choice, except for the Orion design. The leakage model has an effect only in the reconstructed pin power values, particularly for the maximum value when the `FD_B` option is considered.

Table 4.7 Pin power (% difference) for the MX-UX 3x3 PWR motif as a function of *leakage model* and *ADF* option.

		FD_B			FD_H			NO ADF		
		max	**min**	**rms**	**max**	**min**	**rms**	**max**	**min**	**rms**
Canb 2-lvl SPH	NoL	4.85	-5.74	1.11	1.71	-5.68	1.15	5.15	-7.26	1.54
	B1	3.79	-6.74	1.45	1.94	-7.55	1.72	5.16	-9.25	2.14
	P1	3.75	-6.75	1.44	1.94	-7.58	1.72	5.14	-9.26	2.14
DRAGOR-V1	NoL	2.15	-6.13	1.27	2.00	-7.08	1.51	5.01	-8.33	1.80
	B1	2.12	-8.26	1.79	2.17	-9.26	2.09	5.01	-10.30	2.40
	P1	2.13	-8.28	1.79	2.16	-9.28	2.08	5.00	-10.33	2.40

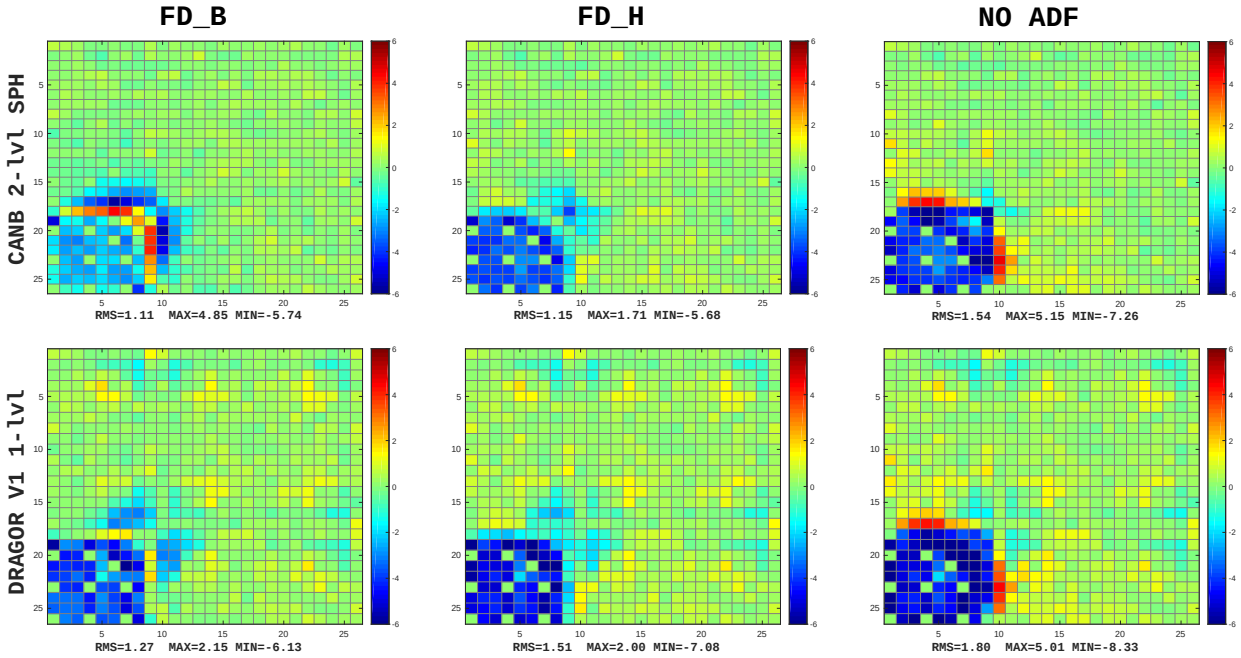

Figure 4.9 Pin power (% difference) error map for the MX-UX 3x3 PWR motif. *Leakage model*=NoL.

4.5 Conclusion

In conclusion, some remarks can be made to address the major sources of discrepancies observed in the results presented in the sensitivity study and during the validation excercise. However, before any consideration, it should be remarked that the computation has been performed with a challenging configuration, where the concentration of boron has been imposed at 0 ppm, and each distinct assembly is far from criticality; this is probably an element that has enhanced the depicted inaccuracies. Several points will be reviewed, and few remarks will be made in an effort to address the foremost sources of imprecision.

Leakage Model

Looking at a realistic configuration adaptable for an industrial application, we should have considered only the results from the B_1 or P_1 homogeneous leakage approximations.

Instead, we opted to present also the results where no leakage approximation is employed, since it generates a better estimation for certain problems, in particular when a MOX assembly is involved. For this configurations, we observed a significant increase in accuracy that involves both the nodal calculation and the reconstruction process. As an example, if we consider the best outcome for the MX-UX configurations for different leakage models, a significant amelioration of the assembly power is exhibited by considering no leakage correction compared to the B_1 or P_1 methods (up to 2% for the MOX assembly). Furthermore, the impact on the **rms** value in the pin power reconstruction is also remarkable (above 0.5% for the cluster 2x2) if no leakage correction is applied on single assembly calculations.

So, although this approximation is hardly applicable for a standard calculation scheme, it exploits the difficulties in the validation of the chosen case of study; it also gives an additional possible comprehension and justification for the imprecisions globally seen. Hence, for certain core configuration, an infinite-lattice approximation in the absence of a leakage correction should be preferred to reduce inaccuracies compared to a corrected spectrum model.

For what concern the P_1 homogeneous model, the general trend is that it produces similar results compared to the B_1 approximation. If we consider the reactivity and the assembly power errors, this assessment is valid for all the configurations analyzed besides limited combinations of calculation options (for example, counting a batch of combinations, only one lattice scheme deviate from the overall bias). The unique validation step in which the P_1 option results marginally more precise than B_1, is observed in the reconstructed pin power maps for the UA-UX 2x2 motif. Moreover, the implementation of ADF is not affected by choice of leakage model, and a similar trend is obtained for the two cases.

It should also mention that the calculation options applied during the validation were sorted according to the overall best outcome of both leakage models. For example, we didn't focus on the separate impact of CDF, MDF or *nodal solver* between the two options.

Hence, even if a recent work strongly supports the use of P_1 rather than the B_1 method[33], for our particular configuration and the methods that we implemented to generate the homogenized parameters, our calculations show comparable solutions coming from the B_1 and P_1 methods. The choice should be then arbitrary.

Finally, a critical leakage model has been tested both for B_1 and P_1 methods. This is the technique usually adopted to perform deterministic simulations on critical reactors. Compared to the method employed, a net degradation has been observed both for the reactivities and the assembly power. On the other hand, the pin power values were slightly more accurate.

ADF

Concerning the ADFs, a distinction should be made according to the leakage model considered.

When B_1 or P_1 models are applied, the implementation of ADFs provides a definite improvement for all calculation schemes under analysis.

Concerning the dehomogenization, it should be then remarked that usually the ADF strongly affects the reconstruction process and tend to increase the peaks along the interfaces, even if the overall outcome is a reduction of the distributed error (decreased in the **rms** deviation). This can be graphically observed for all explicit pin power maps, particularly for the `FD_B` option, that is characterized by a higher magnitude of ADF.

Moving towards the comparison between the two option presented for the ADFs, `FD_B` and `FD_H`, we should recall that the difference between the two options concern the region where the surface flux is recovered (water gap versus the outer pin row). The first assessment is that due to the different magnitude, the `FD_B` option tends to affect mostly the $\boldsymbol{\delta}$ value in the reconstruction process, since it increases the negative and positive error peaks, mostly along the interfaces. Particularly, for the MOX assemblies, it should be underlined the large difference between the values of the ADF for the `FD_B` option (~ 1.4) against the `FD_H` one (slightly above unity).

The outcome then depends on the cluster considered. The `FD_B` option should be generally preferred for the 3x3 motif, for all the configuration and almost for every parameter considered in the validation; only the magnitude of the peak errors is slightly degraded in the dehomogenization. For the configuration containing the rodded assembly, the employment of the ADFs strongly reduces the error in the central part of the motif, leaving only marked

differences at the interface between the UA and UOX assemblies. For the MX-UX case, this impact is less pronounced, and it consists mostly in a slight reduction of the discrepancies in the region of the motif surrounding the central assembly.

Regarding the 2x2 motif, it is more complicated to point out a suggested computation option. A significant limit of the `FD_B` option is displayed at the interface of the MX-UX configuration, where the value are excessively overestimated. Since the `FD_H` are close to unity, for the outer pin row case this effect is almost negligible. In conclusion, for this test case, the `FD_B` option generates more accurate results for the overall nodal solutions, while the `FD_H` is more suited to reduce the error in the reconstruction process.

The inadequacy of the method of computation of ADF is highlighted for this representation; some comment will be made at the end of the chapter. Following the observations made concerning the leakage model, we hypothesize that if the environment is taken into account correctly, a higher effectiveness of ADF should be exhibited.

Finally, when no leakage model is implemented, the effect depends on the chosen assembly and should be evaluated carefully. It's hard to assess a unequivocal impact of the ADF ; the effect tends to be positive for the configurations with MOX assemblies, while their use should be avoided for the rodded ones.

CDF, MDF and GFF

In the study, we presented a broad spectrum of combinations concerning the additional discontinuity parameters required for the dehomogenization process. According to the configuration, they affect the accuracy of the calculation significantly, often soften the peaks that arise in the pin power reconstructed map.

First, we remarked that massive discrepancies over 30% are observed when GFF are not recovered from the lattice calculation. Consequently, their implementation is fundamental in the assessment of the pin power reconstructed values using PARCS.

Concerning CDF and MDF, their impact is less remarkable but is helpful in the refinement of the dehomogenization procedure. As previously discussed, the `FDCM` option is overall the best solution for the MDF, and it may be adopted as a standard for all computations. On the other hand, the choice of the CDF needs to be adjusted to the configuration examined: when assemblies with neutron absorbers are employed, the `FD_C` option results more accurate while with MOX assemblies `FDCP` should be preferred. For the latter, this is probably related to the three zones composition of the Plutonium enrichment; a lower value of CDF seems more suited in this case.

In conclusion, the activation of CDF, MDF and GFF is surely recommended to guarantee the accuracy of the reconstruction.

It should also be remarked that in the case of the *DRAGOR-V1 1lvl* scheme, a volume correction has been applied following the pin power reconstruction, to take into account the dilution of the GFF in the outer row of the assembly due to the inclusion of the water gap in the pin mesh.

Nodal Solver

All the methods currently available with PARCS have been tested during our simulations. Our conclusion is that we should not discriminate the use of the nodal kernel, according to the case analyzed. In fact, during the sensitivity study, we observed that the ANM method should be preferred for both clusters.

It is worth mention that the limitations noted for the NEM method concerning the convergence criteria are probably related to the spatial discretization effect and the inability to actually represent the exact flux distribution at the interface between heterogeneous assemblies.

Lattice scheme

Several lattice schemes have been tested along the validation process to generate more hints for the understanding of the problem. The differences reside in the homogenized cross sections, the homogenized parameters (ADF, CDF and MDF) and the group form functions, and they are also affected by the calculation options chosen during the lattice calculation.

Overall a similarity of the trend is observed between the Canbakan schemes, more or less according to the configuration. The *DRAGOR-V1* scheme instead is the only one displaying a peculiar behavior and a general degradation compared to the other possibilities.

Following the remarks presented in the previous paragraphs, it is then possible to attempt the selection of the calculation options that should be implemented as a possible default standards in the calculation scheme between DRAGON5-PARCS. They are selected among the best overall outcomes achieved between the combination of all the available options.

Hence, is then possible to present a general summary of the results achieved and to have a final comparison of the lattice schemes based on the validation using a “standard” method. We assume that the effects related to the leakage conditions can be separated from the one due to the lattice schemes.

The choices for the computation are given as follows:

- **Leakage Model**: B_1 ;
- **ADF**: `FD_B` ;
- **CDF**: `FD_C` ;
- **MDF**: `FDCM` ;
- **Nodal Solver**: `A2`.

The comparison between lattice schemes is displayed in Table 4.8.

Table 4.8 Comparison of lattice schemes 'default' outcome for configurations UA-UX and MX-UX of 2x2 and 3x3 PWR motifs.

		UA-UX					MX-UX				
	Lattice Scheme	$\boldsymbol{\Delta\rho}$	$\mathbf{rms}_{ass}$	$\boldsymbol{\delta}_{ass}$	$\mathbf{rms}_{pin}$	$\boldsymbol{\delta}_{pin}$	$\boldsymbol{\Delta\rho}$	$\mathbf{rms}_{ass}$	$\boldsymbol{\delta}_{ass}$	$\mathbf{rms}_{pin}$	$\boldsymbol{\delta}_{pin}$
CLU 2x2	*Canb 2-lvl SPH*	-237	0.87	1.74	1.39	5.25	-39	1.33	2.67	2.30	13.75
	DRAGOR-V1	-317	1.36	2.66	1.75	9.88	203	2.21	4.41	2.73	10.46
	Canb 2-lvl w/o SPH	-446	0.54	1.12	1.61	5.83	-157	1.36	2.71	2.33	13.83
	Canb 2-lvl SPH TISO	-211	1.04	2.06	1.34	5.72	19	1.57	3.14	2.38	13.11
	Canb 1-lvl	-141	1.02	2.01	1.32	5.48	109	1.54	3.08	2.50	14.07
CLU 3x3	*Canb 2-lvl SPH*	-90	0.34	1.19	0.73	5.48	-29	0.87	3.01	1.50	10.42
	DRAGOR-V1	41	0.65	2.24	0.90	9.07	165	1.42	4.71	1.79	10.38
	Canb 2-lvl w/o SPH	-222	0.20	0.70	0.86	5.87	-145	0.88	3.04	1.51	10.20
	Canb 2-lvl SPH TISO	-58	0.43	1.47	0.69	5.12	9	1.02	3.47	1.53	10.42
	Canb 1-lvl	-1	0.40	1.39	0.70	5.53	69	0.98	3.38	1.60	10.37

Few considerations can be made. The element that emerges is the overall lack of accuracy presented by the *DRAGOR-V1* scheme compared to the other lattice choices, and it does not seem adequate to be adopted in combination with this core calculation method with PARCS (nodal diffusion solution followed by a dehomogenization procedure).

The choice of using white boundary condition (`TISO` option) generates in most cases a slight degradation of the power distribution; it induces however an amelioration of the discrepancies in reactivity and a reduction of the absolute peaks in the pin power values. The `TSPC` option seems more suited since it produces overall the outcome with a lower value of **rms**, both for the assembly and pin powers.

Concerning the 26-group SPH equivalence, the outcome is affected by the configuration chosen. Compared to the case where this procedure is applied, the nodal solution displays overall a

significant amelioration for the assembly power when rodded assemblies are considered, while for the others elements of validation a slight degradation is usually observed.

The Canbakan single level scheme does not present any distinct advantage with respect to the two-level scheme with SPH, and it is generally less accurate.

In conclusion, the Canbakan two-level scheme with 26-group SPH equivalence using the `FD_B` option seems the overall best alternative to generating proper reactor database for nodal diffusion calculations.

Limit of the Modelization

This work represents a preliminary study for the implementation of a calculation scheme between DRAGON5-PARCS and we did not investigate properly any improvement respect the single assembly calculation performed with DRAGON5.

As an example, the environmental effect is not taken into account, and it can be addressed as the primary source of inaccuracies, particularly for both the MX-UX and UA-UX interfaces.

Actually, the inaccuracies in the core calculation loaded with heterogeneous assemblies originated from the implementation of several approximations in the nodal diffusion calculation.

Several effects are addressed by Downar[34] and should be analyzed for a future improvement of the current methodology:

- Spatial homogenization effect: the infinite-lattice approximation does not account for the environment surrounding the fuel assembly in an actual reactor core. The leakage term that arises at the interfaces of the assembly is poorly represented by the zero current hypothesis that is defined through the reflective boundary condition. Considering, for example, the interface between UOX and MOX assembly, a large thermal flux gradient is generated at the interface due to the differences in the thermal spectrum between the two fuel assemblies. The homogenized cross sections implemented in the diffusion calculation are calculated through infinite-lattice calculation by collapsing the multigroup cross sections using the infinite medium energy-spectrum; however, the exact solution of the heterogeneous problem present a spectrum that deviates significantly respectfully to the infinite single assembly spectrum of each component of the cluster.

- Spatial discretization effect: the current nodal methods may present limitations in the accurate representation of the high thermal flux gradients at the interface between heterogeneous nodes. For example, the quartic polynomial expansion employed for the NEM kernel may predict incorrect solution that may cause increased inaccuracies.

- Energy condensation effect: the two-energy group is a limit in the account of physics effects that happen in intermediate regions of the energy spectrum (like the presence of large resonances for the Pu).
- Transport approximation: the diffusion equation is limited in the representation of the neutron streaming between heterogeneous assemblies. Higher order approximations such SP_3 are more suited to reduce the discrepancies.

The spatial homogenization is probably the primary element that characterized our discrepancies; the single assembly model with reflective boundary condition is a strong limitation, and the environmental effect should be adequately represented.

Over the last three decades, several studies have demonstrated the need for performing corrections to this infinite-lattice homogeneous parameters to mitigate the significant deficiencies that arise in the case of heterogeneous configurations, with large neutron leakage between nodes. Three different approaches are generally considered: correction of the infinite-lattice single assembly computation, mini-core calculation or iterative method between the lattice and core calculation. The last two methods are little-used: the mini-core approach required a particular calculation for each condition that an assembly may face during his operative life, while the iterative process is subjected to an excessive computational burden.

In 1994, Smith proposed the re-homogenization technique[35], a method that does not imply any additional lattice calculation. It is based on the assumption (already adopted for the pin power reconstruction) that the heterogeneous reconstructed flux can be well approximated by the superposition of the flux form function from single-assembly and the flux shape from the nodal calculation. For each global iteration in the nodal calculation, it consists in the recomputation of the homogenized cross section. Based on this work, Pallmtag[36] implemented an empirical correlation method to treat the MX-UX environment.

However, the limit of the previous method is that it does not involve the correction of the assembly discontinuity factor. Rahnema and Nichita[37] then showed the possible inaccuracies that may arise from the rehomogenization of only the cross section and proposed a different method based on the leakage recorrection of all the homogenized parameters. They suggested the parameterization of the leakage effects on the homogenized parameters by assuming a linear behavior of the latter respect the current-to-flux ratio at the node border. The homogenized parameters are tabulated according to perturbation of the boundary conditions.

Following the tabulation approach, Clarno and Adams[38] suggested interpolating the effect induced by neighboring assemblies, in 4 assemblies set such as MOX and UOX, to compute corrected homogenized parameters.

Many other methods have then been proposed and currently belong to a broad spectrum of legacy codes[33, 39]. The main suggestion is to maintain the single assembly framework but to implement a re-homogenization procedure to account for the spatial and spectral effects of the environment.

As for the last remark, it should also be noted that a multigroup SP_3 transport operator can be applied in PARCS, that it may be adequate to the representation of high heterogeneous fluxes. However, it has not been tested during this study.

CHAPTER 5 SIMPLIFIED CORE VALIDATION

This chapter is dedicated to the validation of a simplified PWR core (Figure 5.1), based on the 2-D version of the benchmark c5g7[12]. The core-reflector region represents a challenging problem for deterministic simulation due to the substantial heterogeneity of the neutronic spectrum at the interface between the core and the non-multiplicative region. Therefore an appropriate procedure needs to be applied to account for the sharp alteration in the power distribution introduced by the presence of the reflector.

Historically, the core-reflector region was envisaged using either empirical parameters or predetermined albedo coefficients were imposed as boundary conditions instead of the reflector region[15]. With the advent of 2-group diffusion methods, a further sophistication has been introduced, and explicit reflector nodes have been adopted since then.

The first part of this chapter is committed to the investigation of a technique to model the radial reflector using DRAGON5, such that can be implemented in the calculation scheme DRAGON5-PARCS. The aim is to define equivalent homogenized parameters capable of representing this domain.

Since IRSN is currently developing a standard procedure to proper account the core-reflector region, different alternatives have been explored. At the time the internship took place, a validated methodology was still unavailable hence, of all the possibilities under investigation, we decided to choose one particular methodology that was supposed to suit our calculation scheme adequately. The technique has been proposed by Koebke[40, 41, 42], and it has been applied successfully for PWR nodal diffusion simulation since the late 80's. By now it represents the best alternative evaluated at IRSN. It derives from the application of the nodal equivalence theory for the definition of homogenized parameters, and it is based on a 1-D (slab) representation of a portion of the core-reflector interface.

It should be remarked that at the time the internship took place, the development of the methodology employed by IRSN was still distant from a verified implementation. After the internship, it has been decided to continue the development of the Koebke method starting from the basic approach and design defined by IRSN. Several modifications from the original model have been implemented, and the final method will be presented in this chapter. Following a recent exchange with IRSN, we discovered that meanwhile, IRSN has adopted congruent modifications.

Finally, the proposed method is validated on a simplified core configuration inspired by the

c5g7 benchmark[12]. Moreover, a brief sensitivity study is conducted on the provided reflector model.

5.1 Reflector Modelisation

The 1-D model that we designed for our radial reflector is presented in Figure 5.2.

The region has the spatial dimension of a fuel assembly, and it consists of a stainless steel baffle and a thick water slab. We opted not to include any barrel, in order to define a simpler layout for the validation. The dimension and the material properties has been selected according to guidelines provided by IRSN. The baffle (around $2cm$) is close-fitted to the core, and it borders the water gap of the fuel assembly. On the other hand, the water region filled the remaining space between the limit of the baffle and the edge of the geometry. To account for structural materials, approximately 5% in volume of stainless steel is diluted in the mixture.

It should be remarked that we did not discriminate explicitly between the flat side reflector and the outer corner one (as depicted in Figure 5.1); a pertaining explanation will be held later on in the chapter.

5.1.1 Koebke Approach

The Koebke method is an environment-insensitive reflector model capable of generating equivalent nodal parameters for the radial reflector of a PWR.

The objective is to compute a response matrix representative of the reflector region from one-dimensional (1-D) multigroup transport calculations (so-called spectral calculations), and subsequently, use the computed matrix to define group diffusion coefficients and heterogeneity factors.

The mathematical model employed will be presented in the next paragraphs.

Two-group Analytic Diffusion Solution

The purpose of this paragraph is to derived the solution of the two-group analytic diffusion problem, that is going to be employed for the computation of the response matrix.

Let's consider the steady-state diffusion equation over a control domain in energy group g. The one-speed neutron diffusion equation can be written as[16]:

$$-\nabla \mathbb{D}_g\left(\vec{r}\right)\vec{\nabla}\phi_g\left(\vec{r}\right)+\Sigma_g\left(\vec{r}\right)\phi_g\left(\vec{r}\right)=\sum_{h=1}^{G}\Sigma_{g\leftarrow h}\phi_h\left(\vec{r}\right)+\frac{\chi_g\left(\vec{r}\right)}{K_{eff}}\sum_{h=1}^{G}\nu\Sigma_{f\,h}\left(\vec{r}\right)\phi_h\left(\vec{r}\right) \tag{5.1}$$

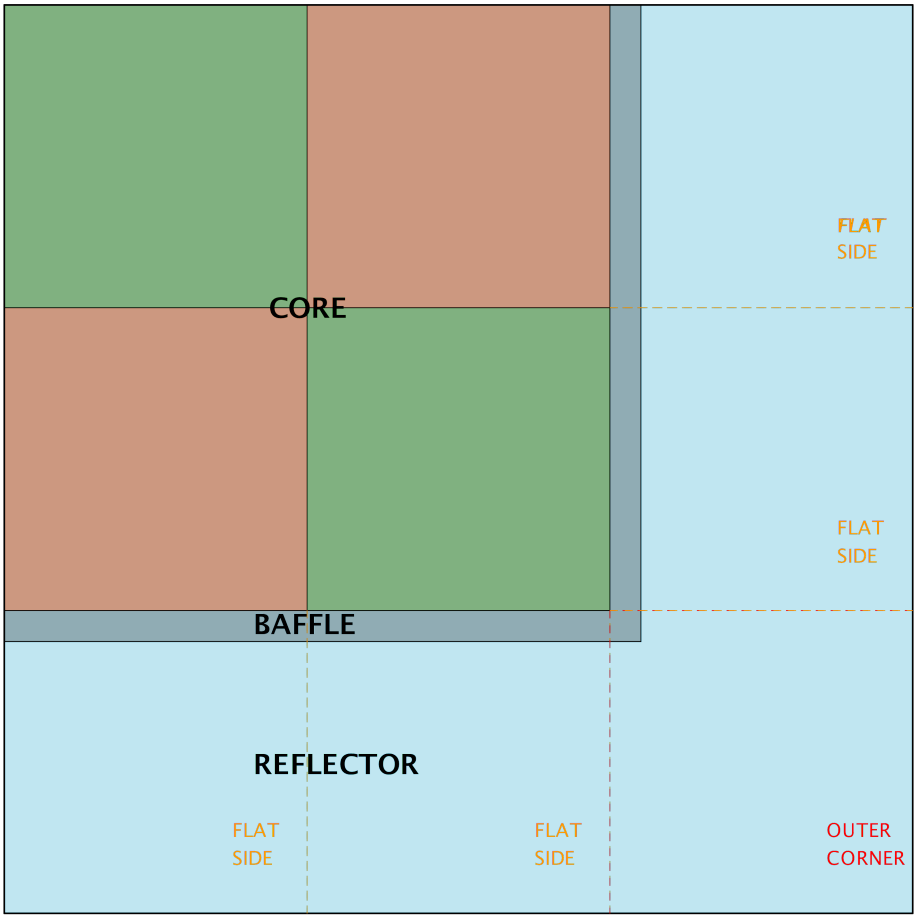

Figure 5.1 Simplified PWR core based on benchmark C5G7.

Let's consider now the particular case when a two group energy-mesh ($G = 2$) is involved. Two approximations can be usually introduced:

1. a neutron cant́ be accelerated from group 2 (thermal) toward group 1 (fast): $\Sigma_{1\leftarrow 2} = 0$;
2. all the secondary neutrons from fission are produced in group 1: $\chi_1 = 1, \chi_2 = 0$.

Assuming moreover that non-directional diffusion coefficients are an acceptable approximation for the calculation, the 2-gr neutron diffusion equation can be written as:

$$\begin{cases} -D_1(\vec{r})\nabla^2\phi_1(\vec{r}) + \Sigma_1(\vec{r})\phi_1(\vec{r}) = \Sigma_{1\leftarrow 1}(\vec{r})\phi_1(\vec{r}) + \dfrac{1}{K_{eff}}\left[\nu\Sigma_{f\,1}(\vec{r})\phi_1(\vec{r}) + \nu\Sigma_{f\,2}(\vec{r})\phi_2(\vec{r})\right] \\ -D_2(\vec{r})\nabla^2\phi_2(\vec{r}) + \Sigma_2(\vec{r})\phi_2(\vec{r}) = \Sigma_{2\leftarrow 2}(\vec{r})\phi_2(\vec{r}) + \Sigma_{2\leftarrow 1}(\vec{r})\phi_1(\vec{r}) \,. \end{cases} \tag{5.2}$$

A simplified 1-D cartesian homogeneous infinite model for the reflector needs to be determined.

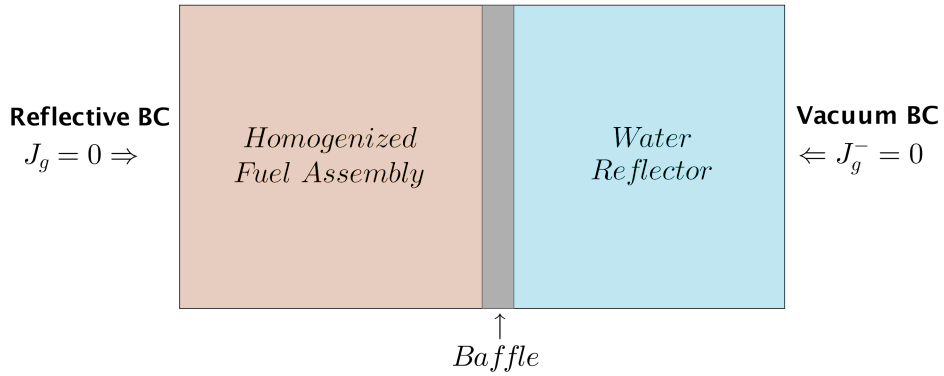

Figure 5.2 1-D model of the radial reflector.

It is a non multiplicative material so $\Sigma_{f\,1}(\vec{r}) = 0$ and $\Sigma_{f\,2}(\vec{r}) = 0$. Furthermore, we assume spatially constant cross sections in the domain (homogenous model).

Before going further, it is useful to simplify the notation. Let's define the total cross section Σ_g as the sum of absorption cross section $\Sigma_{a,g}$ and scattering cross section $\Sigma_{scat,g}$:

$$\Sigma_g = \Sigma_{a,g} + \Sigma_{scat,g} = \Sigma_{f,g} + \Sigma_{capt,g} + \Sigma_{scat,g} \tag{5.3}$$

that in 2-gr results in:

$$\begin{cases} \Sigma_1 = \Sigma_{a,1} + \Sigma_{1\leftarrow 1} + \Sigma_{2\leftarrow 1} \\ \Sigma_2 = \Sigma_{a,2} + \Sigma_{2\leftarrow 2}. \end{cases} \tag{5.4}$$

So the 2-gr neutron diffusion equations for the homogeneous 1-D reflector region can be finally written as:

$$\begin{cases} -D_1\nabla^2\phi_1(x) + [\Sigma_{a,1} + \Sigma_{1\leftarrow 1} + \Sigma_{2\leftarrow 1}]\,\phi_1(x) = \Sigma_{1\leftarrow 1}\phi_1(x) \\ -D_2\nabla^2\phi_2(x) + [\Sigma_{a,2} + \Sigma_{2\leftarrow 2}]\,\phi_2(x) = \Sigma_{2\leftarrow 2}\phi_2 + \Sigma_{2\leftarrow 1}\phi_1(x) \end{cases} \tag{5.5}$$

hence, the system to be solved is:

$$\begin{cases} -D_1\nabla^2\phi_1(x) + [\Sigma_{a,1} + \Sigma_{2\leftarrow 1}]\,\phi_1(x) = 0 \\ -D_2\nabla^2\phi_2(x) + \Sigma_{a,2}\phi_2(x) = \Sigma_{2\leftarrow 1}\phi_1(x). \end{cases} \tag{5.6}$$

Assuming that the flux is null at the extrapolation distance and that the heterogenous flux at

the interface core-reflector is known, the following boundaries condition are defined:

$$\begin{cases} \phi_g\left(x=u\right)=0 \\ \phi_g\left(x=0\right)=\tilde{\phi}_g \end{cases} \tag{5.7}$$

The purpose of the next step is to find an explicit analytic solution for the 2-gr neutron diffusion equation inside the homogeneous reflector region.

Let's start by considering the diffusion equation for the fast energy group:

$$-\nabla^2\phi_1\left(x\right)+\frac{1}{L_1^2}\phi_1\left(x\right)=0 \tag{5.8}$$

where $L_1^2=\dfrac{D_1}{\Sigma_{a,1}+\Sigma_{2\leftarrow 1}}$.

The general solution of this Helmothz equation is a sum of exponential, such that:

$$\phi_1\left(x\right)=c_1e^{-\frac{x}{L_1}}+c_2e^{\frac{x}{L_1}}=\bar{c}_1\sinh\left(\frac{x}{L_1}\right)+\bar{c}_2\cosh\left(\frac{x}{L_1}\right) \tag{5.9}$$

where the more convenient hyperbolic solution is presented, and c_1,c_2,$\bar{c}_1$,$\bar{c}_2$ are constant to be determined. Applying the boundary conditions, the solution of $\phi_1\left(x\right)$ becomes:

$$\phi_1\left(x\right)=\frac{\tilde{\phi}_1}{\sinh\left(\dfrac{u}{L_1}\right)}\sinh\left(\frac{u-x}{L_1}\right) \tag{5.10}$$

On the other hand, for the thermal domain the equation to be solved is the following:

$$-\nabla^2\phi_2\left(x\right)+\frac{1}{L_2^2}\phi_2\left(x\right)=\alpha\phi_1\left(x\right) \tag{5.11}$$

where $L_2^2=\dfrac{D_2}{\Sigma_{a,2}}$ and $\alpha=\dfrac{\Sigma_{2\leftarrow 1}}{D_2}$.

The general solution of this equation can be expressed as the sum of an homogeneous $\phi_2^h\left(x\right)$ and particul $\phi_2^p\left(x\right)$ solution:

$$\phi_2\left(x\right)=\phi_2^h\left(x\right)+\phi_2^p\left(x\right) \tag{5.12}$$

The first element on the RHS is obtained analogously to the fast solution, while the method of Judicious Guessing is applied for the second term. The general solution is then:

$$\phi_2\left(x\right)=\bar{d}_1\sinh\left(\frac{x}{L_2}\right)+\bar{d}_2\cosh\left(\frac{x}{L_2}\right)+\gamma\phi_1\left(x\right) \tag{5.13}$$

where $\gamma = \dfrac{\alpha}{\dfrac{1}{L_2^2} - \dfrac{1}{L_1^2}}$.

In conclusion, consecutive to the application of the boundary conditions, the expression for $\phi_2(x)$ is obtained:

$$\phi_2(x) = \frac{\tilde{\phi}_2 - \gamma\tilde{\phi}_1}{\sinh\left(\dfrac{u}{L_2}\right)} \sinh\left(\frac{u-x}{L_2}\right) + \gamma \frac{\tilde{\phi}_1}{\sinh\left(\dfrac{u}{L_1}\right)} \sinh\left(\frac{u-x}{L_1}\right) \tag{5.14}$$

Definition of Response Matrix

In this section, the response matrix is derived from the two-group analytic diffusion solution previously computed.

First, the response matrix R between the surface fluxes and net currents can be defined at an interface as follows:

$$\phi = \mathbb{R}J \tag{5.15}$$

Applying the Fick's law, a relation between the current and the flux can be computed at the interface core-reflector of the 1-D model:

$$\begin{cases} J_1(x=0) = -D_1 \left.\dfrac{\mathrm{d}\phi_1(x)}{\mathrm{d}x}\right|_{x=0} = \dfrac{D_1}{L_1}\coth\left(\dfrac{u}{L_1}\right)\tilde{\phi}_1 \\ J_2(x=0) = -D_2 \left.\dfrac{\mathrm{d}\phi_2(x)}{\mathrm{d}x}\right|_{x=0} = \dfrac{D_2}{L_2}\coth\left(\dfrac{u}{L_2}\right)\tilde{\phi}_2 + \gamma D_2\tilde{\phi}_1\left(\dfrac{\coth\left(\dfrac{u}{L_1}\right)}{L_1} - \dfrac{\coth\left(\dfrac{u}{L_2}\right)}{L_2}\right) \end{cases} \tag{5.16}$$

The previous equations define a non-linear system where the cotangent term is dependent on the diffusion coefficient. It is then nontrivial to solve directly using the CLE2000 capability as prospected using the methodology developed at IRSN. An approximation on the dimension of the reflector can then be imposed to simplify the problem notably. As proposed by Koebke, we can assume that the width of the water reflector is sufficiently large respect the mean-free-path length of the neutrons in the reflector. As a consequence, since for $u \to \infty$ the cotangent term tend to 1, it is then possible to write the responce matrix $\phi = \mathbb{R}J$ as:

$$\begin{bmatrix} R_{11} & R_{12} \\ R_{21} & R_{22} \end{bmatrix} = \begin{bmatrix} \dfrac{L_1}{D_1} & 0 \\ -\Sigma_{2\leftarrow 1}\dfrac{1}{D_1 D_2}\left(\dfrac{L_2 - L_1}{\dfrac{1}{L_1^2} - \dfrac{1}{L_2^2}}\right) & \dfrac{L_2}{D_2} \end{bmatrix} \tag{5.17}$$

To move forward, a new interface condition is defined to account for the homogenization inaccuracies, based on the Equivalence Theory (ET) by Koebke[40]. This approach is strongly related to the GET, and it will be discussed briefly in the following section.

The homogenous surface flux can then be replaced by the following relation:

$$f_g \tilde{\phi}_g = \phi_g^* \tag{5.18}$$

such that

$$\begin{bmatrix} R_{11} & R_{12} \\ R_{21} & R_{22} \end{bmatrix} = \begin{bmatrix} \dfrac{f_1 L_1}{D_1} & 0 \\ -\Sigma_{2\leftarrow 1} \dfrac{f_2}{D_1 D_2} \left(\dfrac{L_2 - L_1}{\dfrac{1}{L_1^2} - \dfrac{1}{L_2^2}} \right) & \dfrac{f_2 L_2}{D_2} \end{bmatrix} \tag{5.19}$$

Let's assume for now that the elements of the response matrix are already known from previous spectral calculations.

To find the expression for the heterogeneity factors and diffusion coefficients, the previous matrix is then rearranged, and three separate equations are obtained. However, four homogenized parameters (D_1,D_2 and f_1,f_2) need to be computed.

The system can them be solved by imposing a fixed value for one of the parameters to be found. The general approach, reccomended by Koebke[41], is to assume a value $f_1 = 1.0$, considering that no source term exists in the first group.

The system can be re-written to obtain the reflector diffusion coefficients and the thermal heterogeneity factor. Let's consider first the expression of the diffusion coefficients:

$$D_1 = \frac{R_{11}^2}{\Sigma_{a,1} + \Sigma_{2\leftarrow 1}} \tag{5.20}$$

$$D_2 = \frac{R_{22}^2}{f_2 \Sigma_{a,2}} \tag{5.21}$$

Concerning the expression for the thermal heterogeneity factor, few mathematical steps are required. Starting from the expression of R_{21}

$$R_{21} = -\Sigma_{2\leftarrow 1} \frac{f_2}{D_1 D_2} \left(\frac{L_2 - L_1}{\frac{1}{L_1^2} - \frac{1}{L_2^2}} \right) \tag{5.22}$$

$$R_{21} = -\Sigma_{2\leftarrow 1}\frac{f_2}{D_1 D_2}\left(\frac{\left(\frac{D_1}{\Sigma_{a,1}+\Sigma_{2\leftarrow 1}}\right)^{\frac{1}{2}} - \left(\frac{D_2}{\Sigma_{a,2}}\right)^{\frac{1}{2}}}{\frac{\Sigma_{a,1}+\Sigma_{2\leftarrow 1}}{D_1} - \frac{\Sigma_{a,2}}{D_2}}\right) \tag{5.23}$$

$$R_{21}\left[D_2\left(\Sigma_{a,1}+\Sigma_{2\leftarrow 1}\right) - D_1\Sigma_{a,2}\right] = -\Sigma_{2\leftarrow 1}\left[f_2\left(\frac{D_1}{\Sigma_{a,1}+\Sigma_{2\leftarrow 1}}\right)^{\frac{1}{2}} - f_2 D_2\left(\frac{1}{(D_2\Sigma_{a,2})}\right)^{\frac{1}{2}}\right] \tag{5.24}$$

Considering that $R_{22} = f_2\dfrac{1}{(D_2\Sigma_{a,2})^{\frac{1}{2}}}$ and multiplying every term for $(\Sigma_{a,2}\left(\Sigma_{a,1}+\Sigma_{2\leftarrow 1}\right))$, after few mathematical steps the final form is obtained:

$$\begin{aligned}\left[\frac{R_{21}\left(\Sigma_{a,1}+\Sigma_{2\leftarrow 1}\right) - R_{22}\Sigma_{2\leftarrow 1}}{R_{22}^2}\right]\left(\frac{\Sigma_{a,1}+\Sigma_{2\leftarrow 1}}{\Sigma_{a,2}}\right)^{\frac{1}{2}} f_2^2 \\ + \Sigma_{2\leftarrow 1}\left(D_1\Sigma_{a,2}\right)^{\frac{1}{2}} f_2 \\ - R_{21}D_1\Sigma_{a,2}\left[\Sigma_{a,2}\left(\Sigma_{a,1}+\Sigma_{2\leftarrow 1}\right)\right]^{\frac{1}{2}} = 0\end{aligned} \tag{5.25}$$

Finally, a quadratic equation of the form $af_2^2 + bf_2 + c = 0$ needs to be solved to obtain the expression for the thermal heterogeneity factor, where the coefficients are defined as:

$$\begin{cases} a = \left[\dfrac{R_{21}\left(\Sigma_{a,1}+\Sigma_{2\leftarrow 1}\right) - R_{22}\Sigma_{2\leftarrow 1}}{R_{22}^2}\right]\left(\dfrac{\Sigma_{a,1}+\Sigma_{2\leftarrow 1}}{\Sigma_{a,2}}\right)^{\frac{1}{2}} \\ b = \Sigma_{2\leftarrow 1}\left(D_1\Sigma_{a,2}\right)^{\frac{1}{2}} \\ c = -R_{21}D_1\Sigma_{a,2}\left[\Sigma_{a,2}\left(\Sigma_{a,1}+\Sigma_{2\leftarrow 1}\right)\right]^{\frac{1}{2}} \end{cases} \tag{5.26}$$

Comparing the outcome of the diffusion calculation, we took into account only the positive root.

Calculation of the Response Matrix

In the derivation of the expression for the heterogeneity factors and the diffusion coefficients, we have assumed that the element of the response matrix $\mathbb{R}$ were known. Before introducing the method employed for the calculation of these elements, we report few considerations made by Koebke[41] that are useful for the understanding of the environment-insensitive response

matrix approach.

This methodology is based on the assumptions that the response matrix is not influenced by:

- the water density and the thickness of the reflector, if the last one is sufficiently large compared to the mean free path;
- the flux solution of the spectral calculation;
- the state of the neighboring fuel assembly, if the changes in the ratio between microgroup and macrogorup spectral calculations are marginal at the core-reflector interface.

If these conditions are satisfied, it can be assumed that the response matrix is then environment insensitive and depends only on the thickness of the baffle and the boron concentration of the water region in the reflector.

The computation of the response matrix can then be presented.

Let's assume that two spectral calculations have been computed and both the surface fluxes and currents have been extracted.

The response matrix R can be written as a function of these two spectra:

$$\begin{bmatrix} R_{11} & R_{12} \\ R_{21} & R_{22} \end{bmatrix} = \begin{bmatrix} \phi_1^{s_1} & \phi_1^{s_2} \\ \phi_2^{s_1} & \phi_2^{s_2} \end{bmatrix} \begin{bmatrix} J_1^{s_1} & J_1^{s_2} \\ J_2^{s_1} & J_2^{s_2} \end{bmatrix}^{-1} \tag{5.27}$$

The computation of the element of the matrix is then straightforward:

$$\begin{cases} R_{11} = \dfrac{\phi_1^{s_1} J_2^{s_2} - \phi_1^{s_2} J_2^{s_1}}{J_1^{s_1} J_2^{s_2} - J_1^{s_2} J_2^{s_1}} \\ R_{12} = 0.0 \\ R_{21} = \dfrac{\phi_2^{s_1} J_2^{s_2} - \phi_2^{s_2} J_2^{s_1}}{J_1^{s_1} J_2^{s_2} - J_1^{s_2} J_2^{s_1}} \\ R_{22} = \dfrac{\phi_2^{s_2} J_1^{s_1} - \phi_2^{s_1} J_1^{s_2}}{J_1^{s_1} J_2^{s_2} - J_1^{s_2} J_2^{s_1}} \end{cases} \tag{5.28}$$

SET Theory

The GET theory is based on the Equivalence Theory proposed by Koebke[7]. He has been the first to define a new interface condition to be applied in diffusion calculation by the introduction of so-called heterogeneity factor. Equivalent to what has been told in the presentation of the homogenisation problematic, these factors allow to account for the preservation of reaction rate and surface currents from a previous heterogeneous calculation in the nodal diffusion

one. As for the ADF, when symmetric assemblies are considered, and only one direction is characteristic of the behavior of the homogeneous node in the reactor, a simplified approach is introduced where diffusion coefficients and heterogeneity factors are directionally independent. In this framework, the SET theory can then be introduced. It guarantees the preservation of reaction rates for this direction-independent simplified problem. The so-called SET cross section Σ_g^{SET} and diffusion coefficients D_g^{SET} are defined as:

$$\begin{cases} \Sigma_g^{SET} = \frac{\Sigma_g}{f_g} \\ D_g^{SET} = \frac{D_g}{f_g} \end{cases} \tag{5.29}$$

where Σ_g and D_g are flux-volume weighted group cross sections and f_g is the group heterogeneity factor. These SET parameters can then be included in the nodal diffusion calculation without revising the solution method employed by the code.

In conclusion, the flux volume weighted cross section for the reflector need to be renormalized using the heterogeneity factor to produce the required environment-insensitive reflector parameters.

5.1.2 Dragon Reflector Modeling

The method that has been chosen for the development of the reflector model is based on a methodology developed at IRSN, that was available at the time the internship took place.

The first step is the definition of the homogenized parameter of the fuel region in the 1-D model. Depending on the fuel assembly adjacent to the reflector region, a single assembly calculation is performed in infinite-lattice approximation with fundamental mode activated (B_1 homogeneous model). Concerning this point, we observed that the use of a critical leakage model has a positive impact compared to the leakage model with fixed effective multiplication constant. We opted to use the proper adjacent fuel assembly for the definition of distinct homogenized parameters for the reflector. The conclusion from IRSN is that the environmental-insensitive approximation can affect the assembly power with maximum deviation around 0.3%.

At the end of the calculation, the assembly is completely homogenized while the energy group structure is maintained unaltered. The correspondent homogenized parameters are then stored in a macrolib, and the transport calculation on the core-reflector region is initialized. It should be remarked that the 295-gr single-level Canbakan scheme has been employed for this study instead of the ORION design. The nuclear data evaluation considered for the reflector is the same as for the lattice design.

Once the macrolib is generated, containing the mixture for the fuel reflector, the baffle, and the water region, a transport calculation is performed on the 1-D slab geometry employing the discrete ordinates method. Following the indication reported by IRSN, a 16-th order angular discretization of the flux is chosen (S_{16}), with a product of Gauss-Legendre and Gauss-Chebyshev quadrature. A linearly anisotropic scattering source in the laboratory system is adopted. The discretization of the slab is highly refined, notably in the region across the baffle and the initial zone of the water side. A small slice (0.005cm) is defined at the core-reflector (in the baffle) to subsequently recover the surface flux, using the same approach adopted for the definition of the ADF.

Once the transport solution is obtained, the resulting flux is employed to perform two separate spatial homogenizations, first limited to the fuel assembly and then to the reflector region. The first homogenization is performed to compute the current at the interface between the fuel assembly and the reflector, by solving a 1-D balance diffusion equation in the fuel region. This approach takes advantage of the fact that reflective boundary conditions are imposed on the left side of the fuel assembly.

The following expressions are considered:

$$\begin{cases} J_1 = \frac{1}{K_{eff}} \left[\nu\Sigma_{f\,1}\left(\vec{r}\right)\phi_1\left(\vec{r}\right) + \nu\Sigma_{f\,2}\left(\vec{r}\right)\phi_2\left(\vec{r}\right)\right] - \left[\Sigma_1 - \Sigma_{1\leftarrow 1}\right]\left(\vec{r}\right)\phi_1\left(\vec{r}\right) \\ J_2 = \Sigma_{2\leftarrow 1}\left(\vec{r}\right)\phi_1\left(\vec{r}\right) - \left[\Sigma_2 - \Sigma_{2\leftarrow 2}\right]\left(\vec{r}\right)\phi_2\left(\vec{r}\right). \end{cases} \tag{5.30}$$

The second homogenization is then performed on the reflector region to compute the flux-volume weighted homogenized parameters to be included in the reactor database for the non-multiplicative region.

As described in the section regarding SET, two distinct 1-D multigroup transport calculations are required to compute the two-group infinite-reflector response matrix (R) and the flux-volume weighted cross sections. The two different spectra are obtained by considering the same geometry and composition for the reflector and by modifying the boron concentration of the moderator inside the fuel assembly; 600 *ppm* are diluted in the second spectral calculation, while the first one is maintained as the reference value adopted for the lattice validation (0 *ppm*).

Once the two transport solutions are obtained, the diffusion coefficients and heterogeneity factors are computed in terms of the element of the response matrix and the flux-volume weighted cross sections. It should be noted that, following the procedure from IRSN, the absorption and the slowing-down cross sections are evaluated as the average between the two spectral calculations. The renormalized homogenized parameters are then stored directly in a

MULTICOMPO database, before being reprocessed with DONJON and GenPMAXS.

It should be highlighted that the whole procedure for the computation of the response matrix and the definition of the homogenized parameters has been performed directly using the input file of DRAGON and taking advantage of the CLE2000 capability.

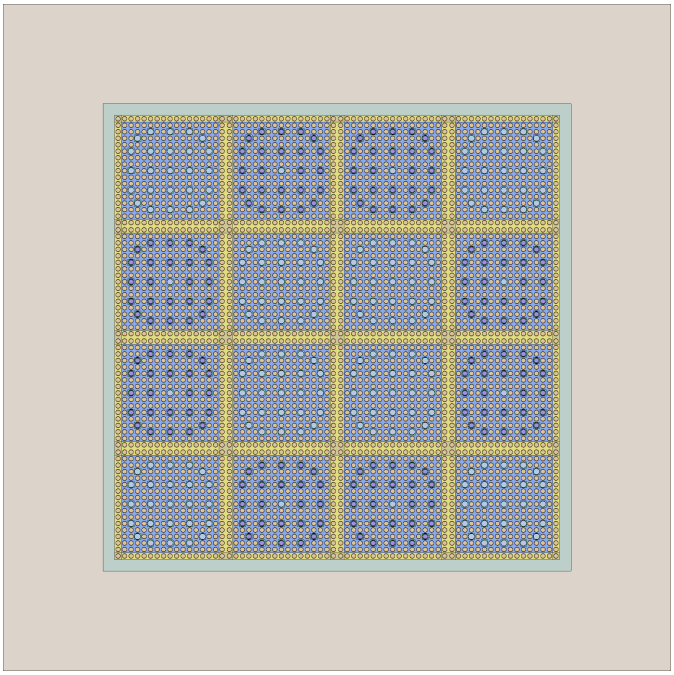

Figure 5.3 Simplified PWR core. MOX (flat sides) and UOX (center & corner) fuel assemblies (geometry output from SERPENT2 computation).

5.1.3 Simplified Core Modeling

The modeling employed for SERPENT2 and PARCS rely on few modifications added to the cluster modelisation to account for the insertion of the non-multiplicative region. To save computational time, in both cases we took advantage of the symmetry of the problem, and we defined quarter-core geometries.

Concerning SERPENT2 we opted to set the whole core by defining a quadrant symmetry through the card usym, and to specify the baffle and the surrounding water region using square surfaces (Figure 5.3). The simulation is again performed with 2000 cycles of 1500000 source neutron each.

The insertion of the reflector nodes in PARCS is trivial and is achieved analogously to the fuel ones. The only significative modification resides in the generation of the PMAX database: the REFLECTOR card need to be activated when the D2P: module is launched, and few keywords

need to be properly set.

5.1.4 Validation of the Simplified Core

The validation is performed employing the calculation options that has been selected at the end of the previous chapter:

CDF: `FD_C` ;

MDF: `FDCM` ;

Nodal Solver: ANM with $2x2$ meshes `A2`.

Furthermore, we maintained the same philosophy adopted before, and we display both the option for the leakage model and the option for the calculation of the ADF.

UX

For the core filled with UX assemblies, a unique trend is displayed by the ADF options `FD_B` and `NO ADF`; this is easily reconducted to the proximity of the first choice to a unity value for the ADFs. On the other hand, the `FD_H` alternative shows a peculiar behavior that we related to the thermal value of the ADF, slightly lower than unity ($= 0.955$).

Concerning the reactivity (Table 5.1), a net overestimation is observed without leakage while a good estimation of the k_{eff} is displayed when either B_1 or P_1 approaches are considered. In particular, the P_1 option is notably less degraded (less than 30 *pcm* compared to the reference).

Table 5.1 k_{eff} and reactivity [*pcm*] for the UX-UX simplified core as a function of leakage model and ADF option. Reference SERPENT2: 1.24432 ± 5pcm.

	FD_B		FD_H		NO ADF	
	k_{eff}	$\Delta\rho$	k_{eff}	$\Delta\rho$	k_{eff}	$\Delta\rho$
NoL	1.24845	266	1.24869	281	1.24850	269
B1	1.24543	72	1.24566	86	1.24547	74
P1	1.24453	14	1.24476	28	1.24457	16

Moving towards the assembly power (Figure 5.4) and the pin power values (Table 5.2), a clear distinction has to be defined between the trend display by the P_1 method compared to the other possibilities. While B_1 and the no leakage approaches are characterized by a uniformity

of behavior, with close discrepancies regardless of the ADF option, the P_1 calculations present significant ameliorations.

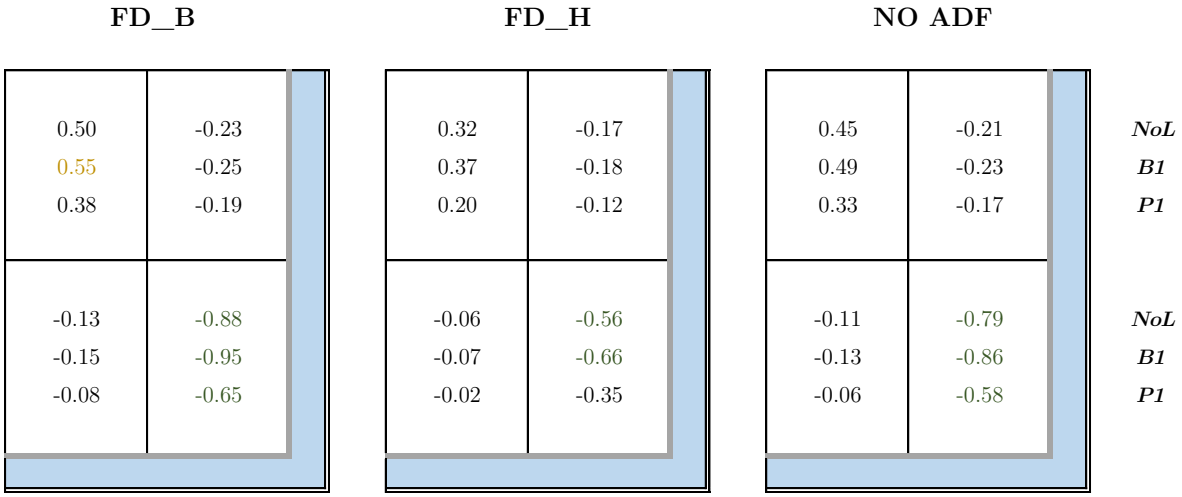

Figure 5.4 Assembly power (% difference) for the UX-UX simplified core as a function of leakage model and ADF option.

In particular, both for the assembly and pin power accuracy, the best outcome is observed with the P_1 leakage model and the `FD_H` option. The impact of the ADFs is minimal due to the homogeneity of the configuration; however, `FD_H` seems overall the best alternative. From the explicit representation of the pin power maps (Figure 5.7), a significant source of discrepancies can be located in the corner pins, the one that faces the corner reflector. This inaccuracy is reasonably due to the 2-D effects originate in the corner region.

Table 5.2 Pin power (% difference) for the UX-UX simplified core as a function of leakage model and ADF option.

	FD_B			FD_H			NO ADF		
	max	**min**	**rms**	**max**	**min**	**rms**	**max**	**min**	**rms**
NoL	14.67	-1.14	1.84	12.76	-1.04	1.40	13.99	-1.10	1.69
B1	14.47	-1.15	1.85	12.56	-1.02	1.42	13.85	-1.11	1.70
P1	13.51	-1.11	1.61	11.60	-1.05	1.19	12.83	-1.08	1.46

UA

Starting from the assessment of the reactivity (Table 5.3), a different behavior is displayed according to the leakage correction and the implementation of the ADF. The impact of the

ADFs can be estimated in 600 *pcm* of gain in reactivity. That being said, when B_1 or P_1 approaches are considered, an initial gap of more than 750 *pcm* is widely reduced by the introduction of the ADFs. On the other hand, without leakage correction, the ADFs leads to a remarkable overestimation of the reactivity (above 550 *pcm*). The difference between `FD_B` and `FD_H` options is around 60 *pcm*.

Table 5.3 k_{eff} and reactivity [*pcm*] for the UA-UX simplified core. Reference SERPENT2: 1.12332 ± 5pcm.

	FD_B		FD_H		NO ADF	
	k_{eff}	$\Delta\rho$	k_{eff}	$\Delta\rho$	k_{eff}	$\Delta\rho$
NoL	1.13098	603	1.13036	555	1.12308	-19
B1	1.12142	-151	1.12068	-210	1.11371	-768
P1	1.12136	-156	1.12060	-216	1.11355	-781

Considering the assembly power (Figure 5.5), it is interesting to remark the impact of the leakage model and moreover, how the choice of ADF affects the tilt of power inside the small core. Without leakage correction and with unity ADFs, the overestimation of the power is located in the assembly facing the side reflector while a depression is displayed both in the corner and the central one. The implementation of the ADFs leads to an inversion of the power distribution in both side and central assemblies. On the contrary, both B_1 and P_1 maintain the same trend despite the introduction of ADF. The impact of the ADFs need to be discriminated for each assembly position: it induces a gain between 2% and 3% for the central and the corner assemblies and more than 6% for the side ones. That means that a clear amelioration from around 8% of discrepancy to less than 2% is achieved with the introduction of the ADFs in the side assemblies when a leakage model is considered. The difference between the ADF options can be estimated in the range between 0.1% and 0.6% according to the position of the assembly in the motif. The corner node is almost insensible to the difference between the two ADF options studied. For this configuration let's also highlight the fact that the P_1 model behaves slightly worst than B_1.

Regarding the pin power discrepancies (Table 5.4), with a leakage correction the improvement in the evaluation of the **rms** value due to the ADF is almost 4% with the `FD_H` option while it decreases of around 0.2% when `FD_B` is considered. Hence, despite what observed in the assembly power, `FD_H` seems the most accurate option. This configuration is characterized by significant high peaks of discrepancies, and the use of ADFs is able only to reduce largely the **min** value. Without fundamental mode, the ADF impact is negative for the **rms** value (gain in inaccuracy around 1%) even if the minimum is notably decreased.

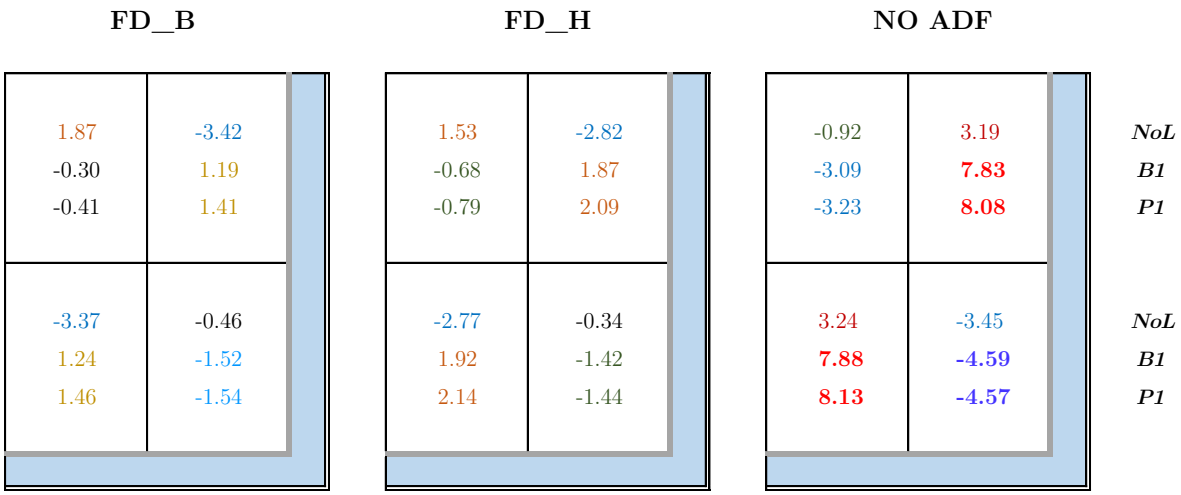

Figure 5.5 Assembly power (% difference) for the UA-UX simplified core as a function of leakage model and ADF option.

Table 5.4 Pin power (% difference) for the UA-UX simplified core as a function of leakage model and ADF option.

	FD_B			FD_H			NO ADF		
	max	**min**	**rms**	**max**	**min**	**rms**	**max**	**min**	**rms**
NoL	13.48	-2.79	4.46	11.25	-2.64	3.93	11.99	-11.83	3.42
B1	14.15	-4.34	2.09	11.99	-5.64	1.88	12.74	-17.90	5.64
P1	13.01	-3.74	1.93	10.85	-5.04	1.65	11.66	-16.81	5.50

MX

The MX-UX core is the last configuration to be considered.

Compared to the previous cases of study, no additional information can be added concerning the accuracy in reactivity (Table 5.5). As previously observed, the leakage model discriminates between over and underestimation of the multiplication factor. The impact of ADF is estimated around 50 *pcm* for the FD_B option, while for FD_H is almost negligible.

Concerning the tilt in the distribution of the assembly power discrepancies, the general trend is again an overestimation of the lateral assemblies, while the corner and central one are deteriorated (Figure 5.6). Only the particular case without leakage and with FD_B option display an opposite trend. It also results in the best outcome due to differences below 0.5% compared to the Monte Carlo reference. According to the position of the assembly, the impact of the ADF option has a wide spectrum of values: it is estimated between 0.4% and 1.1% for FD_H while between 1.5% and 2.0% for the FD_B option.

Table 5.5 k_{eff} and reactivity [pcm] for the MX-UX simplified core. Reference SERPENT2: 1.17388 ± 5pcm.

	FD_B		FD_H		NO ADF	
	k_{eff}	$\Delta\rho$	k_{eff}	$\Delta\rho$	k_{eff}	$\Delta\rho$
NoL	1.17899	369	1.17836	324	1.17825	316
B1	1.17425	27	1.17358	-22	1.17348	-29
P1	1.17370	-13	1.17303	-62	1.17293	-69

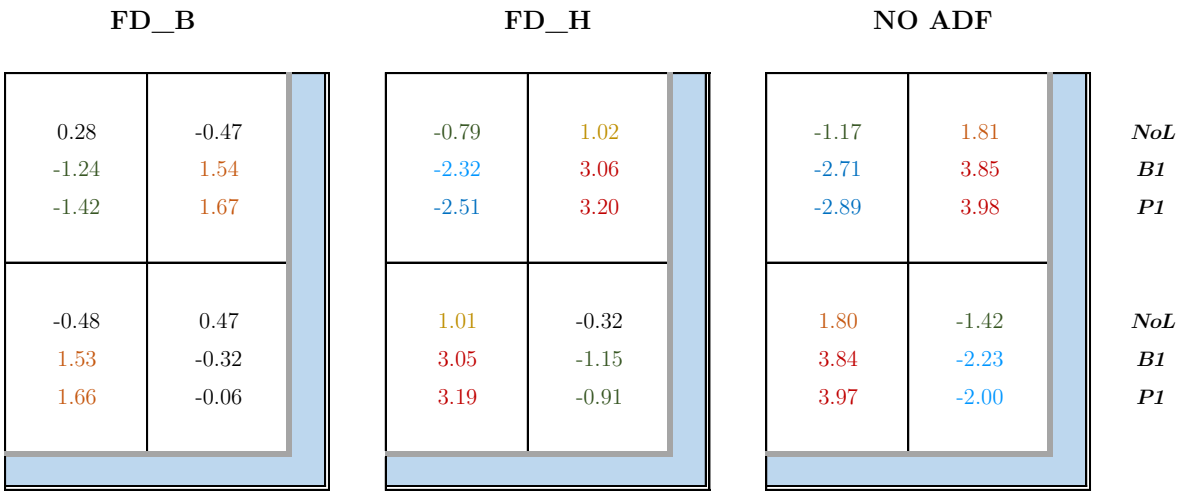

Figure 5.6 Assembly power (% difference) for the MX-UX simplified core as a function of leakage model and ADF option.

In conclusion, the pin power reconstructed values present remarkable negative and positive peaks, constantly above 7.5% such that they reflects in the overall large **rms** values (Table 5.6). The gain associated with the ADFs for B_1 and P_1 approaches is lower than 1% for the **rms** value, as the best case. When no leakage correction is applied the FD_H results in the most accurate, and it displays the lower inaccuracies.

Table 5.6 Pin power (% difference) for the MX-UX simplified core as a function of leakage model and ADF option.

	FD_B			FD_H			NO ADF		
	max	**min**	**rms**	**max**	**min**	**rms**	**max**	**min**	**rms**
NoL	15.02	-10.13	2.21	12.88	-7.77	1.78	14.02	-9.65	2.34
B1	15.47	-9.66	2.83	13.32	-7.41	3.17	14.46	-10.83	3.72
P1	14.33	-9.76	2.80	12.19	-7.65	3.19	13.33	-11.07	3.72

5.2 Sensitivity Study on Koebke Method

Two options in the calculation of the reflector parameters have been tested and are here proposed.

5.2.1 Definition of Fixed Homogenized Parameter

During the derivation of the mathematical model proposed by Koebke, it has been observed that a system of three equations with four unknowns is obtained. A predetermined value needs to be assigned for either the heterogeneity factors or the diffusion coefficients. The method adopted during the validation of the core was to assign a unity value for the fast heterogeneity factor as proposed by Koebke[41].

Besides, other possibilities can be contemplated. Muller[42] suggested that the most straightforward alternative is to impose a value for the diffusion coefficient in the fast energy group, using a flux-volume weighted parameter.

In accordance with this idea three different approaches are examined based on:

1. B1 homogeneous leakage model ;
2. Transport XS ;
3. B1 heterogeneous ECCO model.

The former is the same methodology adopted for the computation of diffusion coefficient for fuel assembly reactor databases. It should be noted that the leakage model is applied on the geometry assembly-reflector, and as a consequence also the diffusion coefficient is unique for the whole region.

The transport XS approach consists of computing the diffusion coefficient as:

$$D_g = \frac{1}{3\Sigma_{tr,g}} \tag{5.31}$$

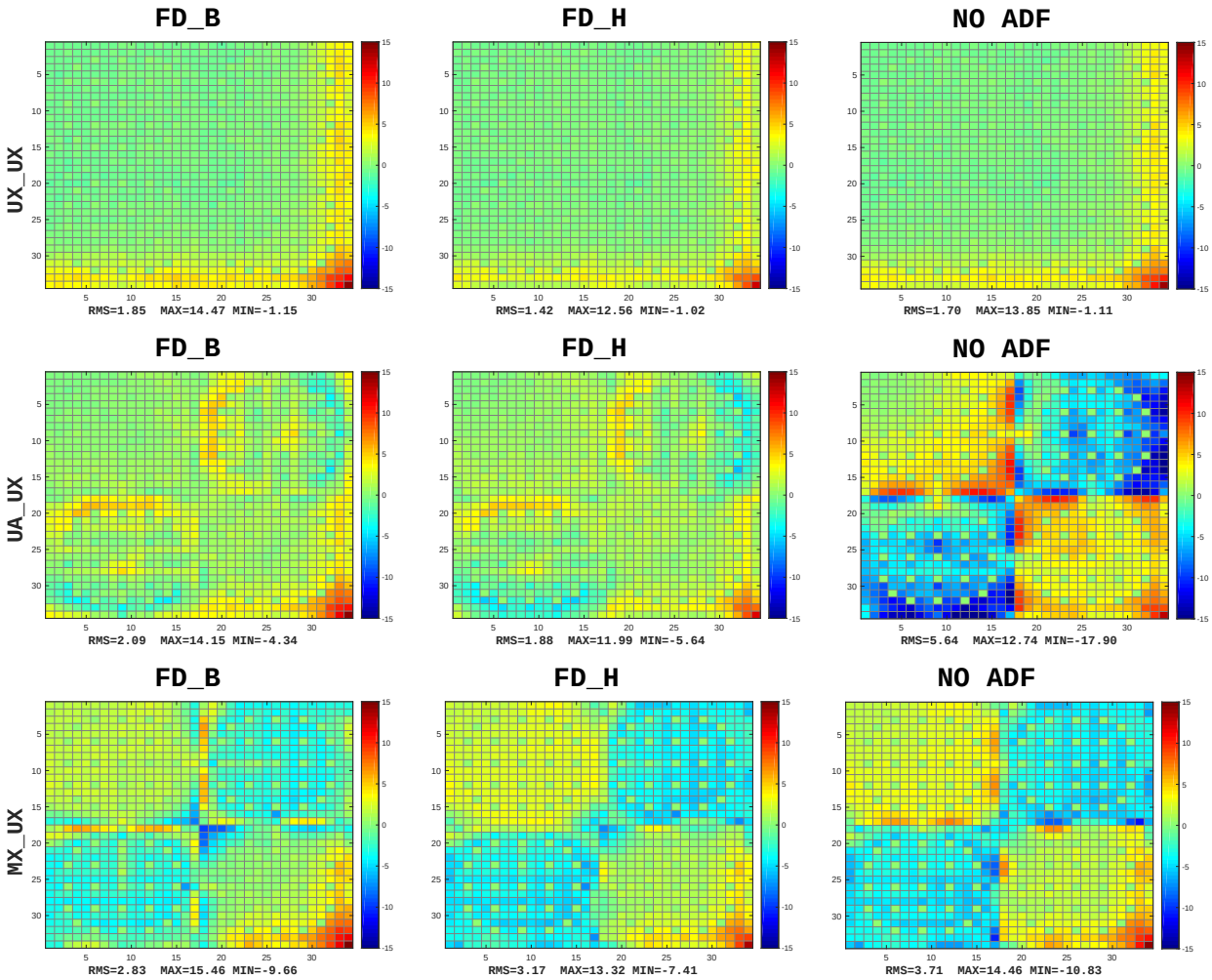

Figure 5.7 Pin power (% difference) error map for the simplified core. *Leakage model*=B1.

where the transport cross section $\Sigma_{tr,g}$ is evaluated as the subtraction of linearly anisotropic component of the scattering cross section $\Sigma_{g,s1}$ from the total cross section ($\Sigma_{tr,g} = \Sigma_g - \Sigma_{g,s1}$).

The last alternative is the computation of the diffusion coefficient using the ECCO heterogeneous leakage model. This method has been developed to represent better the effect of scattering anisotropy on the leakage rate. The main advantage of this method is the possibility to obtain separate diffusion coefficients for the fuel and reflector region, so as to compute improved local parameters.

It should be noted that to employ the ECCO leakage model, reflective boundary conditions need to be applied at both side of the geometry. To simulate the void boundary conditions an absorber slab of approximately half the dimension of the assembly has been located on the right side of the geometry; it is composed of a mixture of Vanadium and Cadmium. To define the proper geometry and composition, plus to evaluate the quality of this absorber, a Monte Carlo simulation with an explicit representation of the geometry has been conducted and both the k_{eff} and the flux distribution along the geometry has been assessed. To reduce the amount of information inserted in this study, we opted to present briefly only one configuration (UX-UX) and to include the remaining results in the appendices.

Before examining the outcome of the diffusion simulation is worth observing the actual value of the computed parameters, after being renormalized using the heterogeneity factors. These are the reflector homogenized parameters that are used in the diffusion calculation (Table 5.7).

Table 5.7 Reflector homogenized parameters for UX configuration.

	f_1	$B_{1,HOMO}$	Σ_{tr}	$B_{1,ECCO}$
$\Sigma_{t,1}$	2.977E−02	2.575E−02	3.014E−02	2.362E−02
$\Sigma_{t,2}$	2.116E−01	1.830E−01	2.142E−01	1.571E−01
$\Sigma_{a,1}$	1.946E−03	1.683E−03	1.970E−03	1.545E−03
$\Sigma_{a,2}$	2.116E−01	1.830E−01	2.142E−01	1.571E−01
$\Sigma_{2\leftarrow1}$	2.782E−02	2.407E−02	2.817E−02	2.207E−02
D_1	9.084E−01	1.050E+00	8.973E−01	1.090E+00
D_2	1.528E−01	1.766E−01	1.509E−01	2.425E−01
f_1	1.000E+00	1.156E+00	9.877E−01	1.287E+00
f_2	1.132E−01	1.309E−01	1.118E−01	1.514E−01

The option that derives from the transport cross section is the closest to the standard Koebke choice ($f_1 = 1$), with a difference lower than 1.5%. Concerning the leakage option, the differences become quite important, and the general trend is the overestimation of the diffusion coefficient that is counterbalanced by an opposite tendency for the cross sections (both absorption and removal). Notably, the variations are around 15% for the B1 homogeneous

model and above 20% for the heterogeneous one. For the latter, the difference in the evaluation of the thermal diffusion coefficient is around 60%.

Let's consider now the results from the diffusion calculation (Tables 5.8, 5.9 and Figure 5.8). For a matter of simplicity, we are going to consider only the outcome from fuel assemblies computed using B_1 leakage model.

Table 5.8 k_{eff} and reactivity $[pcm]$ for the UX-UX simplified core. Comparison between different methods to compute Koebke homogenized parameters. Reference SERPENT2: 1.24432 ± 5pcm.

	FD_B		FD_H		NO ADF	
	$\boldsymbol{k_{eff}}$	$\boldsymbol{\Delta\rho}$	$\boldsymbol{k_{eff}}$	$\boldsymbol{\Delta\rho}$	$\boldsymbol{k_{eff}}$	$\boldsymbol{\Delta\rho}$
$\boldsymbol{f_1}$	1.24543	72	1.24566	86	1.24547	74
$\boldsymbol{B_{1,HOMO}}$	1.24525	60	1.24548	75	1.24529	63
$\boldsymbol{\Sigma_{tr}}$	1.24544	73	1.24567	87	1.24548	75
$\boldsymbol{B_{1,ECCO}}$	1.24601	109	1.24626	125	1.24606	112

Considering the standard Koebke method as the reference for this discussion, the first observation is the negligible impact of using the transport cross section instead of fixing unity value for the fast heterogeneity factor. The outcome is almost identical in the two cases.

The B1 homogeneous approach instead induces a constant degradation of almost all the elements considered for the validation. The fact of considering a unique core-reflector homogenized region in the definition of the fast diffusion coefficient to some degree induces a negative impact on the definition of proper homogenized parameters.

The most interesting result is obtained with the B1 ECCO model. It represents the most accurate alternative concerning the power distributions (Figure 5.8 and Table 5.9). From the comparison of the assembly power distribution and the discrepancies observed in the pin power, it can be assumed that the main advantage of this method is a specially improved treatment of the corner fuel assembly, the most critical part of all the configurations.

In conclusion, despite the increased computational time required for the calculation, it may be worthwhile to consider this method to improve the accuracy of the reflector homogenized parameters.

5.2.2 Two-dimensional Effect

A final remark should be then made concerning the so-called two-dimensional (2-D) effect, a consequence of the inadequacy of the 1-D model to represent the corner reflector region.

This backlash is primarily observed when two different fuel assemblies face a corner reflector.

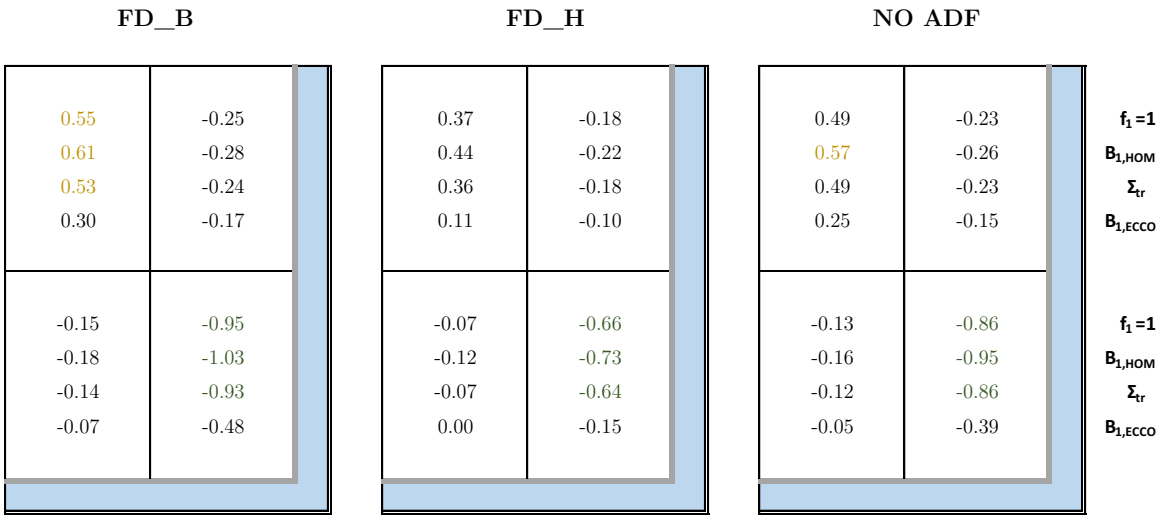

Figure 5.8 Assembly power (% difference) for the UX-UX simplified core as a function of leakage model and ADF option. Compared to reference SERPENT2.

Table 5.9 Pin power (% difference) for the UX-UX simplified core. Comparison between different methods to compute Koebke homogenized parameters.

	FD_B			FD_H			NO ADF		
	max	**min**	**rms**	**max**	**min**	**rms**	**max**	**min**	**rms**
$\boldsymbol{f_1}$	14.47	-1.15	1.85	12.56	-1.02	1.42	13.85	-1.11	1.70
$\boldsymbol{B_{1,HOMO}}$	13.31	-1.19	1.91	11.40	-1.05	1.47	12.69	-1.15	1.76
$\boldsymbol{\Sigma_{tr}}$	14.60	-1.15	1.85	12.69	-1.01	1.41	13.92	-1.10	1.70
$\boldsymbol{B_{1,ECCO}}$	10.65	-1.15	1.44	8.60	-1.14	1.01	9.97	-1.12	1.28

In our case, however, the fuel assemblies are not connected directly to the outer reflector, and we supposed that the misevaluation of the baffle is probably the main concern, particularly for the reconstructed pin power value in the corner assembly.

Two approaches can be considered to account for this issue: use additional empirical factors or perform 2-D spectral calculations[42]. Since in the GenPMAXS manual[32] a correction of the down-scattering is proposed, we decided to test the implementation of this technique. The correction factor is defined as:

$$corr_{2D} = \frac{L_{fa} - L_{baf}}{L_{fa}} \tag{5.32}$$

where $corr_{2D}$ is the correction factor, L_{fa} the lattice assembly pitch and L_{baf} the baffle width.

We implemented this correction by multiplying the down scattering cross section of the corner reflector for the previously defined factor. We observed just a little improvement in our calculations, in the range of few pcm in reactivity and few tens of percent for the assembly and pin powers. This modification does not have a significant impact on the accuracy.

5.3 Conclusion

This chapter has been dedicated to the development of a reflector model to be implemented in the calculation scheme DRAGON5-PARCS, and to the validation on a simplified PWR core.

The chosen method is the one proposed by Koebke for the generation of environment-insensitive reflector parameters. It involves the computation of heterogeneity factors in terms of a characteristic response matrix and flux-volume weighted homogenized parameters. These heterogeneity factors are then used to re-normalized the homogenized parameters that will be utilized in the nodal diffusion calculation.

The primary conclusion is that the implemented reflector model is giving interesting results concerning the accuracy in reactivity and assembly power, with a good agreement compared to the Monte Carlo reference. Taking into account that a small reactor has been examined, discrepancies in assembly power below 2% (in the worst case), have to be considered as a promising result.

The less positive outcome is that a significant degradation is observed in the pin power reconstruction process along the core-reflector interface, especially in the corner assembly adjacent to the reflectors. For the latter, a two-dimensional effects may be of primary importance in the wrong evaluation, and a corrective method should be developed.

The most likely explanation for the degradation of the core-reflector interface is that the

infinite-lattice approximation employed for the computation of GFF play a central role in this issue: this region diverges deeply from the adopted approximation and should be treated separately in the transport calculation. The silver lining can then be found by considering the UX-UX configuration: it is strictly a local effect, and it has a minor impact on the inner part of the core, and so in the core power distribution. That being said, the refinement of the reflector model and the definition of improved GFF at the interface core reflector may lead to a significant reduction of these inaccuracies.

Concerning the ADF, a largely positive impact can be assessed for the core calculation when the fundamental mode is activated during lattice calculation. The magnitude of amelioration is consistent with what obtained in the previous chapter. Actually, the reflector parameters are already re-normalize before being employed in the diffusion calculation, so they are not involved whether the ADF are activated or not in the diffusion calculation. Not much additional information can be gathered concerning the impact of ADF compared to the previous cases.

A remark should be instead made regarding the impact of the P_1 leakage model on the corner assembly and the significant reduction of the tilt in the assembly power. Actually, it results in the most accurate alternative, and it allows a significant reduction of the peak pin power values in the corner region.

At the end of the present chapter, a brief investigation for an amelioration of the standard Koebke method has been examined. An interesting outcome has been displayed when the ECCO leakage model is adopted to increase the accuracy in the evaluation of the diffusion coefficient in the fast domain.

CHAPTER 6 CONCLUSION

A calculation scheme has been implemented between the lattice code DRAGON5 and the nodal code PARCS, and the pin power reconstruction has been tested. Five lattice schemes have been studied, and a reactor database containing the homogenized parameters have been created in each case to perform the nodal diffusion calculation. The scheme DRAGON5-PARCS has been examined initially on a 2x2 and 3x3 motifs, and subsequently on a simplified core configuration based on the benchmark c5g7. All the results have been validated with a stochastic calculation using SERPENT2.

The first part has been dedicated to the validation of the lattice scheme used to generate the homogenized parameters required for the nodal calculation. These calculations have been performed on a single assembly in infinite lattice approximation considering different leakage models. A comparison of the lattice schemes currently adopted by EPM and IRSN was shown, and a preliminary investigation of the sources of discrepancies has been conducted.

The second part of the work focuses on the validation of the diffusion calculation performed with PARCS and the analysis of the influence of the leakage model and the methodology to compute ADF on the nodal solution and the pin power reconstruction process. The diffusion calculations have been executed on a simplified core configuration to treat issues where the environmental effects are particularly enhanced. Several limitations of the implemented model derive from the infinite-medium approximation used to perform the lattice calculation.

The final chapter focuses on the introduction of an adequate reflector methodology for the calculation scheme DRAGON5-PARCS and the validation on a simplified PWR core. The method proposed by Koebke was chosen to generate the reflector reactor database, and was implemented using the lattice code DRAGON5. Positive results were obtained both in the accuracy of reactivity and the assembly power distribution. On the other hand, regarding the reconstructed pin power values, some issues were observed at the core-reflector and in the corner zone. In this case, a two-dimensional effect may be accounted as a main contributor in the inaccuracies.

Besides the implementation of the calculation scheme, the main result of this study was to observe the net impact of the use of ADF with regard to the assembly power map and the reactivity. Moreover, the positive influence of the ADFs was assessed for the reconstruction process. The magnitude of the improvement varies for each particular case, as shown in the comparison between the UA-UX and the MX-UX cluster and core configurations.

Regarding the leakage model, the P_1 approximation shown similar results compared to the B_1 option, the choice should then be arbitrary. Only in the core validation, a remarkable improvement has been observed by using the P_1 approach to increase the accuracy in the corner assembly and subsequently to reduce the tilt in the power distribution. Even if it may present better results in some particular case, the calculation without leakage model has not been finally considered due to its applicability in a practical reactor. In fact, the multiplication factor that can be obtained is usually distant from the one of a realistic core, and a critical spectrum is not achieved.

In conclusion, the Canbakan two-level scheme with SPH using the `FD_B` option seems the overall best alternative to generating proper reactor database for nodal diffusion calculations. On the other side, the *DRAGOR-V1 1lvl* scheme does not present sufficient accuracy to be adopted in combination with this core calculation method.

Several alternatives for the calculation has been examined, and a combination of options have been proposed for the DRAGON5-PARCS calculation scheme. It should also be recalled that this is a preliminary investigation in the coupling between DRAGON5 and PARCS. Either way, important tests have been conducted to verify the efficiency of the calculation scheme. The primary sources of error have been analyzed and will be addressed for future improvements of the model.

6.1 Perspectives

Since the current work was dedicated to the implementation of a first calculation scheme between DRAGON5 and PARCS (unique association in the deterministic code panorama performed at LNR), several problematics have been faced, and several limitations in the modeling have been considered. Few suggestions are then considered for the near future amelioration of the current method.

6.1.1 Treatment of Environment Effect

The infinite-lattice approximation has been one of the major element in the refinement of our calculation scheme. In the fourth chapter, we highlighted several approaches that have been studied to account for this problematic, and we suggested to direct the next effort to the definition of a technique that would provide for the re-normalization of the homogenized parameter generated using an infinite-lattice approach.

In the immediate next future, it would also be interesting to test cluster geometries to estimate the inaccuracies induced by this environmental effect, as a preliminary study for the

development of an adequate technique to be included in the calculation scheme.

Following a similar approach, to account for the inaccuracies at the MX-UX interface, lattice calculations on an eight of assembly should be performed including additional rows of a UX assembly. Since the zero net current approximation would lose validity, the main concern would be the evaluation of appropriate homogenized parameters.

6.1.2 Reflector Modeling

The next step for the amelioration of the calculation scheme is probably to consider the methodology suggested in the GenPMAXs manual for the generation of the reflector equivalent nodal parameters. They suggest computing appropriate discontinuity factors for the reflector by performing a diffusion calculation on a 1-D reflector node using the same nodal methods as the one employed in PARCS for the refinement of the coupling coefficients. To define these unique homogenous solution, currents and surface fluxes are required from a previous transport calculation performed on a core-reflector cell.

By now a heterogeneous geometry has already been developed using the DRAGON5 lattice code. However, the `D2P:` module is currently unable to guarantee the flux of information between DRAGON5 and GenPMAXS required to access this option successfully. Few modifications will be implemented in the near future to allow for this capability. The same methodology can be employed to account for the impact of neighboring fuel assemblies.

6.1.3 Validation on a Realistic PWR Core

The last step is to consider the validation on a realistic PWR reactor, where the large dimension can reduce some discrepancies that have been observed in our simplified core model; furthermore, a critical reactor could be interesting to reduce the impact of the leakage approximation.

REFERENCES

[1] S. Pignet et al. The IRSN ORION project: development of new capabilities for neutronics deterministic simulations dedicated to safety analysis. In *Conference: PHYSOR 2016, Unifying Theory and Experiments in the 21st Century, At Sun-Valley, Idaho, USA*, 2016.

[2] Richard Sanchez, Igor Zmijarevi, Mireille Coste-Delclaux, Emiliano Masiello, Simone Santandrea, Emanuele Martinolli, Laurence Villate, Nadine Schwartz, and Nathalie Guler. APOLLO2 year 2010. *Nuclear Engineering and Technology*, 42(5):474–499, 2010.

[3] Alain Hébert. DRAGON5 and DONJON5, the contribution of École polytechnique de Montréal to the SALOME platform. *Annals of Nuclear Energy*, 87, Part 1:12–20, 2016.

[4] Joel Rhodes, Kord Smith, and Deokjung Lee. CASMO-5 development and applications. In *Proc. ANS Topical Meeting on Reactor Physics (PHYSOR-2006)*, pages 10–14, 2006.

[5] JJ Lautard, S Loubière, and C Fedon-Magnaud. CRONOS: a modular computational system for neutronic core calculations. In *IAEA Specialists Mtg. on Advanced Calculational Methods for Power Reactors, Cadarache, France, September 10-14 (1990)*, 1990.

[6] T Downar et al. PARCS v2. 6 US NRC core neutronics simulator theory manual. *Purdue University/NRC*, 2004.

[7] Kord S Smith. Assembly homogenization techniques for light water reactor analysis. *Progress in Nuclear Energy*, 17(3):303–335, 1986.

[8] Richard Sanchez. Assembly homogenization techniques for core calculations. *Progress in Nuclear Energy*, 51(1):14–31, 2009.

[9] Rémi Maurice Jean Vallerent. Développement et validation de schémas de calcul à double niveau pour les réacteurs à eau sous pression. Master's thesis, École Polytechnique de Montréal (Canada), 2009.

[10] A. Canbakan and A. Hébert. Accuracy of a 2-level scheme based on a subgroup method for pressurized water reactor fuel assembly models. *Annals of Nuclear Energy*, 81:164–173, 2015.

[11] Richard Chambon. Implementation of pin power reconstruction capabilities in the DRAGON system. Technical Report IGE-349, École Polytechnique de Montréal (Canada), 2015.

[12] EE Lewis et al. Benchmark specification for deterministic 2-d/3-d MOX fuel assembly transport calculations without spatial homogenization (C5G7 MOX). *NEA/NSC*, 2001.

[13] Rachid Sekkouri. *Analyse des différentes techniques d'homogénéisation et des schémas de calcul du cœur des réacteurs à eau sous pression*. PhD thesis, Université de Paris 11, 1995.

[14] Jaakko Leppänen. Serpent–a continuous-energy Monte Carlo reactor physics burnup calculation code. *VTT Technical Research Centre of Finland*, 4, 2013.

[15] R.J.J. Stammler and M. J. Abbate. *Methods of Steady-State Reactor Physics in Nuclear Design*. Academic Press Inc, 1983.

[16] Alain Hébert. *Applied reactor physics*. Presses internationales Polytechnique, Montréal, 2 edition, 2016.

[17] Paul Reuss. *Neutron physics*. EDP sciences, 2012.

[18] T Downar, D Lee, Y Xu, and T Kozlowski. Theory manual for the PARCS neutronics core simulator. *School of Nuclear Engineering, Purdue University, W. Lafayette, Indiana*, 47907, 2004.

[19] Alain Kavenoky. The SPH homogeneization method. Technical report, CEA Centre d'Etudes Nucleaires de Cadarache, 1978.

[20] Alain Hébert and Pierre Benoist. A consistent technique for the global homogenization of a pressurized water reactor assembly. *Nuclear Science and Engineering*, 109(4):360–372, 1991.

[21] A Hébert and G Mathonniere. Development of a third-generation superhomogeneisation method for the homogenization of a pressurized water reactor assembly. *Nuclear Science and Engineering*, 115(2):129–141, 1993.

[22] Patrick Blanc Tranchant. *Élaboration et qualification de schémas de calcul de référence pour les absorbants dans les réacteurs à eau pressurisée*. PhD thesis, Université Aix-Marseille-1, 1999.

[23] Alain Santamarina, Claire Collignon, and Christian Garat. French calculation schemes for light water reactor analysis. *The Physics of Fuel Cycles and Advanced Nuclear Systems: Global Developments (PHYSOR 2004)*, 2004.

[24] JF Vidal et al. New modelling of LWR assemblies using the APOLLO2 code package. *Proc. Joint Int. Top. Mtg. on Mathematics & Computation and Supercomputing in Nuclear Applications (M&C+ SNA 2007)*, pages 15–19, 2007.

[25] Axel Canbakan. Validation d'un nouveau calcul de référence en évolution pour les réacteurs thermiques. Master's thesis, École Polytechnique de Montréal (Canada), 2014.

[26] Noureddine Hfaiedh. *Nouvelle méthodologie de calcul de l'absorption résonnante*. PhD thesis, Université Louis Pasteur (Strasbourg), 2006.

[27] A Hébert. Refinement of the santamarina-hfaiedh energy mesh between 22.5 eV and 11.4 keV. In *International Conference on the Physics of Reactors, Interlaken, Switzerland*, 2008.

[28] Alain Hébert. Development of the subgroup projection method for resonance self-shielding calculations. *Nuclear Science and Engineering*, 162(1):56–75, 2009.

[29] A. Hébert G. Marleau and R. Roy. A user guide for DRAGON version5. Technical Report IGE-335, École Polytechnique de Montréal (Canada), 2015.

[30] Luca Liponi, Alain Hébert, and Julien Taforeau. Calculation and verification of assembly discontinuity factors for the DRAGON/PARCS code sequence. In *Int. Conf. on Mathematics & Computational Methods (M&C) Applied to Nuclear Science and Engineering; Jeju, Korea*, 2017.

[31] R. Chambon A. Hébert, D. Sekki et al. A user guide for DONJON 5. Technical Report IGE-344, École Polytechnique de Montréal (Canada), 2016.

[32] Y Xu and T Downar. GenPMAXS code for generating the PARCS cross section interface file pmaxs. *Purdue University, School of Nuclear Engineering, West Lafayette, IN, USA*, 2006.

[33] K Smith. Nodal diffusion methods: Understanding numerous unpublished details. In *Conference: PHYSOR 2016, Unifying Theory and Experiments in the 21st Century, At Sun-Valley, Idaho, USA*, 2016.

[34] TJ Downar, CH Lee, and G Jiang. An assessment of advanced nodal methods for MOX fuel analysis in light water reactors. In *Proceedings of the PHYSOR 2000 ANS International Topical Meeting on Advances in Reactor Physics and Mathematics and Computation into the Next Millennium. Pittsburgh, Pennsylvania*, 2000.

[35] Kord S Smith. Practical and efficient iterative method for LWR fuel assembly homogenization. *Transactions of the American Nuclear Society*, 71, 1994.

[36] Scott Palmtag and Kord S Smith. Two-group spectral corrections for MOX calculations. In *Proc. Int. Conf. Physics of Nucl. Sci. and Tech*, volume 1, page 3, 1998.

[37] F Rahnema and Eleodor M Nichita. Leakage corrected spatial (assembly) homogenization technique. *Annals of Nuclear Energy*, 24(6):477–488, 1997.

[38] Kevin T Clarno and Marvin L Adams. Capturing the effects of unlike neighbors in single-assembly calculations. *Nuclear Science and Engineering*, 149(2):182–196, 2005.

[39] Aldo Dall'Osso. A spatial rehomogenization method in nodal calculations. *Annals of Nuclear Energy*, 33(10):869–877, 2006.

[40] K Koebke. Advances in homogenization and dehomogenization. In *Joint ANS/ENS international topical meeting on advances in mathematical methods for the solution of nuclear engineering problems; Munich, Germany*, 1981.

[41] K Koebke, H Haase, L Hetzelt, and H-J Winter. Application and verification of the simplified equivalence theory for burnup states. *Nuclear Science and Engineering*, 92(1):56–65, 1986.

[42] Erwin Ziegfried Müller. *EQUIVA-2: A code for generating environmental-insensitive equivalent nodal parameters for PWR reflector regions.* Atomic Energy Corporation of South Africa, 1991.

APPENDIX A 13-gr Isotopic Absorption Reaction Rates Comparison

Table A.1 13-gr absorption rate accuracy for UX and UA assemblies (sensitivity study).

			U235		U238		U235		U238	
	Group	**Sup. Limit**	**Δr**	**Δa**	**Δr**	**Δa**	**Δr**	**Δa**	**Δr**	**Δa**
Canb 1-lvl	*1*	19.6 MeV	-1.3	-2.0	-1.3	-23.9	-1.5	-2.2	-1.5	-27.1
SHEM295	*2*	2.23 MeV	-1.2	-3.7	-1.2	-18.7	-1.4	-4.6	-1.4	-22.2
	3	494 keV	-0.1	-0.6	-0.5	-7.8	-0.5	-2.9	-0.9	-15.0
	4	11.1 keV	0.4	3.1	-0.2	-6.7	0.0	-0.2	-0.6	-18.3
	5	748 eV	0.0	0.8	-0.5	-19.6	-0.4	-8.2	-0.9	-39.3
	6	76.3 eV	0.0	0.0	-1.2	-11.8	-0.5	-5.6	-1.9	-18.3
	7	39.7 eV	0.2	2.5	-1.1	-23.3	-0.3	-3.6	-1.7	-33.9
	8	22.5 eV	0.4	1.6	-0.7	-16.2	0.0	0.1	-1.3	-29.1
	9	19 eV	-0.2	-4.6	-1.4	-7.1	-0.7	-14.2	-1.9	-9.3
	10	7.6 eV	-2.4	-13.0	-0.4	-16.4	-3.3	-16.0	-1.0	-42.1
	11	4 eV	-0.6	-14.6	-0.8	-5.5	-1.0	-20.3	-1.2	-7.2
	12	0.625 eV	-0.6	-51.1	-0.7	-7.0	-0.6	-35.4	-0.7	-5.0
	13	190 meV	0.3	116.2	0.2	10.8	0.6	144.5	0.5	14.7
	tot			34.8		-153.3		31.5		-252.0
Orion 1-lvl	*1*	19.6 MeV	-0.1	-0.1	-0.1	-1.4	0.4	0.7	0.4	8.3
SHEM295	*2*	2.23 MeV	-0.2	-0.7	-0.2	-2.9	0.2	0.8	0.3	5.2
	3	494 keV	-0.1	-0.4	-0.5	-8.4	0.3	1.6	-0.2	-2.8
	4	11.1 keV	0.2	1.3	-0.9	-24.9	0.6	5.2	-0.5	-13.1
	5	748 eV	-0.2	-3.9	-0.9	-39.4	0.3	5.7	-0.5	-19.6
	6	76.3 eV	-0.3	-3.0	-1.1	-10.7	0.2	2.7	-0.8	-7.6
	7	39.7 eV	-0.3	-3.6	-0.9	-17.9	0.1	1.5	-0.4	-8.8
	8	22.5 eV	-0.1	-0.5	-0.3	-7.9	0.4	1.5	0.0	0.9
	9	19 eV	-0.6	-13.5	-1.6	-8.4	-0.2	-3.1	-1.2	-6.0
	10	7.6 eV	-1.9	-10.4	-1.3	-57.1	-1.8	-8.7	-0.9	-35.8
	11	4 eV	-0.7	-18.7	-0.9	-6.5	-0.3	-6.6	-0.5	-3.1
	12	0.625 eV	-0.8	-75.7	-0.9	-9.8	-0.5	-28.8	-0.5	-3.9
	13	190 meV	0.3	120.2	0.2	9.8	0.1	14.9	0.0	-0.1
	tot			-9.1		-185.5		-12.7		-86.4
DRAGOR-V1 1lvl	*1*	19.6 MeV	12.9	22.5	12.7	271.6	13.5	23.5	13.4	283.9
XMAS172	*2*	2.23 MeV	-2.4	-7.8	-16.2	-227.5	-1.7	-5.5	-15.2	-218.2
	3	494 keV	-2.9	-15.3	-2.6	-41.7	-2.4	-13.7	-2.2	-36.7
	4	11.1 keV	6.9	61.0	4.4	125.5	7.3	67.1	4.8	142.9
	5	748 eV	-1.9	-39.1	-2.9	-124.5	-1.4	-29.6	-2.4	-104.0
	6	76.3 eV	7.0	87.7	24.0	315.3	7.6	93.1	23.7	306.4
	7	39.7 eV	-14.5	-156.8	-21.3	-360.3	-14.1	-148.3	-20.7	-341.9
	8	22.5 eV	48.8	365.9	4.5	109.5	48.5	349.4	4.8	112.9
	9	19 eV	-14.1	-266.2	-21.6	-93.9	-13.6	-243.4	-21.5	-89.1
	10	7.6 eV	3.0	16.8	-2.0	-88.8	3.2	16.6	-1.6	-64.2
	11	4 eV	-0.9	-22.0	-1.0	-7.1	-0.5	-10.6	-0.7	-3.9
	12	0.625 eV	0.3	29.3	0.3	2.6	0.5	30.0	0.4	3.1
	13	190 meV	-0.1	-27.5	-0.2	-7.6	-0.4	-89.8	-0.4	-12.4
	tot			48.4		-126.8		38.8		-21.3

Table A.2 13-gr absorption rate accuracy for MX assembly (sensitivity study).

			U235		**U238**		**Pu239**		**Pu240**		**Pu241**	
	Group	**Sup. Limit**	**Δr**	**Δa**	**Δr**	**Δa**	**Δr**	**Δa**	**Δr**	**Δa**	**Δr**	**Δa**
Canb 1-lvl	*1*	19.6 MeV	-1.4	-0.1	-1.4	-25.6	-1.4	-4.2	-1.4	-1.8	-1.4	-0.6
SHEM295	*2*	2.23 MeV	-1.1	-0.2	-1.1	-17.2	-1.2	-6.7	-1.1	-2.3	-1.2	-1.0
	3	494 keV	-0.1	0.0	-0.5	-7.6	-0.2	-1.1	-0.1	-0.1	-0.4	-0.5
	4	11.1 keV	0.2	0.1	-0.2	-6.3	1.3	10.4	1.6	2.2	0.0	-0.1
	5	748 eV	0.3	0.3	-0.8	-34.1	0.4	11.9	-0.8	-4.3	0.2	0.8
	6	76.3 eV	-0.1	-0.1	0.9	7.4	0.2	3.6	1.0	4.9	-0.5	-0.8
	7	39.7 eV	-0.1	-0.1	-1.4	-25.4	1.2	4.2	0.7	2.1	1.3	3.6
	8	22.5 eV	-1.5	-0.4	-0.3	-5.7	-1.0	-3.7	7.0	12.5	-0.3	0.0
	9	19 eV	-1.6	-1.8	-1.8	-7.4	-0.1	-4.2	-1.5	-0.1	0.1	0.7
	10	7.6 eV	-3.0	-0.8	-0.8	-30.4	-2.4	-5.3	-1.7	-0.2	-0.1	-0.6
	11	4 eV	-1.0	-0.7	-1.1	-4.6	-1.3	-16.8	-1.0	-103.3	-0.9	-2.2
	12	0.625 eV	-1.4	-1.1	-1.5	-2.8	-1.0	-153.7	-1.3	-15.8	-1.4	-16.7
	13	190 meV	1.8	6.9	1.7	12.3	1.0	175.0	1.5	29.6	1.1	38.5
	tot			1.9		-147.3		9.3		-76.7		21.3
Orion 1-lvl	*1*	19.6 MeV	0.0	-0.3	-5.5	-0.3	-0.9	-0.3	-0.4	-0.3	-0.1	-0.3
SHEM295	*2*	2.23 MeV	-0.1	-0.2	-3.8	-0.3	-1.9	-0.3	-0.6	-0.3	-0.3	-0.3
	3	494 keV	0.0	-0.1	-8.7	-0.2	-1.0	-0.2	-0.1	-0.4	-0.5	-0.1
	4	11.1 keV	0.0	0.8	-23.9	-1.1	8.0	1.3	1.7	-0.3	-0.6	0.2
	5	748 eV	0.0	-1.0	-53.0	-1.6	2.4	-1.4	-7.6	-0.1	-0.6	2.8
	6	76.3 eV	-0.2	-0.5	7.9	-1.0	-5.2	0.4	1.9	-0.8	-1.2	-1.3
	7	39.7 eV	-0.4	0.0	-20.5	1.0	2.6	-0.6	-1.8	1.0	2.8	1.9
	8	22.5 eV	-0.5	-1.4	2.6	-4.4	-6.4	5.0	8.8	-0.2	0.0	-14.0
	9	19 eV	-2.2	-1.8	-8.7	0.2	-32.2	-1.8	-0.1	-0.3	-2.6	8.8
	10	7.6 eV	-0.7	-2.3	-64.8	-1.9	-5.7	-1.9	-0.2	-0.1	-1.1	-2.1
	11	4 eV	-0.9	-1.4	-5.5	-2.0	-20.2	-0.9	-94.9	-1.1	-2.6	-0.4
	12	0.625 eV	-1.4	-1.8	-3.4	-1.8	-144.8	-1.5	-18.1	-1.4	-16.4	-1.6
	13	190 meV	5.2	1.2	8.9	2.1	161.5	1.5	29.3	1.1	37.5	1.7
	tot			-8.7		-11.3		-0.8		-3.2		-4.8
DRAGOR-V1 1lvl	*1*	19.6 MeV	12.3	1.2	12.0	255.6	12.0	41.8	11.8	17.5	12.7	6.0
XMAS172	*2*	2.23 MeV	-2.5	-0.4	-16.4	-215.6	-3.3	-18.8	-7.5	-14.3	-2.6	-2.2
	3	494 keV	-2.8	-0.8	-2.5	-37.7	-4.0	-24.0	-4.5	-3.5	-3.3	-4.2
	4	11.1 keV	6.8	3.3	4.5	121.5	5.8	49.5	3.3	4.7	5.2	9.6
	5	748 eV	-1.5	-1.7	-2.8	-110.5	-0.2	-5.1	-2.1	-10.7	0.3	1.5
	6	76.3 eV	6.4	4.0	24.9	287.7	4.7	95.4	45.0	385.6	8.4	13.7
	7	39.7 eV	-16.1	-9.5	-17.7	-280.1	0.9	3.1	-5823.4	-281.6	-6.9	-17.7
	8	22.5 eV	39.5	16.3	4.9	106.0	49.9	377.3	25.2	56.1	95.3	181.0
	9	19 eV	-16.2	-16.2	-26.0	-84.5	-12.2	-413.0	-40.4	-1.4	-19.4	-156.2
	10	7.6 eV	0.4	0.1	-2.6	-96.5	-35.2	-59.1	-1.4	-0.2	1.7	16.4
	11	4 eV	-1.9	-1.3	-1.8	-7.3	-2.0	-25.0	-1.2	-121.4	-1.5	-3.6
	12	0.625 eV	-1.2	-1.0	-1.5	-2.8	-0.6	-96.6	-1.6	-18.9	-0.6	-7.4
	13	190 meV	0.6	2.3	0.4	3.2	0.0	1.0	0.7	13.5	0.3	8.7
	tot			-3.9		-61.0		-73.6		25.4		45.6

APPENDIX B Validation of 2x2 PWR Assembly Cluster

Here we report the validation of the 2x2 PWR motif; it is the same validation excercise proposed for the 3x3 PWR motif.

UA

Let's consider first the accuracy of the multiplication factor (Table B.1); the overall most precise outcome is observed when no leakage model is implemented, and it is characterized by a switch between underestimation to overestimation of the reactivity due to the ADFs. Concerning, the `B1` and `P1` leakage models, the outcome is slightly degraded, but the ADFs lead to a net improvement. Globally, higher discrepancies are observed compared to the 3x3 motif, and an increased impact of ADFs is displayed. Especially for the Canbakan scheme, the implementation of ADFs leads to an increase in reactivity close to 570 *pcm* for the `FD_B` option, while approximately 30 *pcm* lower for the `FD_H` one. For the *DRAGOR-V1* the magnitude is reduced, and it does not discriminate between the two ADF options. The `FD_B` option results in the best approach with leakage correction.

Table B.1 k_{eff} and reactivity [*pcm*] for the UA-UX 2x2 PWR motif with reflective BC as a function of *leakage model* and *adf* option. Calculation option employed: *nodal kernel*=`A2`.

		`FD_B`		`FD_H`		`NO ADF`	
		k_{eff}	$\Delta\rho$	k_{eff}	$\Delta\rho$	k_{eff}	$\Delta\rho$
Canb 2-lvl SPH	`NoL`	1.20342	280	1.20271	231	1.19510	-298
	`B1`	1.19597	-237	1.19516	-294	1.18792	-804
	`P1`	1.19599	-236	1.19517	-293	1.18788	-807
DRAGOR-V1	`NoL`	1.20239	209	1.20251	218	1.19591	-242
	`B1`	1.19482	-317	1.19481	-318	1.18851	-762
	`P1`	1.19483	-317	1.19481	-318	1.18846	-765
Canb 2-lvl w/o SPH	`NoL`	1.20051	79	1.19980	30	1.19210	-508
	`B1`	1.19299	-446	1.19218	-503	1.18486	-1021
	`P1`	1.19302	-444	1.19220	-502	1.18483	-1023
Canb 2-lvl SPH + TISO	`NoL`	1.20380	307	1.20334	275	1.19578	-250
	`B1`	1.19634	-211	1.19575	-252	1.18858	-757
	`P1`	1.19636	-210	1.19577	-251	1.18854	-759
Canb 1-lvl	`NoL`	1.20476	373	1.20409	327	1.19644	-204
	`B1`	1.19735	-141	1.19649	-201	1.18920	-713
	`P1`	1.19740	-137	1.19654	-197	1.18919	-714

Considering now the assembly power (Figure B.1 and Table B.2), a similar trend as for the reactivity is observed on the impact of the leakage correction. If no leakage model is

considered, the ADFs lead to a net alteration of the tilt in the power distribution, while a significant reduction of the inaccuracies is observed when B_1 or P_1 models are considered. The leakage choice does not influence the extent of the variation due to the ADF. Considering the Canbakan scheme, for the `FD_B` option, it can be estimated at approximately 5.5% for the UA assembly, while close to 2.5% for the UX one. If the `FD_H` option is chosen, a slight reduction compared to `FD_B` is observed. Hence, independently of the ADF option, a clear amelioration due to the ADFs is found when a leakage correction is considered (from more than 6% to less approximately 1%). When the Orion scheme is considered the impact is partially reduced, and the difference between the two ADF alternatives is almost negligible.

Table B.2 Assembly power (% difference) for the UA-UX 2x2 PWR motif with reflective BC as a function of *leakage model* and *adf* option. Calculation option employed: *nodal kernel*=`A2`.

		`FD_B`				`FD_H`				`NO ADF`			
		#1	**#2**	**#3**	**#4**	**#1**	**#2**	**#3**	**#4**	**#1**	**#2**	**#3**	**#4**
Canb 2-lvl SPH	`NoL`	1.49	-3.03	-2.99	1.35	1.26	-2.55	-2.50	1.12	-1.27	2.80	2.85	-1.40
	`B1`	-0.46	1.08	1.15	-0.59	-0.72	1.64	1.71	-0.86	-3.18	6.85	6.93	-3.31
	`P1`	-0.43	1.01	1.09	-0.56	-0.69	1.57	1.65	-0.83	-3.17	6.82	6.89	-3.30
DRAGOR-V1	`NoL`	1.16	-2.36	-2.29	1.03	1.18	-2.40	-2.33	1.05	-0.97	2.15	2.23	-1.10
	`B1`	-0.75	1.70	1.77	-0.88	-0.77	1.73	1.80	-0.90	-2.87	6.18	6.25	-2.99
	`P1`	-0.72	1.64	1.71	-0.86	-0.74	1.67	1.74	-0.87	-2.85	6.15	6.22	-2.98
Canb 2-lvl w/o SPH	`NoL`	1.67	-3.43	-3.36	1.53	1.43	-2.94	-2.86	1.30	-1.11	2.45	2.52	-1.24
	`B1`	-0.26	0.65	0.73	-0.39	-0.52	1.22	1.29	-0.66	-3.00	6.46	6.54	-3.13
	`P1`	-0.22	0.58	0.65	-0.36	-0.49	1.14	1.21	-0.62	-2.98	6.43	6.50	-3.11
Canb 2-lvl SPH + TISO	`NoL`	1.35	-2.76	-2.69	1.22	1.20	-2.44	-2.37	1.06	-1.31	2.89	2.96	-1.44
	`B1`	-0.56	1.29	1.37	-0.69	-0.76	1.72	1.79	-0.89	-3.20	6.88	6.96	-3.33
	`P1`	-0.53	1.23	1.31	-0.66	-0.73	1.65	1.73	-0.86	-3.18	6.85	6.93	-3.31
Canb 1-lvl	`NoL`	1.36	-2.78	-2.71	1.23	1.13	-2.30	-2.22	1.00	-1.41	3.09	3.16	-1.54
	`B1`	-0.55	1.26	1.34	-0.68	-0.83	1.86	1.93	-0.96	-3.30	7.10	7.18	-3.43
	`P1`	-0.51	1.18	1.26	-0.64	-0.79	1.78	1.85	-0.92	-3.28	7.07	7.14	-3.41

The last element that we consider is the validation of the pin power reconstruction (Table B.3). The outcome followed what evaluated for the assembly power. The ADF induces greater accuracy when a leakage model has been applied to the lattice calculation, while an overall negative effect is noticed in the other case. Let's consider as reference the Canbakan scheme. Without leakage, the impact of ADF is negative even if the $\boldsymbol{\delta}$ between positive and negative error peaks is notably reduced (more than 8%, particularly for the `FD_H` option). Concerning the B_1 and P_1 leakage models, the implementation of ADF leads instead to a remarkable improvement in the calculation: the **rms** value decreases as much as 3%, while the $\boldsymbol{\delta}$ above 15%. The `FD_H` option is notably more accurate compared to the `FD_B` one.

A comparison of the reconstructed power maps (Figure B.3) can then be helpful to assess the impact of the `FD_H` option in the distribution of errors; a decreased magnitude of inaccuracies

	FD_B		FD_H		NO ADF		
CANB 2-lvl	1.46 -0.46 -0.43	-3.00 1.08 1.01	1.24 -0.72 -0.69	-2.51 1.64 1.57	-1.29 -3.18 -3.17	2.84 **6.85** **6.82**	*NoL* *B1* *P1*
	-2.93 1.15 1.09	1.33 -0.59 -0.56	-2.44 1.71 1.65	1.10 -0.86 -0.83	2.91 **6.93** **6.89**	-1.42 -3.31 -3.30	*NoL* *B1* *P1*
DRAGOR V1	1.16 -0.75 -0.72	-2.36 1.70 1.64	1.18 -0.77 -0.74	-2.40 1.73 1.67	-0.97 -2.87 -2.85	2.15 **6.18** **6.15**	*NoL* *B1* *P1*
	-2.29 1.77 1.71	1.03 -0.88 -0.86	-2.33 1.80 1.74	1.05 -0.90 -0.87	2.23 **6.25** **6.22**	-1.10 -2.99 -2.98	*NoL* *B1* *P1*

Figure B.1 Assembly power (% difference) for the UA-UX 2x2 PWR motif as a function of *leakage model* and *ADF* option.

is remarked along the interfaces between the heterogeneous assemblies. The same conclusion can also be made for the *DRAGOR-V1* scheme, except that the extent of the impact is decreased and that the difference between the ADF options is negligible.

Overall, it should be highlighted that the overall best choice is provided by a combination of the P_1 leakage model with the `FD_H` option for ADF. Notably, the most accurate case is obtained with the Canbakan single level scheme (**rms** = 1.10). In conclusion, concerning the lattice schemes employed, an overall consistency is obtained throughout the available choices, except for the *DRAGOR-V1*; a large degradation is remarked both for the assembly power and pin power map.

MX

Compared to the previous configuration UA-UX, when MOX assemblies are considered, the magnitude of the discrepancies are notably reduced.

First, the accuracy of the reactivity (Table B.4) displays a range of errors difficult to interpret;

Table B.3 Pin power (% difference) for the UA-UX 2x2 PWR motif as a function of *leakage model* and *adf* option.

		FD_B			FD_H			NO ADF		
		max	**min**	**rms**	**max**	**min**	**rms**	**max**	**min**	**rms**
Canb 2-lvl SPH	NoL	7.85	-2.38	4.07	7.29	-2.36	3.75	9.93	-8.02	2.63
	B1	4.62	-0.64	1.39	4.04	-1.16	1.21	10.68	-10.04	4.05
	P1	4.37	-0.94	1.39	3.79	-1.45	1.17	10.37	-10.37	3.96
DRAGOR-V1	NoL	9.01	-3.83	3.45	9.13	-3.88	3.50	9.91	-5.25	2.65
	B1	5.16	-4.73	1.75	4.89	-4.71	1.73	10.65	-8.17	4.06
	P1	5.28	-4.63	1.67	5.33	-4.60	1.66	10.33	-8.32	3.97
Canb 2-lvl w/o SPH	NoL	8.32	-2.80	4.42	7.90	-2.80	4.10	9.91	-7.98	2.70
	B1	4.94	-0.89	1.61	4.35	-0.89	1.36	10.67	-10.01	3.83
	P1	4.71	-1.10	1.65	4.12	-1.18	1.37	10.36	-10.36	3.75
Canb 2-lvl SPH + TISO	NoL	7.65	-2.43	3.92	7.41	-2.44	3.71	9.94	-8.03	2.62
	B1	4.65	-1.08	1.34	3.94	-1.63	1.22	10.69	-10.00	4.05
	P1	4.33	-1.37	1.32	3.70	-1.93	1.18	10.38	-10.34	3.97
Canb 1-lvl	NoL	7.76	-2.15	3.88	7.22	-2.15	3.57	9.78	-8.05	2.58
	B1	4.57	-0.91	1.32	3.97	-1.37	1.17	10.51	-10.02	4.18
	P1	4.33	-1.09	1.30	3.72	-1.32	1.10	10.22	-10.40	4.09

the leakage model may have a positive or negative impact according to the case evaluated. Overall, it seems that the most reliable results can be obtained with the two-level Canbakan scheme without 26-gr SPH equivalence. As in the previous configuration, the implementation of ADF is positive for both fundamental mode methods, while it generates a deterioration without leakage. The only exception is presented by the *DRAGOR-V1* lattice scheme, for which in both cases the use of ADF produces the worst results. The ADFs induce a increase in reactivity between 30 *pcm* and 50 *pcm* for the FD_B option, and few pcm with FD_H.

Let's consider next the assembly power (Figure B.2 and Table B.5). Despite the leakage correction, the impact of ADF is always widely positive, and the magnitude is mainly constant. For the MOX assembly, the improvement can be estimated around 2% considering the FD_B option, while slightly above 0.5% for the FD_H one. Regarding the UOX assembly, between 1% and 1.5% with FD_B and around 0.5% with FD_H. The computations without leakage correction produce values very close to the reference, and particularly the best option is displayed by the Canbakan two-level scheme with SPH equivalence using the FD_B option.

Finally, the reconstructed pin power accuracy is assessed (Table B.6). The impact of the leakage model follows the observation made for the assembly power, where the option without leakage correction is more accurate. Let's focus then on the Canbakan schemes. The impact of the ADFs leads to a remarkable amelioration, which varies according to the case and the option of ADF chosen. Without leakage correction, the best option is represented by FD_H,

Table B.4 k_{eff} and reactivity [*pcm*] for the MX-UX 2x2 PWR motif as a function of *leakage model* and *adf* option.

		FD_B		FD_H		NO ADF	
		k_{eff}	$\Delta\rho$	k_{eff}	$\Delta\rho$	k_{eff}	$\Delta\rho$
Canb 2-lvl SPH	NoL	1.27655	118	1.27588	76	1.27575	68
	B1	1.27401	-39	1.27329	-83	1.27312	-94
	P1	1.27400	-40	1.27327	-84	1.27311	-95
DRAGOR-V1	NoL	1.28051	360	1.28003	330	1.27998	327
	B1	1.27794	203	1.27744	172	1.27735	167
	P1	1.27795	203	1.27745	172	1.27736	167
Canb 2-lvl w/o SPH	NoL	1.27462	-1	1.27394	-43	1.27382	-51
	B1	1.27209	-157	1.27137	-202	1.27120	-212
	P1	1.27207	-158	1.27135	-203	1.27118	-213
Canb 2-lvl SPH SPH + TISO	NoL	1.27748	175	1.27687	137	1.27675	130
	B1	1.27495	19	1.27429	-21	1.27414	-31
	P1	1.27493	18	1.27428	-22	1.27412	-32
Canb 1-lvl	NoL	1.27892	263	1.27822	220	1.27810	213
	B1	1.27642	109	1.27565	62	1.27549	52
	P1	1.27639	108	1.27563	61	1.27547	51

due to a net reduction of the **max** and **min** error peaks (decrease in $\boldsymbol{\delta}$ close to 5%), that affects positively the **rms** value. On the other side, with both B_1 and P_1 leakage models, a duality in trend is observed due to ADF option. While the FD_B option presents an increased refinement on the **rms** value compared to the FD_H one (close to 1% and 0.5% respectively), the impact of FD_H in the reduction of $\boldsymbol{\delta}$ is double compared to FD_B. Such that the errors at the interface between heterogeneous nodes are strongly reduced when the flux is recovered in the outer pin row (FD_H option). The explicit map in Figure B.4, highlights the impact of the ADF choice. The *DRAGOR-V1* scheme displays an exception since the FD_B results in all cases the most accurate option.

In conclusion, the ADF leads to a clear amelioration of the power distribution. FD_B is the best option to improve the assembly power and reduce the overall pin power errors; FD_H has a lower impact on the power, but it induces smaller peaks at the interface between nodes. The leakage model also has an impact on the overall amelioration originated by the ADFs, particularly on the pin power distribution. The Orion scheme is overall more degraded compared to the other alternatives, and the effect of ADF is reduced.

Table B.5 Assembly power (% difference) for the MX-UX 2x2 PWR motif as a function of *leakage model* and *adf* option.

		FD_B				FD_H				NO ADF			
		#1	**#2**	**#3**	**#4**	**#1**	**#2**	**#3**	**#4**	**#1**	**#2**	**#3**	**#4**
Canb 2-lvl SPH	NoL	0.00	0.03	0.01	-0.04	-0.95	1.33	1.31	-0.99	-1.44	1.99	1.97	-1.48
	B1	-1.10	1.53	1.51	-1.14	-2.08	2.86	2.84	-2.12	-2.60	3.56	3.55	-2.64
	P1	-1.09	1.52	1.50	-1.13	-2.08	2.86	2.84	-2.12	-2.60	3.56	3.55	-2.64
DRAGOR-V1	NoL	-0.72	1.01	0.99	-0.76	-1.30	1.80	1.78	-1.34	-1.67	2.30	2.29	-1.71
	B1	-1.84	2.53	2.51	-1.88	-2.43	3.33	3.31	-2.47	-2.84	3.88	3.86	-2.88
	P1	-1.84	2.53	2.51	-1.88	-2.43	3.33	3.31	-2.47	-2.84	3.88	3.86	-2.88
Canb 2-lvl w/o SPH	NoL	-0.02	0.07	0.05	-0.06	-0.98	1.36	1.34	-1.02	-1.47	2.02	2.00	-1.51
	B1	-1.12	1.55	1.53	-1.16	-2.11	2.89	2.87	-2.15	-2.63	3.60	3.58	-2.67
	P1	-1.12	1.55	1.53	-1.16	-2.10	2.88	2.86	-2.14	-2.63	3.60	3.58	-2.67
Canb 2-lvl SPH + TISO	NoL	-0.20	0.30	0.28	-0.24	-1.03	1.43	1.42	-1.07	-1.50	2.07	2.05	-1.54
	B1	-1.30	1.80	1.78	-1.34	-2.17	2.98	2.96	-2.21	-2.67	3.65	3.63	-2.71
	P1	-1.30	1.80	1.78	-1.34	-2.17	2.98	2.96	-2.21	-2.67	3.65	3.63	-2.71
Canb 1-lvl	NoL	-0.19	0.29	0.27	-0.23	-1.16	1.61	1.59	-1.20	-1.66	2.28	2.26	-1.70
	B1	-1.27	1.76	1.74	-1.31	-2.29	3.14	3.12	-2.33	-2.81	3.85	3.83	-2.85
	P1	-1.27	1.75	1.73	-1.31	-2.29	3.14	3.12	-2.33	-2.81	3.85	3.83	-2.85

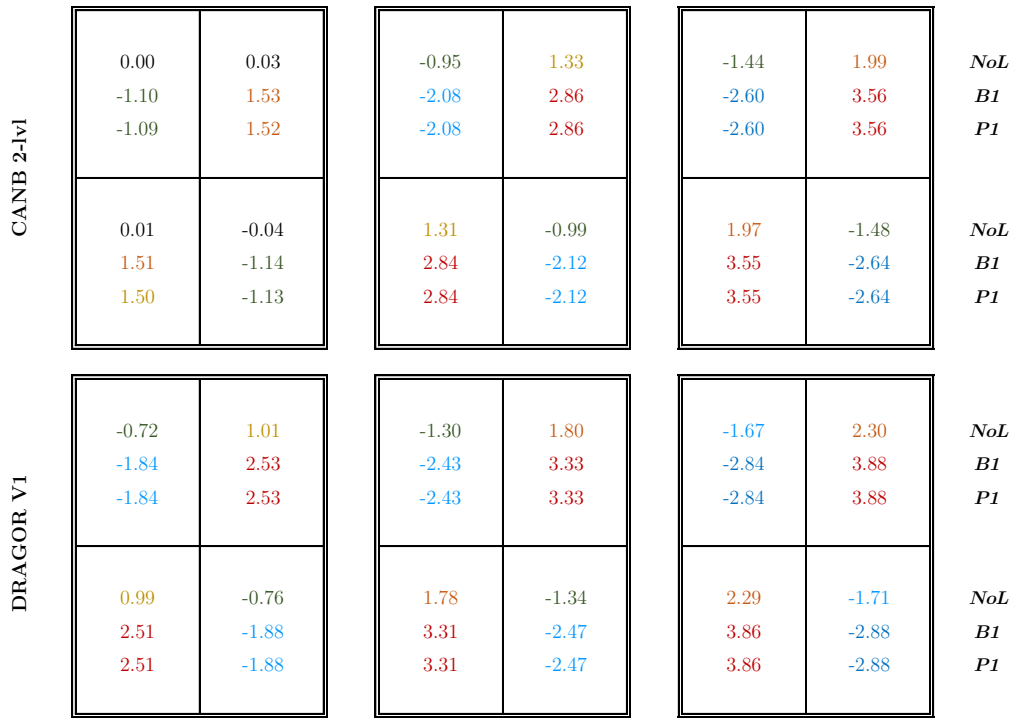

Figure B.2 Assembly power (% difference) for the MX-UX 2x2 PWR motif as a function of *leakage model* and *ADF* option.

Table B.6 Pin power (% difference) for the MX-UX 2x2 PWR motif as a function of *leakage model* and *adf* option.

		FD_B			FD_H			NO ADF		
		max	**min**	**rms**	**max**	**min**	**rms**	**max**	**min**	**rms**
Canb 2-lvl SPH	NoL	6.11	-6.68	1.56	2.60	-4.80	1.42	6.26	-6.52	1.95
	B1	5.64	-5.94	2.23	3.37	-5.19	2.67	7.00	-6.84	3.18
	P1	5.57	-6.02	2.21	3.38	-5.21	2.65	6.93	-6.94	3.16
DRAGOR-V1	NoL	4.50	-4.44	1.63	3.10	-4.91	1.94	6.23	-5.38	2.30
	B1	4.07	-6.40	2.73	4.07	-6.89	3.20	6.96	-6.85	3.56
	P1	4.01	-6.26	2.72	4.06	-6.76	3.18	6.90	-6.79	3.55
Canb 2-lvl w/o SPH	NoL	6.10	-6.71	1.57	2.53	-4.57	1.44	6.23	-6.31	1.97
	B1	5.63	-5.99	2.25	3.31	-5.26	2.69	6.97	-6.65	3.20
	P1	5.56	-6.09	2.24	3.33	-5.23	2.68	6.90	-6.74	3.19
Canb 2-lvl SPH + TISO	NoL	5.83	-6.11	1.50	2.81	-5.49	1.54	6.30	-7.15	2.01
	B1	5.36	-5.54	2.32	3.55	-5.82	2.79	7.03	-7.48	3.25
	P1	5.30	-5.64	2.30	3.54	-5.92	2.77	6.96	-7.58	3.24
Canb 1-lvl	NoL	6.07	-6.76	1.67	2.55	-4.61	1.65	6.20	-6.34	2.14
	B1	5.61	-6.09	2.43	3.56	-5.61	2.92	6.93	-6.66	3.40
	P1	5.53	-6.18	2.42	3.58	-5.58	2.91	6.85	-6.76	3.39

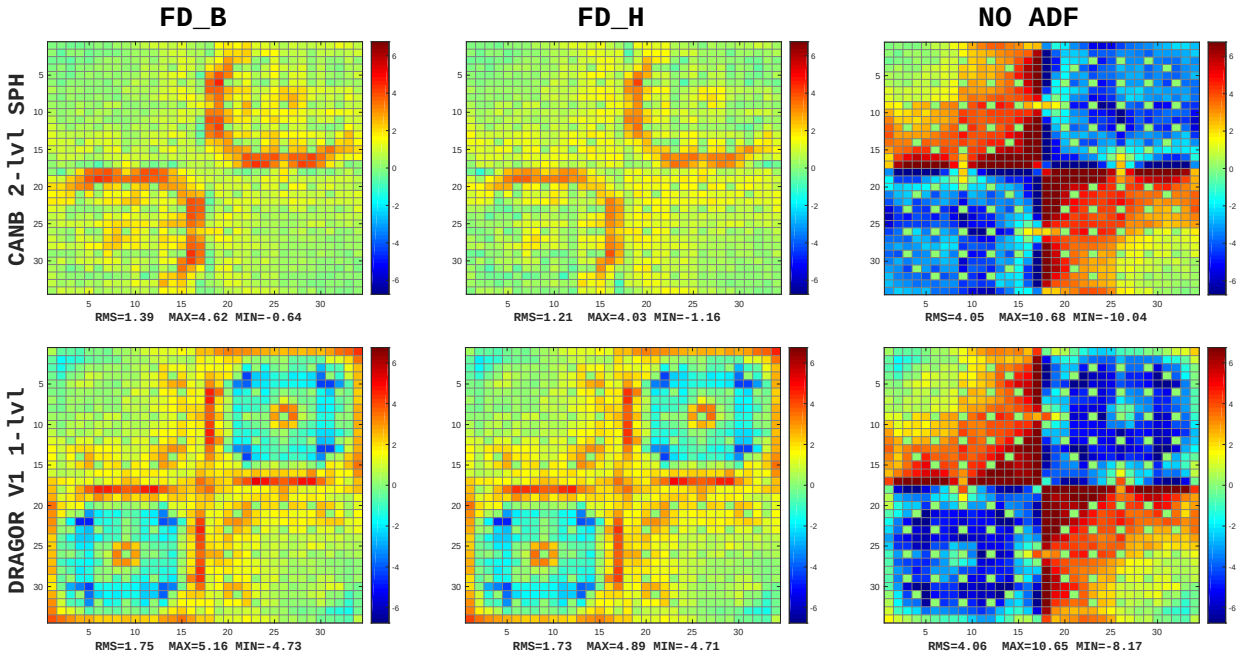

Figure B.3 Pin power (% difference) error map for the UA-UX 2x2 PWR motif as a function of *leakage model* and *adf* options. *Leakage model*=B1.

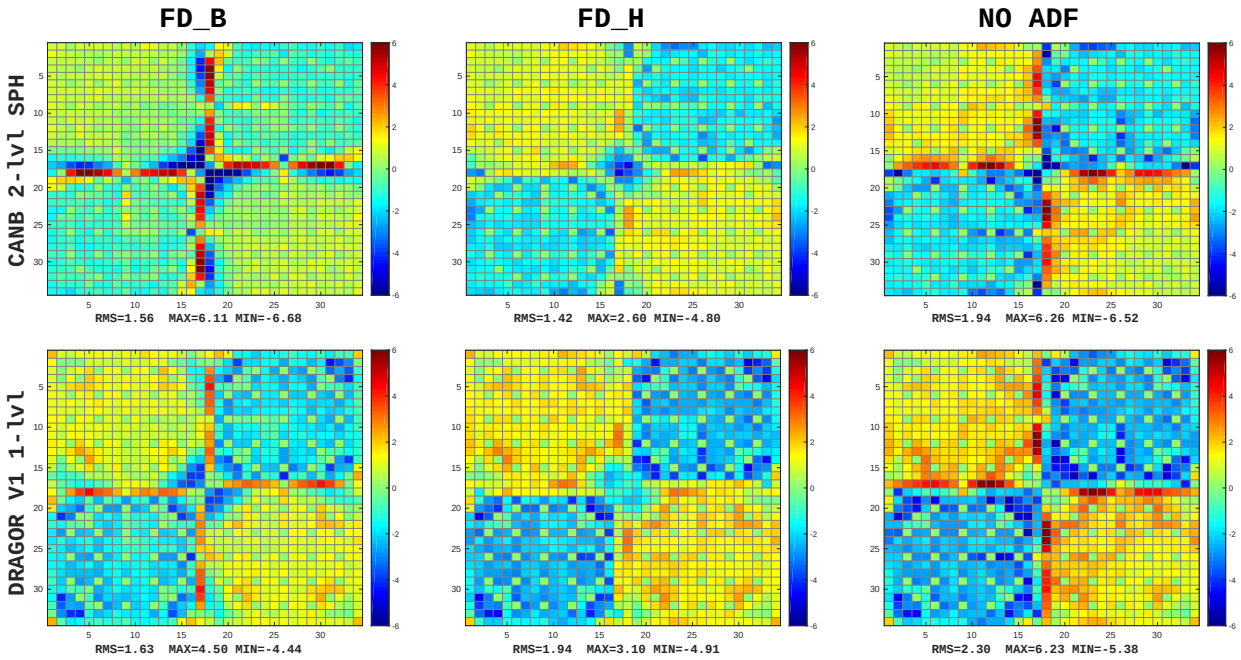

Figure B.4 Pin power (% difference) error map for the MX-UX 2x2 PWR motif as a function of *leakage model* and *adf* option. *Leakage model*=`NoL`.

APPENDIX C Validation of 3x3 PWR Assembly Cluster - Additional Tables

UA

Table C.1 k_{eff} and reactivity [*pcm*] for the UA-UX 3x3 PWR motif as a function of *leakage model* and *adf* option.

		FD_B		FD_H		NO ADF	
		k_{eff}	$\Delta\rho$	k_{eff}	$\Delta\rho$	k_{eff}	$\Delta\rho$
Canb 2-lvl w/o SPH	NoL	1.34047	-108	1.34025	-120	1.33781	-256
	B1	1.33843	-222	1.33818	-236	1.33587	-365
	P1	1.33841	-223	1.33816	-237	1.33583	-367
Canb 2-lvl SPH SPH + TISO	NoL	1.34340	55	1.34326	47	1.34086	-86
	B1	1.34136	-58	1.34118	-69	1.33890	-195
	P1	1.34134	-59	1.34116	-70	1.33887	-197
Canb 1-lvl	NoL	1.34444	112	1.34423	101	1.34180	-34
	B1	1.34239	-1	1.34213	-16	1.33982	-144
	P1	1.34238	-2	1.34212	-16	1.33980	-145

Table C.2 Assembly power (% difference) for the UA-UX 3x3 PWR motif as a function of *leakage model* and *adf* option.

		FD_B			FD_H			NO ADF		
		Crn	**Ctr**	**Side**	**Crn**	**Ctr**	**Side**	**Crn**	**Ctr**	**Side**
Canb 2-lvl w/o SPH	NoL	0.22	-3.95	0.32	0.22	-3.28	0.22	0.24	4.06	-0.83
	B1	-0.01	0.53	-0.07	-0.01	1.26	-0.17	0.01	8.40	-1.19
	P1	-0.02	0.46	-0.05	-0.01	1.20	-0.15	0.01	8.36	-1.18
Canb 2-lvl SPH + TISO	NoL	0.16	-3.22	0.28	0.17	-2.74	0.21	0.18	4.53	-0.83
	B1	-0.07	1.25	-0.10	-0.07	1.81	-0.18	-0.05	8.85	-1.20
	P1	-0.08	1.20	-0.09	-0.08	1.76	-0.16	-0.06	8.81	-1.18
Canb 1-lvl	NoL	0.14	-3.29	0.32	0.14	-2.63	0.22	0.15	4.72	-0.82
	B1	-0.10	1.14	-0.06	-0.10	1.93	-0.17	-0.08	9.06	-1.19
	P1	-0.11	1.09	-0.04	-0.11	1.86	-0.15	-0.09	9.03	-1.17

Table C.3 Pin power (% difference) for the UA-UX 3x3 PWR motif as a function of *leakage model* and *adf* option.

		FD_B			FD_H			NO ADF		
		max	**min**	**rms**	**max**	**min**	**rms**	**max**	**min**	**rms**
Canb 2-lvl w/o SPH	NoL	8.55	-1.37	2.22	7.96	-1.39	2.03	8.46	-8.29	1.65
	B1	4.31	-1.56	0.86	3.65	-1.25	0.69	8.09	-11.55	2.32
	P1	4.31	-1.66	0.88	3.65	-1.24	0.71	7.99	-11.68	2.30
Canb 2-lvl SPH + TISO	NoL	7.91	-1.43	1.97	7.50	-1.44	1.85	8.40	-8.35	1.63
	B1	3.74	-1.38	0.69	3.20	-1.30	0.59	8.00	-11.55	2.40
	P1	3.67	-1.49	0.70	3.18	-1.25	0.60	7.91	-11.68	2.38
Canb 1-lvl	NoL	7.87	-1.31	1.98	7.30	-1.27	1.79	8.14	-8.62	1.63
	B1	3.69	-1.84	0.70	3.00	-1.36	0.55	7.74	-11.85	2.45
	P1	3.67	-1.96	0.71	3.00	-1.31	0.55	7.64	-11.99	2.42

MX

Table C.4 k_{eff} and reactivity [*pcm*] for the MX-UX 3x3 PWR motif as a function of *leakage model* and *adf* option.

		FD_B		FD_H		NO ADF	
		k_{eff}	$\Delta\rho$	k_{eff}	$\Delta\rho$	k_{eff}	$\Delta\rho$
Canb 2-lvl w/o SPH	NoL	1.35565	-101	1.35539	-115	1.35533	-119
	B1	1.35484	-145	1.35456	-160	1.35447	-165
	P1	1.35482	-146	1.35454	-162	1.35444	-167
Canb 2-lvl SPH SPH + TISO	NoL	1.35850	54	1.35827	41	1.35821	38
	B1	1.35767	9	1.35742	-5	1.35734	-9
	P1	1.35766	8	1.35740	-6	1.35732	-10
Canb 1-lvl	NoL	1.35963	115	1.35936	100	1.35929	97
	B1	1.35878	69	1.35848	53	1.35840	48
	P1	1.35877	68	1.35847	52	1.35838	47

Table C.5 Assembly power (% difference) for the MX-UX 3x3 PWR motif as a function of *leakage model* and *adf* option.

		FD_B			FD_H			NO ADF		
		Crn	**Ctr**	**Side**	**Crn**	**Ctr**	**Side**	**Crn**	**Ctr**	**Side**
Canb 2-lvl	NoL	-0.30	0.80	0.16	-0.33	2.97	-0.25	-0.31	4.25	-0.53
w/o SPH	B1	-0.44	2.49	-0.03	-0.48	4.75	-0.45	-0.46	6.14	-0.75
	P1	-0.44	2.49	-0.03	-0.48	4.75	-0.45	-0.46	6.14	-0.75
Canb 2-lvl	NoL	-0.31	1.18	0.10	-0.34	3.09	-0.26	-0.31	4.29	-0.53
SPH + TISO	B1	-0.45	2.90	-0.11	-0.48	4.89	-0.47	-0.47	6.18	-0.75
	P1	-0.46	2.90	-0.10	-0.49	4.88	-0.46	-0.47	6.19	-0.74
Canb 1-lvl	NoL	-0.36	1.07	0.17	-0.39	3.29	-0.25	-0.36	4.56	-0.53
	B1	-0.49	2.76	-0.03	-0.53	5.10	-0.46	-0.51	6.46	-0.75
	P1	-0.49	2.75	-0.03	-0.53	5.10	-0.46	-0.52	6.47	-0.75

Table C.6 Pin power (% difference) for the MX-UX 3x3 PWR motif as a function of *leakage model* and *adf* option.

		FD_B			FD_H			NO ADF		
		max	**min**	**rms**	**max**	**min**	**rms**	**max**	**min**	**rms**
Canb 2-lvl	NoL	4.83	-5.81	1.12	1.62	-5.52	1.16	5.10	-7.10	1.56
w/o SPH	B1	3.77	-6.56	1.46	1.85	-7.36	1.74	5.11	-9.07	2.15
	P1	3.74	-6.57	1.45	1.85	-7.39	1.73	5.08	-9.10	2.15
Canb 2-lvl	NoL	4.55	-5.29	1.10	1.75	-6.09	1.21	5.12	-7.59	1.58
SPH + TISO	B1	3.48	-7.09	1.49	1.99	-7.96	1.79	5.14	-9.58	2.18
	P1	3.45	-7.11	1.49	1.99	-7.98	1.79	5.11	-9.60	2.17
Canb 1-lvl	NoL	4.78	-6.02	1.19	1.61	-5.95	1.27	4.90	-7.54	1.65
	B1	3.74	-6.83	1.55	1.84	-7.82	1.86	4.90	-9.52	2.25
	P1	3.71	-6.84	1.55	1.84	-7.83	1.85	4.87	-9.53	2.25

APPENDIX D Sensitivity Study on Koebke Method

Here we report the results of the diffusion calculations on the simplified core obtained during the sensitivity study on the Koebke method. Only the UA-UX and MX-UX are presented. In addition, the computed homogenized parameters are included.

UA

Table D.1 Reflector homogenized parameters for UA configuration.

	f_1	$B_{1,HOMO}$	Σ_{tr}	$B_{1,ECCO}$
$\Sigma_{t,1}$	2.951E−02	2.548E−02	2.994E−02	2.381E−02
$\Sigma_{t,2}$	2.047E−01	1.767E−01	2.076E−01	1.658E−01
$\Sigma_{a,1}$	1.844E−03	1.591E−03	1.871E−03	1.474E−03
$\Sigma_{a,2}$	2.047E−01	1.767E−01	2.076E−01	1.658E−01
$\Sigma_{2\leftarrow1}$	2.767E−02	2.388E−02	2.807E−02	2.234E−02
D_1	9.154E−01	1.060E+00	9.022E−01	1.087E+00
D_2	1.811E−01	2.098E−01	1.785E−01	2.074E−01
f_1	1.000E+00	1.158E+00	9.856E−01	1.260E+00
f_2	1.123E−01	1.301E−01	1.106E−01	1.373E−01

Table D.2 k_{eff} and reactivity $[pcm]$ for the UA-UX simplified core. Comparison between different methods to compute Koebke homogenized parameters. Reference SERPENT2: 1.12332 ± 5pcm.

	FD_B		FD_H		NO ADF	
	k_{eff}	$\Delta\rho$	k_{eff}	$\Delta\rho$	k_{eff}	$\Delta\rho$
f_1	1.12142	-151	1.12068	-210	1.11371	-768
$B_{1,HOMO}$	1.12136	-155	1.12062	-214	1.11365	-773
Σ_{tr}	1.12143	-150	1.12069	-209	1.11371	-768
$B_{1,ECCO}$	1.12160	-137	1.12086	-196	1.11389	-754

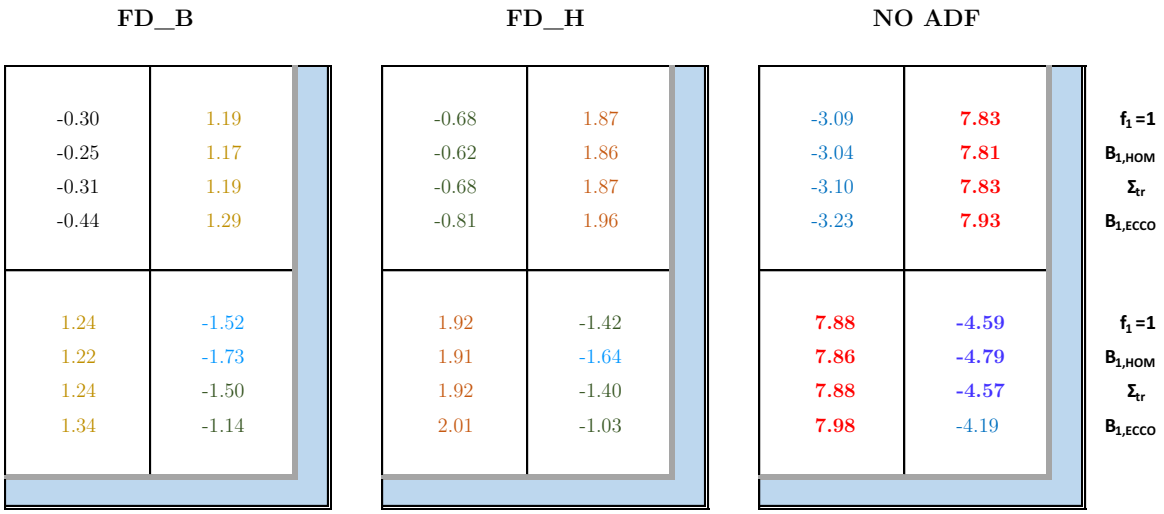

Figure D.1 Assembly power (% difference) for the UA-UX simplified core. Comparison between different methods to compute Koebke homogenized parameters.

Table D.3 Pin power (% difference) for the UA-UX simplified core. Comparison between different methods to compute Koebke homogenized parameters.

	FD_B			FD_H			NO ADF		
	max	**min**	**rms**	**max**	**min**	**rms**	**max**	**min**	**rms**
f_1	14.15	-4.34	2.09	11.99	-5.64	1.88	12.74	-17.90	5.64
$B_{1,HOMO}$	13.48	-4.13	2.16	11.32	-5.43	1.92	12.13	-17.67	5.63
Σ_{tr}	14.22	-4.34	2.08	11.99	-5.64	1.88	12.80	-17.93	5.64
$B_{1,ECCO}$	10.91	-4.90	1.91	8.75	-6.20	1.83	10.68	-18.87	5.73

MX

Table D.4 Reflector homogenized parameters for MX configuration.

	f_1	$B_{1,HOMO}$	Σ_{tr}	$B_{1,ECCO}$
$\Sigma_{t,1}$	2.890E−02	2.515E−02	2.958E−02	2.347E−02
$\Sigma_{t,2}$	1.551E−01	1.349E−01	1.587E−01	1.545E−01
$\Sigma_{a,1}$	1.764E−03	1.535E−03	1.805E−03	1.421E−03
$\Sigma_{a,2}$	1.551E−01	1.349E−01	1.587E−01	1.545E−01
$\Sigma_{2\leftarrow1}$	2.714E−02	2.362E−02	2.778E−02	2.205E−02
D_1	9.489E−01	1.090E+00	9.271E−01	1.145E+00
D_2	4.630E−02	5.321E−02	4.524E−02	1.468E−01
f_1	1.000E+00	1.149E+00	9.770E−01	1.255E+00
f_2	1.417E−01	1.628E−01	1.384E−01	1.412E−01

Table D.5 k_{eff} and reactivity [pcm] for the MX-UX simplified core. Comparison between different methods to compute Koebke homogenized parameters. Reference SERPENT2: 1.17388 ± 5pcm.

	FD_B		FD_H		NO ADF	
	k_{eff}	$\Delta\rho$	k_{eff}	$\Delta\rho$	k_{eff}	$\Delta\rho$
f_1	1.17425	27	1.17358	-22	1.17348	-29
$B_{1,HOMO}$	1.17412	17	1.17345	-31	1.17335	-39
Σ_{tr}	1.17426	28	1.17359	-21	1.17349	-28
$B_{1,ECCO}$	1.17456	49	1.17400	9	1.17394	4

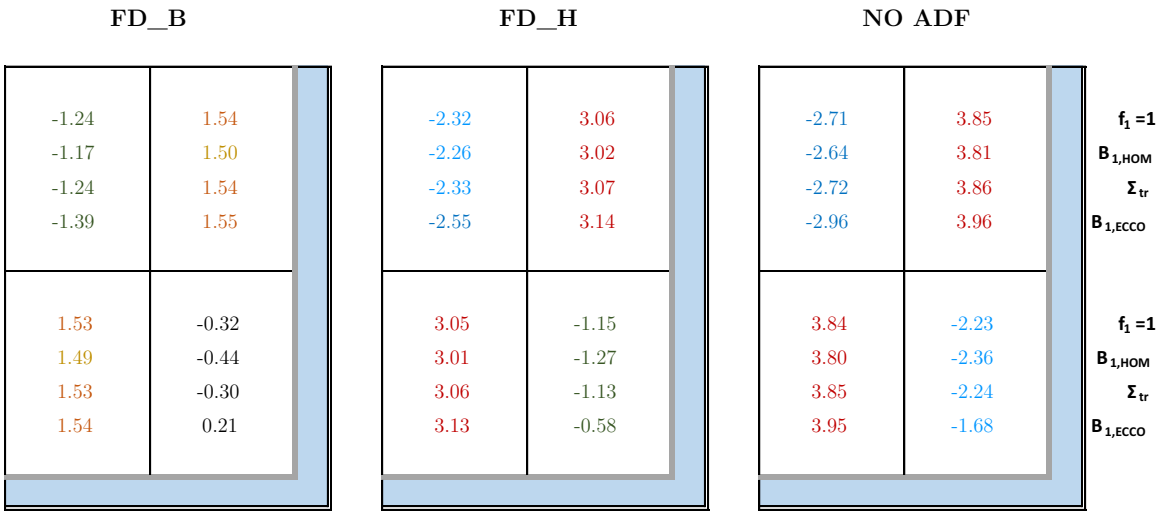

Figure D.2 Assembly power (% difference) for the MX-UX simplified core. Comparison between different methods to compute Koebke homogenized parameters.

Table D.6 Pin power (% difference) for the MX-UX simplified core. Comparison between different methods to compute Koebke homogenized parameters.

	FD_B			FD_H			NO ADF		
	max	min	rms	max	min	rms	max	min	rms
f_1	15.47	-9.66	2.83	13.32	-7.41	3.17	14.46	-10.83	3.72
$B_{1,HOMO}$	14.52	-9.67	2.81	12.38	-7.32	3.12	13.51	-10.54	3.68
Σ_{tr}	15.53	-9.66	2.83	13.45	-7.44	3.17	14.58	-10.86	3.72
$B_{1,ECCO}$	11.81	-9.68	2.71	9.55	-7.55	3.17	10.74	-11.07	3.73